Long term atmosphere/biosphere exchange of CO_2 in Hungary

Geography/Earth Sciences Doctoral Program,
Eötvös Loránd University
Program leader: Prof. Péter MÁRTON
Supervisor: Dr. Tamás WEIDINGER
Scientific adviser: Dr. László HASZPRA

Eötvös Loránd University,
Department of Meteorology
2001

Contents

Abstract

The objective of this dissertation is to clarify the role of a relatively large Hungarian biosphere region in the carbon cycle. This is accomplished by determining the Net Ecosystem carbon dioxide Exchange (NEE) of an active agricultural region and a small grassland area in Hegyhátsál (western Hungary) using the eddy covariance (EC) technique. NEE is determined as the sum of the CO_2 EC flux at 82 m and the rate of change of CO_2 storage below the measuring level for the regional scale system. NEE of the grassland is determined directly from the carbon dioxide fluxes measured at 3 m. The temperature dependence of nighttime ecosystem respitation and photosynthetically active photon flux density (PPFD) dependence of daytime NEE is analyzed. The missing measurement intervals are filled with the modified CO_2 flux data determined from the parallel profile measurements or with data calculated from the temperature and light dependences. Maximum values of carbon dioxide uptake reached 1.5 mg CO_2 m^{-2} s^{-1} (34.1 μmol m^{-2} s^{-1}) during summertime, and soil decomposition resulted in net carbon dioxide loss during wintertime. The agricultural region sequestered 134 gC m^{-2} in 1997, 146 gC m^{-2} in 1998, and 92 gC m^{-2} in 1999. The grassland sequestered 86 gC m^{-2} in 1999 and 247 gC m^{-2} in 2000. The year-round NEE values are comparable with results from boreal environment, temperate croplands or in some cases with results from temperate deciduous forests. More scientific data are needed to understand the behaviour of the ecosystem and to constrain the results.

Chapter 1

Introduction

Water vapor and carbon dioxide are the main atmospheric constituents controlling the Earth's climate. The atmospheric content of water vapor, which is the most important greenhouse gas, is not influenced *directly* by human activity. The atmospheric content of carbon dioxide, which has been increasing since the beginning of the industrial revolution from ∼280 ppm in 1800, to almost 370 ppm today (Fig. 1.1), is influenced by human activity (Schimel, 1995; Barnola et al., 1995; Etheridge et al., 1996; World Data Center for Greenhouse Gases website, 2001; Carbon Dioxide Information Analysis Center website, 2001). This CO_2 increase may enhance the greenhouse effect of the atmosphere generating global climatic change (IPCC, 1996; Matyasovszky et al., 1999; Bartholy et al., 2001; IPCC website, 2001). The global transport of carbon (partly in the form of CO_2) among the large reservoirs (Fig. 1.2) is called the *global carbon cycle*. Carbon dioxide emitted into the atmosphere together with the uptake by the terrestrial sinks and oceans governs the carbon dioxide content observed by the global sampling networks. Currently 40-60% of the anthropogenically released carbon dioxide remains in the atmosphere. Our current knowledge is ambiguous whether the rest of the CO_2 is being detached by oceans or by terrestrial sinks (soil or vegetation) (Baldocchi et al., 1996).

During the last decade several scientists (e.g. Keeling et al., 1989; Tans et al., 1989, 1990; Enting and Mansbridge, 1991; Musselman and Fox, 1991; Tans, 1991; Quay et al., 1992; Sarmiento and Sundquist, 1992; Siegenthaler and Sarmiento, 1993; Sundquist, 1993; Conway et al., 1994; Dixon et al., 1994; Hesshaimer et al., 1994; Ciais et al., 1995ab; Denning et al., 1995; Keeling et al.,

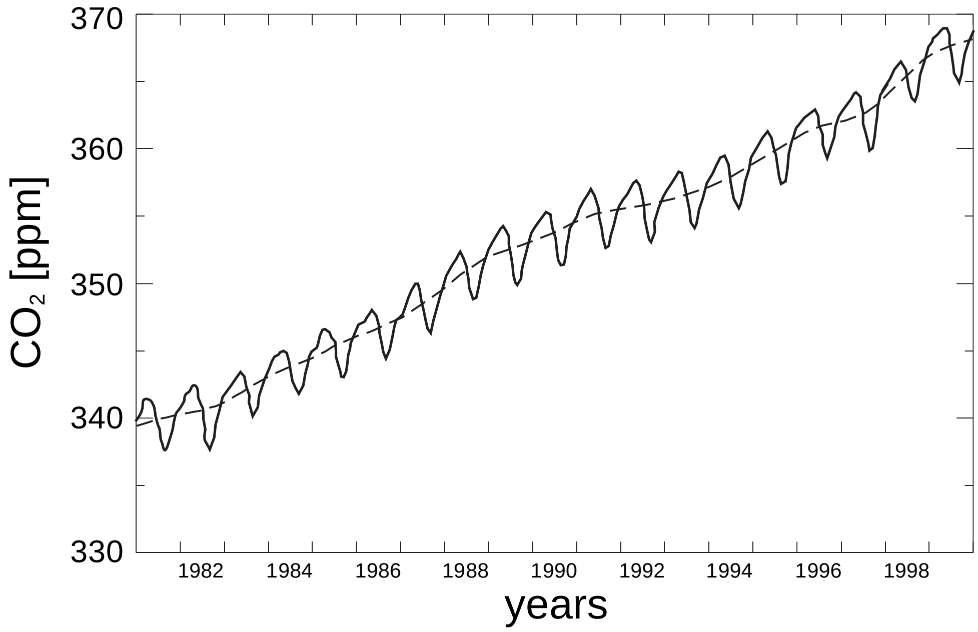

Figure 1.1: The global average atmospheric carbon dioxide mixing ratio (solid line) and the long term trend of the growth (dashed line) between 1981 and 1999 (NOAA CMDL website, 2000).

1996; Taguchi, 1996), based on measurements and model calculations, concluded that there should be a large CO_2 sink in the Northern Hemisphere to balance the observed global carbon budget. Some of these papers suggests that this "missing sink" (~1.4 Gt carbon/year after Schimel, 1995) must be the terrestrial biosphere in the northern temperate latitudes. The 3D atmospheric transport models used for global carbon cycle studies are using CO_2 concentration time series measured by the global sampling network (Tans et al., 1996) as input data. The sources or sinks are inferred from the generally small horizontal concentration gradients of CO_2 measured by the existing sparse measuring network. Thus locating, characterizing and quantifying the "missing sink" requires additional, very high precision CO_2 measurements in the relevant geographical regions (Tans, 1991; Wofsy et al., 1993). In addition to the continuous, long-term monitoring of the CO_2 mixing ratio (see Haszpra, 1995; Haszpra, 1999a,b regarding the Hungarian measurements), the better constrain of the models also requires continuous, long-term measurements of the vertical concentration distribution and that of the atmosphere/biosphere CO_2 exchange. The measurement of atmosphere/biosphere exchange of carbon dioxide can be used to determine the annual net ecosystem

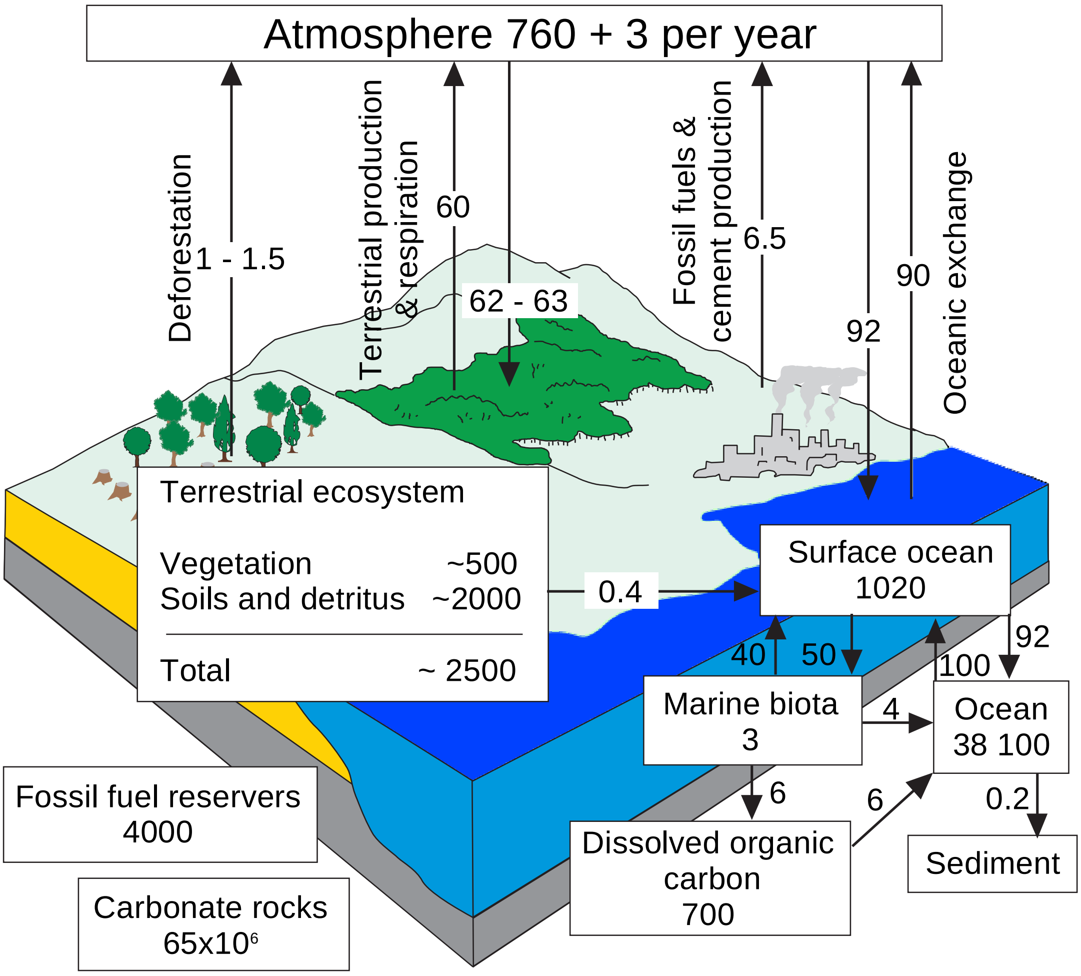

Figure 1.2: Schematic diagram of the global carbon cycle during the 1990's. The carbon content of the reservoirs (shown in boxes) are given in 10^{15} gC, the fluxes are given in 10^{15} gC/year (10^{15} gC = 1 Gt C). The atmospheric content is increasing by 3 GtC per year (Bolin et al., 1997; Schimel et al., 1996, Jogh Grace website).

exchange (NEE) and to examine biophysical processes that control carbon release or uptake by the vegetation (Tans et al., 1996).

As the environmental conditions significantly influence how much CO_2 is absorbed or released by the terrestrial ecosystems, the short term, expedition-like measurements are unable to catch up their environment/climate dependent behaviour (Baldocchi et al., 1996). Direct and long term carbon flux measurements are needed in order to clarify the role of different regions situated under different climatic conditions, and to investigate the behaviour of the different ecological systems. For this purpose a network of tower-based eddy covariance (EC) measurements has been established in Europe (EUROFLUX), North America (AmeriFlux), and is growing globally (FLUXNET website, 2001).

Hungary is located in the northern temperate zone, in the middle of the European continent. The model of Fung et al. (1987), based on satellite data, already suggested that the region might play important role in the global carbon budget, or at least in the generation of the seasonal variation of the atmospheric CO_2 mixing ratio. To contribute to the better definition of the "missing sink" it was decided that, in the framework of a U.S.-Hungarian scientific cooperation, a long-term monitoring site would be established in Hungary.

Since most of the studies concentrate on woodlands or other single species (e.g. Wofsy et al., 1993; Vermetten et al., 1994; Valentini et al., 1995, 1996, 2000; Grace et al., 1995, 1996; Black et al., 1996; Baldocchi et al., 1996, 1997; Grelle and Lindroth, 1996; Greco and Baldocchi, 1996; Hensen et al., 1997; Hollinger et al., 1998; Lindroth et al., 1998; Saigusa et al., 1998; Anthoni et al., 1999; Yamamoto et al., 1999; Baldocchi et al., 2000; Aubinet et al., 2000; Markkanen et al., 2001; see Table 1 in Grelle, 1997), there have been fewer studies conducted over mixed vegetation. Our main goal was to obtain *regionally representative* atmosphere/biosphere flux data and data about the vertical distribution of carbon dioxide in the lower atmosphere. Then the regionally representative, long term carbon budget can be extrapolated to a wider region as long as the soil/vegetation types and the climate forces are similar to those of the region of measurements. In our special case we may try to extrapolate the results to the whole country (with some qualification) to estimate the vegetation's net carbon dioxide budget in Hungary. Without exact measurements of this kind, one can not tell whether the area behaves as a net source or sink of CO_2 in a seasonal or annual scale.

As the main purpose of the study is to obtain regionally representative mixing ratio and flux data, we sought an existing tall tower located as far as possible from direct anthropogenic sources (Bakwin et al., 1995). Considering the possibilities, the television transmitter tower of Hegyhátsál had been chosen for the project.

Funded by the U.S.-Hungarian Scientific and Technological Joint Fund and by the Hungarian National Scientific Research Fund, in cooperation with the NOAA Carbon Cycle Group, measurements of CO_2 mixing ratio profiles and other meteorological elements began at the end of September 1994 (Haszpra, 1999a). Direct flux measurements began in April 1997 at the height of 82 m. The source area (i.e. the region which is actually "seen" by the instrument) of the measured atmosphere/biosphere CO_2 exchange is enhanced as a result of the tower height and it might cover different vegetation types.

Funded by the Agency of Industrial Science and Technology and by the Bilateral Intergovernmental S&T Cooperation, at the end of 1998 the measurements were extended with a new direct flux measuring system developed by the National Institute for Resources and Environment (NIRE, Tsukuba, Japan). The height of this second direct flux measuring system is 3 m. The scale of this measurement is much smaller compared to the 82 m level measurements, thus the results will be representative to the close proximity of the tower. The smaller scale measurements however enables us to detect possible systhematic errors associated with the larger scale measuring system.

The tower is also a NOAA/CMDL global air sampling network site (site code: HUN) (Conway et al., 1994). Air is sampled once per week using glass flasks and the samples are analyzed at NOAA/CMDL for CO_2, CH_4, CO, H_2, N_2O and SF_6, and at the Institute for Arctic and Alpine Research of the University of Colorado for the stable isotopes of C and O in CO_2 (^{*13}C and ^{*18}O) (Trolier et al., 1996).

The main goal of the dissertation is to determine the net ecosystem exchange of CO_2 for the region based on *long term* measurements carried out at Hegyhátsál. Two approaches are used to calculate the atmosphere/biosphere exchange of CO_2 (the profile method and the eddy covariance method), the methodology and applicability of both method is discussed in detail. Methodology and results from the second (Japanese) EC system are also discussed and compared to the regionally representative measurements.

The objective of the dissertation is carbon dioxide balance, thus the tests that ensure the correctness of the calculations are performed based on the CO_2 time series, and the correction routines are developed to ensure the most precise carbon flux calculations possible. For the same reason some tasks are not performed: e.g. the correction of the water vapor flux loss caused by the spectral degradation of the water vapor signal, and the spectral correction of the damaged temperature fluctuation time series. These topics are research areas for possible future workers on the existing huge database.

In the body of the text, the turbulent fluxes of momentum, sensible heat, latent heat and carbon dioxide are reported as positive if directed away from the surface. A positive value for net radiation and photosynthetically active photon flux density indicates a net flux of energy directed to the surface. Negative NEE signifies a net gain of CO_2 by the ecosystem and positive NEE indicates loss of CO_2 by the ecosystem.

UTC+1 h is used systematically in the dissertation as the measure of time during days. This is different from the regular time during the daylight saving time periods.

The dates of the figures demonstrating the spectral analysis were chosen to best demonstrate the overall behaviour of the measuring system. The time mismatch between the figures is intentional. The weekly time periods for data comparison in chapter 3.3 was selected to ensure appropriate data coverage.

The structure of the dissertation is as follows:

In Chapter 2 overview is given about the measuring site, the measurements and the data processing algorithms. The chapter is divided into 4 sections. The first section describes the measuring site. The next section presents the profile measurements together with the data correction routines. The similarity method used for the calculations based on the profile data is discussed in detail. The third section is devoted to the direct flux measurements, the equipment and data processing. The last section briefly describes the second, Japanese EC system.

In Chapter 3 the results of the calculations are shown, the interpretation and error estimates of the results are given. A method is described which can be used to “tweak” the erroneous profile NEE data in order to patch the gaps of the direct measuring system. A new method is introduced which can be used to calculate more reliable carbon dioxide storage profiles below the measuring level. This is important since the net ecosystem exchange of the vegetation, which is located at the surface, can only be determined if one takes into account the rate of change of CO_2 storage in the air layer located below the measuring level.

The last chapter summarizes the results of the dissertation and outlines future plans.

Parts of the material presented here has already appeared in publications (Barcza et al., 1996, 1997, 1999; Haszpra and Barcza, 2001; Haszpra et al., 2001).

Chapter 2

The measurements

In this chapter the measuring system will be described first (2.1). The profile method is introduced in section 2.2, together with the neccessary corrections. A method for calculating turbulent fluxes by means of the similarity theory will be presented. The direct flux measurements carried out at 82 m above the ground will be given in section 2.3. The monitoring system and the calibration will be described in detail. Data processing section is divided into subsections to deal with all the neccessary steps. In the last section (2.4) the Japanese system will be described. Their equipment will be described briefly, then the steps of calibration and data processing will be discussed.

2.1 Measuring site

The measurements are carried out on a 117 m tall (137 m with antenna), free-standing TV and radio transmitter tower at various heights. The tower is owned by Antenna Hungária Corporation. The lower 56 m is a 7.75 m diameter cylinder made of reinforced concrete, while the upper 61 m is a steel cylinder of 1.82 m diameter (Fig. 2.1). As shown in Figure 2.2, the tower is located in a flat region of western Hungary (46^o 57' N, 16^o 39' E), at an altitude of 248 m above sea level. Figure 2.3 shows the land use map of the area. The tower is surrounded by agricultural fields (mostly crops and fodder of annually changing types) and forest patches. The distribution of vegetation types within 10 km of the tower are as follows: 60% arable land, 30% forest and woodland, 10% other (vineyard, settlements, etc.). It is not greatly different from the average for the Western Hun-

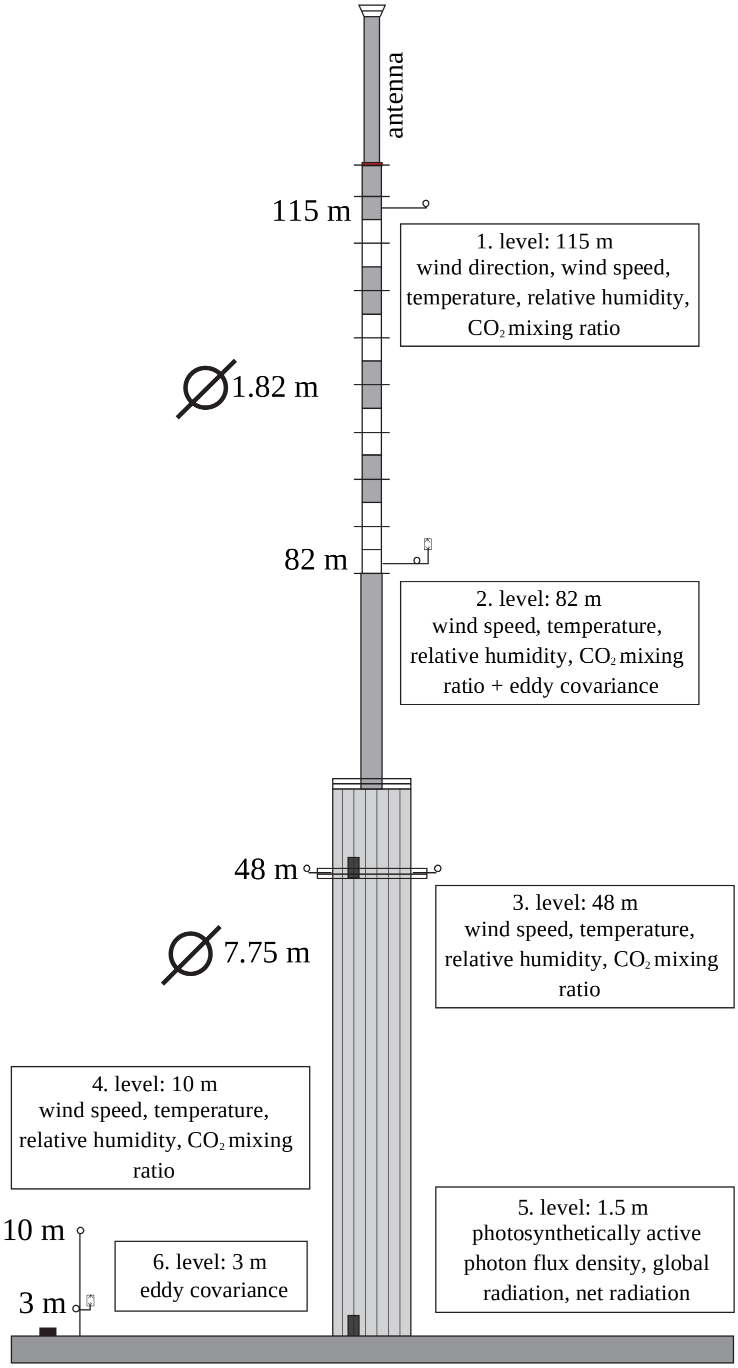

Figure 2.1: The layout of the TV and radio transmitter tower and the instrumentation.

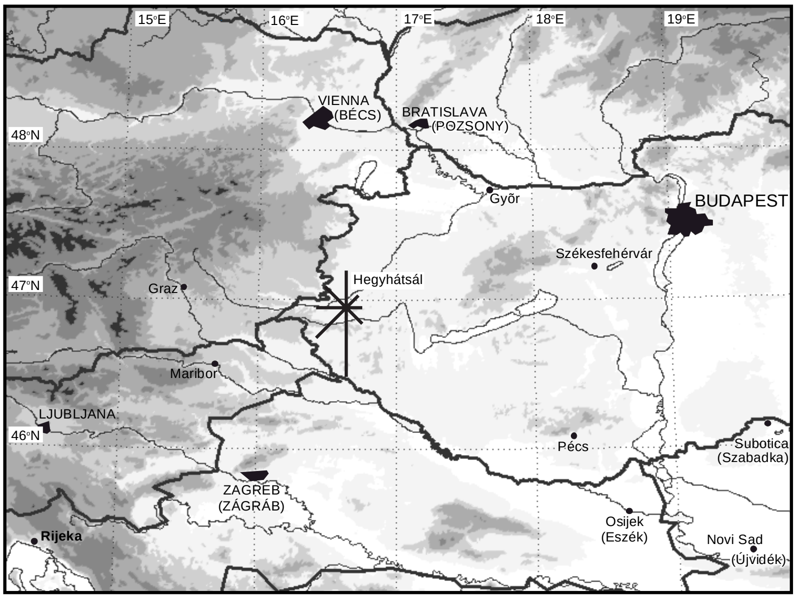

Figure 2.2: Shaded relief map showing the location of the measuring site, and the frequncy distribution of wind direction at Hegyhátsál.

garian Landscape Unit (7,300 km^2) or the whole country (93,000 km^2) (65.5% arable land, 19.5% forest and woodland, 14% other). The soil type in the region of the tower is *"Lessivated brown forest soil"* (Alfisol, according to USDA system). These soils have clay migration and moderate acidity as well as the more widespread humification, leaching and clay formation (Stefanovits, 1971). The upper layer is generally 10-20 cm thick, and its organic matter content is 5-8%.

Human habitations within 10 km of the tower are small villages (100-400 inhabitants). The nearest village is Hegyhátsál (170 inhabitants) about 1 km to the northwest. There is no notable industrial activity in this dominantly agricultural region. Local roads have mostly low levels of traffic. One of the few main roads of the region, which carries 3600 vehicles per day on average, passes approximately 400 m to the southwest of the tower. Yet, the site can be considered as rural in the highly industrialized, densely populated Central Europe.

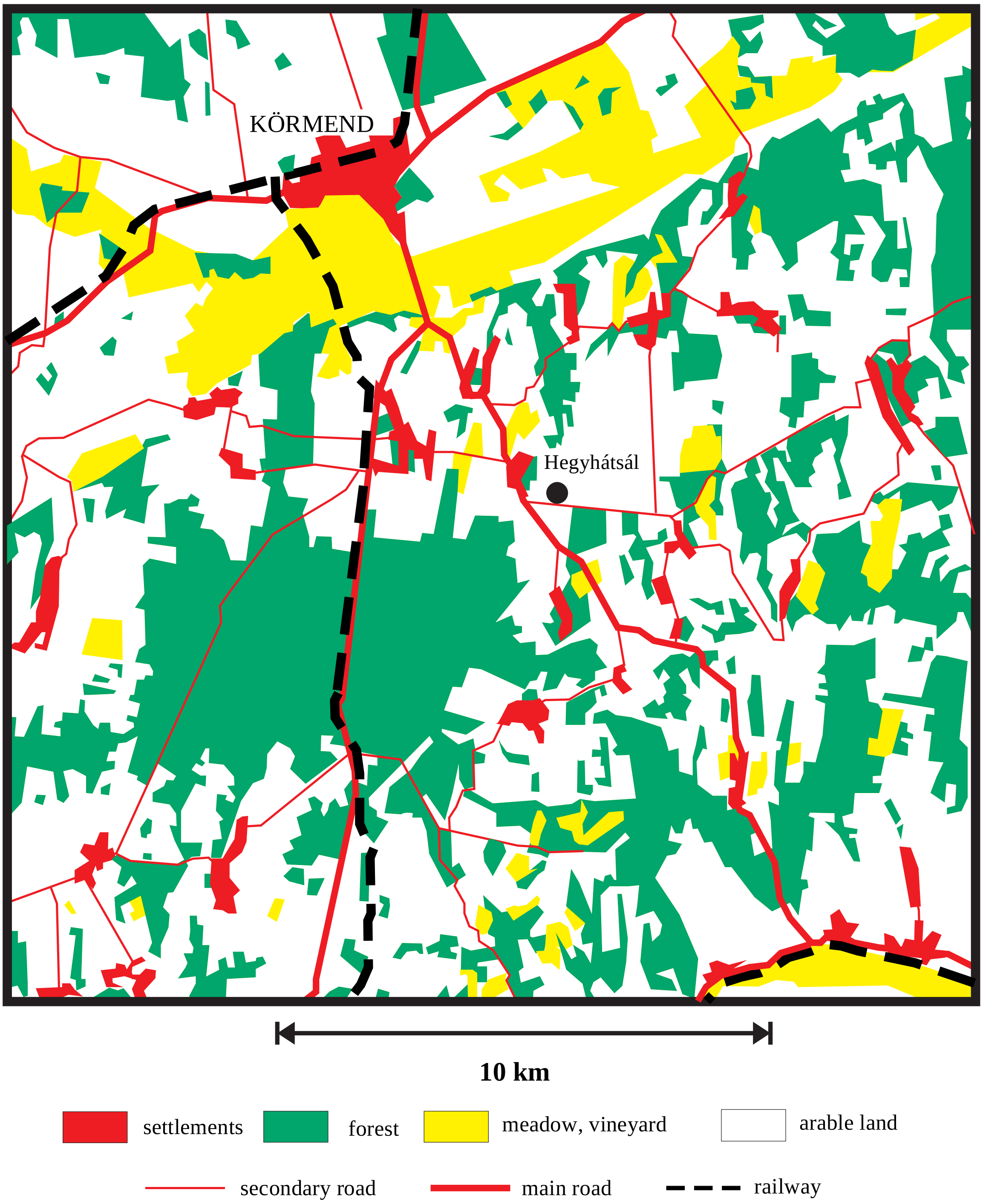

Figure 2.3: Land use map of the surroundings of the measuring site.

2.2 The profile system

2.2.1 Measuring system for the vertical profile of the CO_2 mixing ratio

Measurements of the vertical profiles of CO_2 mixing ratio, temperature, humidity and wind began at the end of September 1994.

Mixing ratios of CO_2 are measured at 10, 48, 82 and 115 m above the ground (Fig. 2.1). Air is pumped through 9.5 mm (outer) diameter tubes to a CO_2 analyzer located in the TV transmitter building. A 47 mm diameter particle filter is located at the inlet of each tube. The set-up for CO_2 analysis is very similar to that described by Zhao et al. (1997a), which was used for the measurements reported in Bakwin et al. (1995, 1998). Diaphragm pumps are used to draw air continuously through each of the tubes from the four monitoring levels at a flow rate of about 2 l min^{-1}. After the pump, the air at 40 kPa overpressure enters a glass trap for liquid water which is cooled in a regular household refrigerator, to dry the air to a dew point of 3-4^{o}C. Liquid water is forced out through an orifice at the bottom of each trap.

The four inlet tubes and the standard gases are connected to a computer controlled, 16-position valve, that selects which monitoring level or standard gas is sampled by the analyzer. The valve head is protected by 7 mm in-line filters. Ambient air flows continuously through the multiport valve so that the system is constantly flushed. The (expensive) standard gases are shut off when not in use by means of computer-controlled solenoid valves. The air leaving the multiport valve through its common outlet is further dried to a dew point of about -25^{o}C by passage through a 182 cm long Nafion drier, so that the water vapor interference and dilution effect are less than 0.1 ppm equivalent CO_2 (Zhao et al., 1997a). The Nafion drier is purged in a counter-flow arrangement using waste sample air that has been further dried by passage through anhydrous $CaSO_4$.

Analysis for CO_2 is carried out using an infrared gas analyzer (IRGA) (LI-COR model LI-6251). A constant sample flow rate of 100 cm^3 min^{-1} is maintained by a mass flow controller. The reference cell of the CO_2 analyzer is continuously flushed at a flow rate of 5-10 cm^3 min^{-1} with a compressed reference gas of 330-340 ppm CO_2 in air (Messer Hungarogáz). The analyzer is calibrated by four standards covering 330-420 ppm CO_2, that were prepared by NOAA/CMDL

(Kitzis and Zhao, 1999).

The basic measuring cycle is two minutes, consisting of one minute flushing and one minute signal integration. Each one minute average and standard deviation is based on 6-7 measurements. The multiport valve steps through the four monitoring levels in eight minutes. Every 32 minutes, after four 8 minutes measuring cycles, the standard gas with the lowest CO_2 mixing ratio is selected and analyzed for 2 minutes, and we term this measurement a zero. After every sixth cycle (every 202 minutes, that is 4x8 min sampling and 2 min zero five times, and one 4x8 min sampling without the zero) a full four-point calibration is carried out. The reference and sample cells of the CO_2 analyzer are not pressure or temperature controlled. The zero measurements are used to account for any short-term drift of the analyzer due to changes in ambient pressure or temperature. A quadratic response function is fit to each set of calibration gas measurements. The zero offset and response function are linearly interpolated in time to obtain values appropriate to calculate CO_2 mixing ratio from the instrument response.

The off-line postprocessing of the profile data consists of the calculation of the response functions for the CO_2 analyzer and the conversion of the voltage data into physical units. If the change in the response function causes more than 2 ppm change between two consecutive calibrations, the data for the period is rejected. Such periods are rare, and almost always caused by significant change in room temperature. The usual change of the response function is below 0.3 ppm. It should be noted that the drift equally influences all monitoring levels, therefore the relative mixing ratio profile is correct even if the absolute accuracy is temporarily lower than usual. As this type of error is random, the long-term accuracy of the values is close to that of the standards (about 0.1 ppm, Zhao et al., 1997b).

For data acquisition and system control for the CO_2 profiles and meteorological data we use a 286 PC with 1 MByte RAM and a 40 MByte hard disk. The analog signals of the CO_2 analyzer and mass flow controller are read by a multiplexer-A/D converter (PCL-711B). The data acquisition and system control software is written in Turbo Pascal (Borland) and runs under MS DOS 5.0. During the data integration period the computer consecutively reads data from the meteorological sensors at each monitoring level through its serial port (RS232), then it reads the CO_2 analyzer and the mass flow controller through the PCL-

711B card. The profile system generates 5 MByte/month of data which is stored on a floppy diskette after compression. The data are mailed or carried to our laboratory in Budapest, where data corrections and data processing are performed.

2.2.2 Temperature, humidity, wind and radiation measurements

At the highest monitoring level, 115 m above the ground, wind speed (Vaisala WAA15A), wind direction (Vaisala WAV15A) and air temperature/humidity sensors (Vaisala HMP35D) are mounted along with the air sampling tube at the end of a 4.4 m long instrument arm. The arm projects toward north. The analog signals of the meteorological sensors are digitized by means of a 12 bit A/D converter and are transmitted to the data acquisition computer via an RS232 serial link. Proper shielding of the cables and sensors, as well as digitizing of the signals, are essential to avoid picking up of noise in the long cables, which may be caused by the nearby high power antennas. Grounding is also important to minimize the possibility of damage from lightning.

The meteorological instrumentation at 82 m above the ground is similar, but a wind direction sensor is not installed there. In April 1997 a sonic anemometer was installed at this level for eddy flux measurements (see Section 2.3.2).

At the 48 m level, the flow distortion caused by the large diameter of the tower (7.75 m) makes it impractical to build a mounting arm long enough to avoid its influence on the meteorological instruments. Instead, two 2.5 m long instrument arms were mounted on opposite (north and south) sides of the tower (Fig. 2.4). Anemometers are installed on both arms and a temperature/humidity sensor and air sample inlet tube are mounted only on the north arm. The flow distortion caused by the tower influences both anemometers and can cause wind speed distortion in excess of 35% of the real wind speed (Fig. 2.5). The measured wind speed is corrected based on the theoretical laminar flow pattern around a cylindrical body using wind direction information from the 115 m level. The two components of the horizontal wind speed around a cylindrical body can be written in the cartesian coordinate system as:

$$u = |v_0| \left\{ \cos\varphi_0 \left[1 - \frac{R^2}{r^2} \cos 2\left(\varphi_0 - \varphi\right) \right] - \frac{R^2}{r^2} \sin\varphi_0 \sin 2\left(\varphi_0 - \varphi\right) \right\} , \qquad (2.1)$$

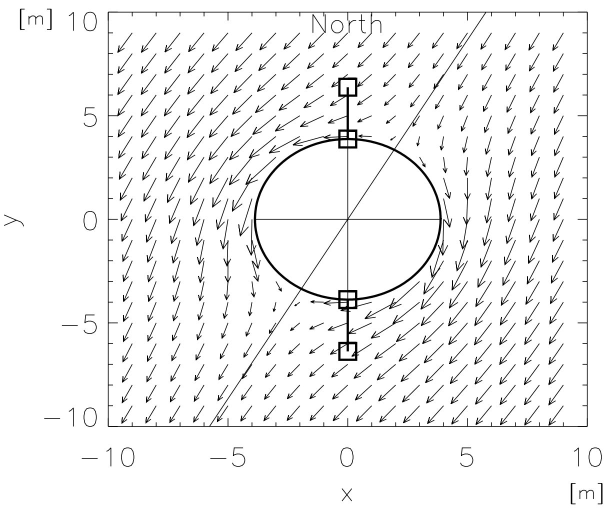

Figure 2.4: Theoretical laminal wind flow pattern around the cylindrical body of the tower in the cartesian coordinate system. The two mounting arms are also indicated. The diameter of the tower is 7.75 m, while the length of the mounting arms is 2.5 m. The length of the arrays are proportional to the wind speed. Wind direction is 30^o.

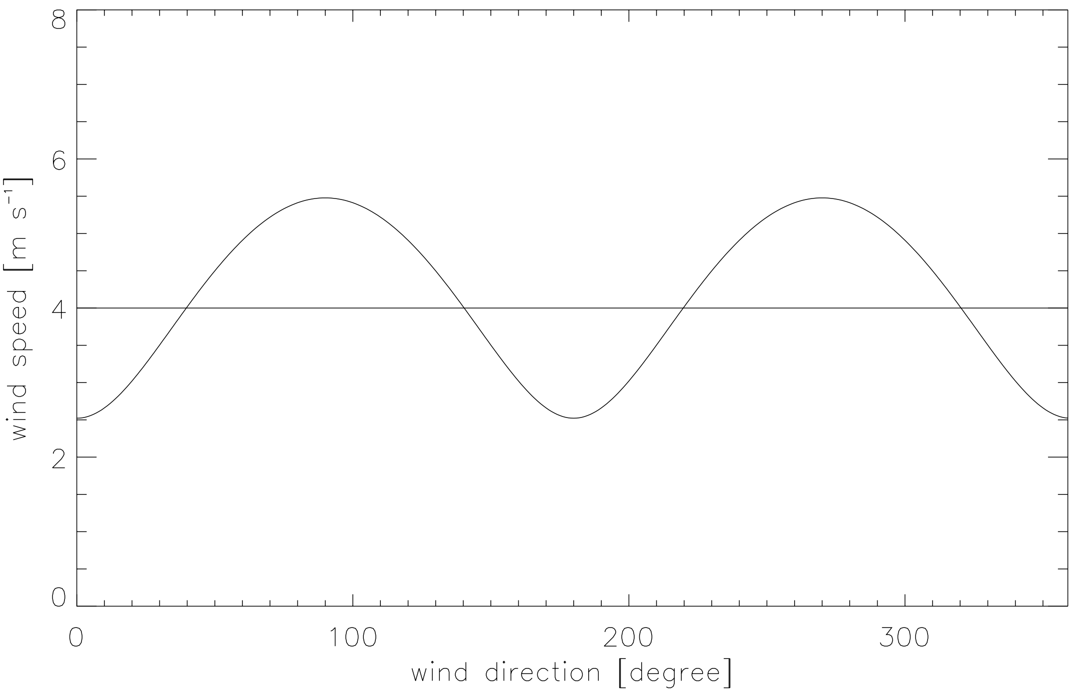

Figure 2.5: Wind direction dependency of the wind vector deflection caused by the tower at 48 m. The undisturbed wind speed was 4 m s^{-1}. The configuration of the mounting arms are shown in fig. 2.4.

$$v = |v_0| \left\{ \sin\varphi_0 \left[1 - \frac{R^2}{r^2} \cos 2\left(\varphi_0 - \varphi\right) \right] + \frac{R^2}{r^2} \cos\varphi_0 \sin 2\left(\varphi_0 - \varphi\right) \right\} , \qquad (2.2)$$

where v_0 is the undisturbed wind speed, φ_0 is the angle of the wind vector ($\varphi_0 = 270^o$-wind direction), R is the radius of the cylinder, r and φ are polar coordinates of the point of interest (Nagy, 1989). The cartesian coordinate system's x axis points towards east and y axis points towards north. The meaning of the wind direction corresponds to the meteorological standard.

Tower-induced von Kármán vortices can also distort the average wind vector in the downwind direction, thus only the wind speed value of the anemometer located on the upwind side of the tower is used for the reconstruction of the wind speed value. The reconstruction routine uses the measured u and v to calculate v_0 based on eq. 2.1 and eq. 2.2 as follows:

$$v_0 = \frac{v_{48}}{\sqrt{1 - 2\frac{R^2}{r^2}\cos 2\left(\varphi_0 - \varphi_b\right) + \frac{R^4}{r^4}}} , \qquad (2.3)$$

where v_{48} is the (distorted) wind speed value of the anemometer located upwind and φ_b is the angle of the boom (90^o or 270^o for the northern and southern side anemometer, respectively).

The same procedure is applied at 82 m and at 115 m without the possibility to distinguish between more or less disturbed signal of two anemometers, but the shadow effect of the tower is not so severe here, since the radius of the tower is considerably smaller than at 48 m (see Fig. 2.1).

Figure 2.6 illustrates the corrected and uncorrected wind speed data for six months. Comparing to a theoretical log-linear wind profile (Webb, 1970; Stull, 1988; Weidinger et al., 2000) the corrected data give considerably lower root mean square error than the uncorrected profile and the corrected data exhibits a more realistic wind profile.

In sunny weather, solar heating of the TV tower body may cause overestimates in the air temperature at the 48 m level, when the wind blows from the SW-SE sector. The temperature is corrected based on the assumption that during daytime unstable atmospheric conditions the mean temperature at 48 m should fit the lapse rate determined by the 10 m and 82 m temperature values. Based on Monin-Obukhov similarity, an approximate relationship between the difference in temperature at 10 m and 82 m and the deviation of the 48 m temperature from

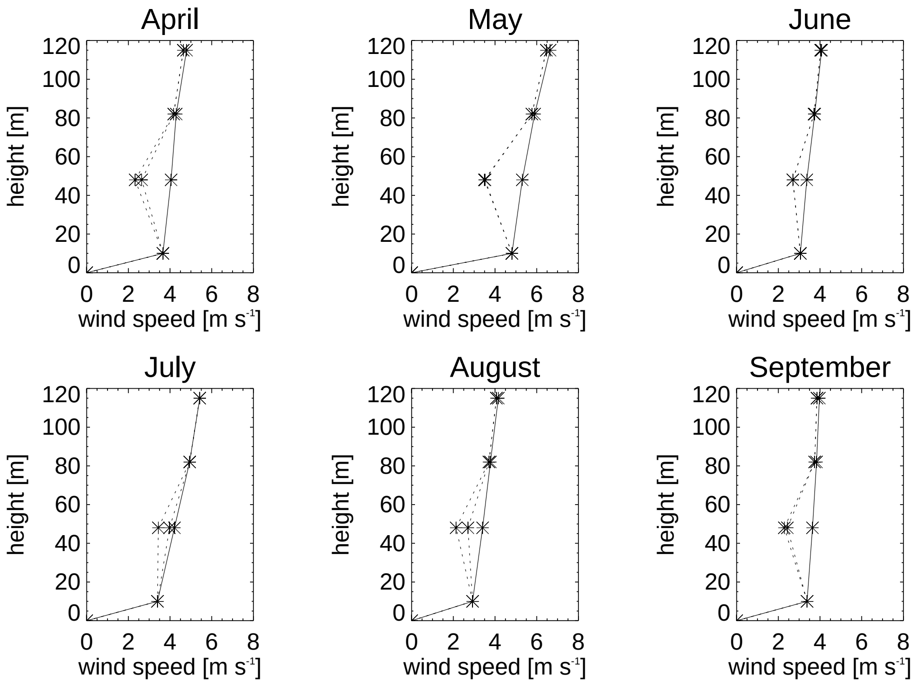

Figure 2.6: Monthly average wind profiles derived from wind speed data measured during daytime for 1997. The dashed lines represent the profiles from the uncorrected data, while the solid line shows the profiles after corrections.

a linear interpolation of temperature with height is:

$$t_{48} \cong t_{10} - (t_{10} - t_{82})\frac{48 - 10}{82 - 10} - 0.3(t_{10} - t_{82})\,. \tag{2.4}$$

The applied correction procedure preserves the variability of the observed temperature time series at 48 m while correcting the smoothed mean value during the critical time periods. The variability (the difference between the smoothed mean value and the measured values) then added to the adjusted mean value to estimate the real temperature value at 48 m.

Figure 2.7 shows the uncorrected and corrected temperature minus the values calculated from 2.4 for three months in 1997. The bias in uncorrected temperature for southerly wind directions is obvious from the figure. As it is expected, the correction has no effect for non-critical wind directions. The figure shows that the undisturbed temperature values are somewhat higher than expected from eq. 2.4, so the correction routine adjust the erroneous values in such a way that the result will exhibit similar behaviour like the correct ones. The humidity sensor measures the relative humidity for its actual environmental condition, therefore

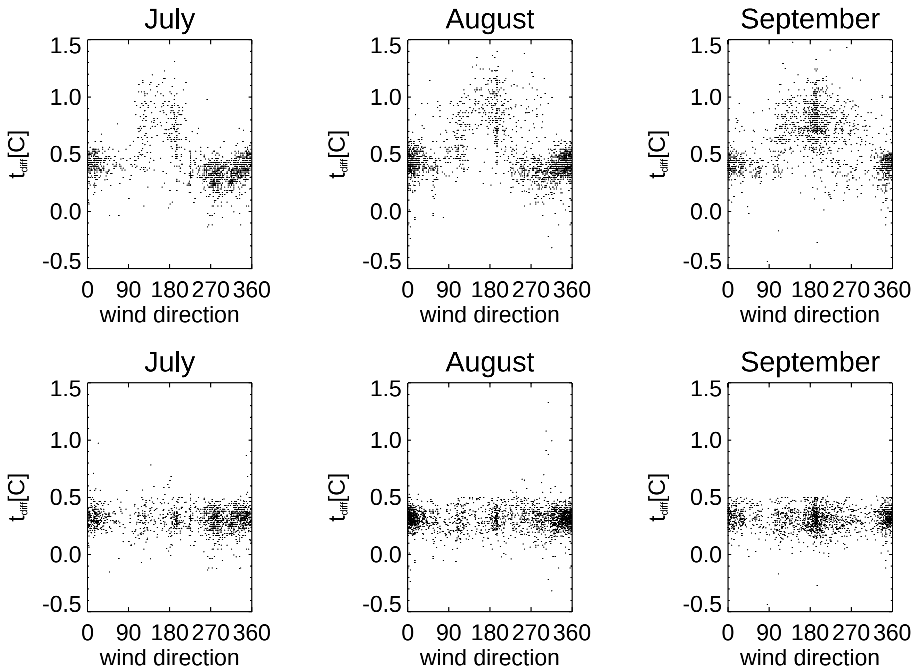

Figure 2.7: The uncorrected and corrected temperature minus the values calculated from eq. 2.4 (t_{diff}) for three months in 1997. Upper plots: uncorrected data; lower plots: corrected data.

the measured (uncorrected) temperature is used for calculation of the absolute humidity.

Relative humidity also needs correction since the Vaisala sensors may suffer from zero and span drift. Since span drift can not be recognized easily (L. Haszpra, personal communication), efforts were done to correct for the effect of zero shift. This was attained by substracting a specific value from the relative humidity data determined from long term data selecting saturated (i.e. foggy) conditions. Thus the corrected data can not exceed 100%.

For measurements at 10 m above the ground, a mast was erected about 70 m from the transmitter building and tower. Wind speed, temperature, and humidity sensors are the same as the ones mounted at the tower. Instruments for radiation measurements are mounted at 2 m height on the mast, including a global solar radiation sensor (Kipp & Zonen model CM2), a radiation balance sensor (REBS model Q*6) and a photosynthetically active photon flux density (PPFD) sensor (LI-COR model LI-190SZ Quantum Sensor). Sensors for soil temperature and soil heat flux (Campbell Scientific model HFT-3) have been installed recently near the mast.

2.2.3 Fluxes calculated by means of the similarity theory

The system was designed to enable us to calculate vertical flux of carbon dioxide from the long term profile measurements. The critical evaluation of the accuracy with which the fluxes can be determined will be given later.

Estimates of the vertical mass transport of CO_2 and other scalars at the surface can be obtained by using surface layer (the lowest 10% of the planetary boundary layer) similarity theory (e.g., see Dyer and Hicks, 1970; Businger et al., 1971; Foken and Skeib, 1983; Businger, 1986; Stull, 1988; Yagüe and Cano, 1994; Saigusa et al., 1998; Hensen et al., 1997; Weidinger et al., 2000), if the vertical profiles of wind speed and air temperature are also available. Applicability of the similarity theory has several preconditions (see Foken and Wichura, 1996 for detailed overview). Briefly, the turbulent field must be horizontally homogeneous and stationary with an appropriate homogeneous area up to a distance of approximately $100z$ (where z is the measuring height) around the measuring site.

In our case, the unusually large height differences between the measuring levels cause uncertainty in the estimate of the similarity profiles but also contributes to improved estimates of the (often small) mixing ratio and temperature gradients. Difficulty arises during nighttime stable conditions when we are restricted to use data measured by the two lowest levels (10 m and 48 m) for the estimate of fluxes to ensure that the utilized data reside in the surface layer (Stull, 1988; Yagüe and Cano, 1994). During unstable conditions we use data of the three lowest levels, up to 82 m height. At night, the 82 m level is often above the inversion layer, and so it is completely decoupled from the ground. Also, the precondition of homogeneous fetch is not fulfilled in our case. Consequently, the results acquired from the similarity theory are expexted to have errors.

As there are three measuring levels located inside the surface layer during unstable conditions, the surface layer fluxes can be inferred using profile fitting technique instead of the less precise flux-gradient relationships which utilize data from only two levels.

According to the Monin-Obukhov similarity theory, the non-dimensional wind, temperature, and scalar profiles can be expressed in the horizontally homogeneous and stationary surface layer as:

$$\phi_m(\frac{z}{L}) = \frac{kz}{u_*}\frac{\partial u}{\partial z} , \tag{2.5}$$

$$\phi_h(\frac{z}{L}) = \frac{kz}{\theta_*}\frac{\partial \theta}{\partial z} , \tag{2.6}$$

$$\phi_s(\frac{z}{L}) = \frac{kz}{s_*}\frac{\partial s}{\partial z} , \tag{2.7}$$

or with the integrated forms as :

$$u = \frac{u_*}{k}[\ln \frac{z}{z_0} - \psi_m(\frac{z}{L})] , \tag{2.8}$$

$$\theta - \theta_0 = \frac{\theta_*}{k}[\ln \frac{z}{z_0} - \psi_h(\frac{z}{L})] \tag{2.9}$$

$$s - s_0 = \frac{s_*}{k}[\ln \frac{z}{z_0} - \psi_s(\frac{z}{L})] , \tag{2.10}$$

with

$$\psi_m\left(\frac{z}{L}\right) = \int_{z_0/L}^{z/L} \frac{(1-\phi_m)}{\zeta} d\zeta , \tag{2.11}$$

$$\psi_h\left(\frac{z}{L}\right) = \int_{z_0/L}^{z/L} \frac{(1-\phi_h)}{\zeta} d\zeta , \tag{2.12}$$

$$\psi_s\left(\frac{z}{L}\right) = \int_{z_0/L}^{z/L} \frac{(1-\phi_s)}{\zeta} d\zeta , \tag{2.13}$$

where u, θ and s are mean quantities of horizontal wind speed, potential temperature ($\theta \cong T + 0.0098z$, where T is the absolute temperature) and scalar mixing ratio (e.g. water vapor or any other trace gas) at height z above the zero plane displacement, θ_0 is the surface potential temperature, $k = 0.4$ (Högström, 1996) is the von Kármán constant, z_0 is the roughness length, ϕ_m, ϕ_h and ϕ_s are the dimensionless wind shear, temperature and scalar concentration gradients respectively, u_* is the friction velocity (defined as $\sqrt{|\tau|/\rho}$ with τ is the Reynolds' stress and ρ is the air density), θ_* is the temperature scale ($\theta_* = -\overline{w'\theta'}/u_*$), s_* is the scalar scale ($s_* = -\overline{w's'}/u_*$), $\zeta = z/L$ with L is the Obukhov length:

$$L = \frac{u_*^2\overline{T}}{kg\theta_*} , \tag{2.14}$$

where $\overline{T}$ is the reference absolute temperature for the surface layer (calculated as the average temperature of the surface layer from the temperature profile measurements) and $\zeta = z/L$. Note that the water vapor buoyancy correction is neglected for the calculation of L (Högström, 1988).

It is generally accepted that $\phi_s = \phi_h$ since for both potential temperature and other scalars the turbulent exchange is governed by the same turbulent field thus the physical process of the transport is similar.

The functional forms of ϕ_m and ϕ_h are determined by field measurements (Högström, 1988). Due to the large scatter of the experimental data many different functions can be found in the literature (e.g. Dyer, 1970; Businger et al., 1971; Foken and Skeib, 1983; Högström, 1988, 1996; Weidinger et al., 2000). For our purposes the revised similarity functions of Högström (1996) are used, which are best fits to large quantities of experimental data. For unstable situations these are as follows:

$$\phi_m = (1 - 19\frac{z}{L})^{-1/4} , \tag{2.15}$$

$$\phi_h = 0.95(1 - 11.6\frac{z}{L})^{-1/2} , \tag{2.16}$$

and for stable situations:

$$\phi_m = 1 + 5.3\frac{z}{L} , \tag{2.17}$$

$$\phi_h = 0.95 + 8\frac{z}{L} . \tag{2.18}$$

Functions ψ_m and ψ_h are as follows for unstable conditions ($L < 0$) after Benoit (1977):

$$\psi_m = \ln\left[\left(\frac{1+x}{2}\right)^2\left(\frac{1+x^2}{2}\right)\right] - 2\arctan(x) + \frac{\pi}{2} , \tag{2.19}$$

$$\psi_h = 2\ln\left[\frac{1+y}{2}\right] , \tag{2.20}$$

where $x = (1 - 19z/L)^{1/4}$ and $y = (1 - 11.6z/L)^{1/2}$.

For stable conditions ($L > 0$):

$$\psi_m = -5.3\frac{z - z_0}{L} , \tag{2.21}$$

$$\psi_h = 0.05\ln\frac{z}{z_0} - 8\frac{z - z_0}{L} . \tag{2.22}$$

Note that ψ_h=ψ_s since $\phi_s = \phi_h$.

Before the application of the profile fitting technique, wind direction dependent roughness length (z_0) is determined dividing the wind directions into 120 sectors (analogous to the wind direction classification of the eddy covariance system, see chapter 2.3.4.3). The idea behind the calculation method is that surface layer fluxes can also be inferred from measurements taken at only two levels using flux-gradient relationships instead of the more precise flux-profile method. Flux-gradient relationships do not utilize z_0 since during the iteration the values of u_* and θ_* are determined from two level's data thus z_0 is rejected (e.g. considering eq. 2.8 for two different levels and substracting them will lead to an equation which does not contain z_0). After u_* and L had been determined eq. 2.8 can be used to determine z_0 for a specific height, wind direction and wind speed:

$$z_0 = z \exp\left[-\frac{uk}{u_*} - \psi_m\left(\frac{z}{L}\right)\right] . \tag{2.23}$$

Values of z_0 are determined from the long term profile measurements classified by wind direction. Data measured during unstable atmospheric conditions are used, utilizing wind speed data from 48 m and 10 m. The calculated z_0 values are averaged in 3 degree intervals of the wind direction. Because of the huge scatter of data, only one average z_0 is used in each sector through the years. The average roughness length is 0.15 m, the minimum value is 0.06 m, and the maximum is 0.24 m.

For zero plane displacement $d = 0.7$ m is used considering that the measuring tower is surrounded by arable land presumably with low vegetation. It should be noted that the calculations are not sensitive to the choice of d since the measuring levels are located relatively high above the vegetation (Weidinger et al., 2000).

The algorithm of calculation is as follows.

First the bulk Richardson number is determined based on data measured by the two lowest level (Yagüe and Cano, 1994; Stull, 1988):

$$Ri \cong \frac{g}{\theta_0} \frac{(\theta_2 - \theta_1)(z_2 - z_1)}{(u_2 - u_1)^2} , \tag{2.24}$$

where g is the acceleration due to gravity, subscript 2 indicates level 2 (48 m), and subscript 1 indicates level 1 (10 m).

Then, it is determined whether the situation was stable or unstable based on the potential temperature profile. This could be decided based on the bulk Richardson number, but the temperature profile may differ from the theoretical, strictly monotonous change with height especially during the morning transition period from stable to unstable stratification, thus at higher altitudes (e.g. at 82 m) the temperature value may not fit the lapse rate determined by the two lowest level. Also, during daytime, well-mixed conditions, the temperature profile is close to the dry adiabatic lapse rate (0.0098 K m^{-1}), which means that small fluctuations of the average temperature at one level can cause deviations from the strictly monotonous profiles.

Next, initial Obukhov length is estimated which is required to start the iteration.

If the conditions are unstable $L_{initial}$ is calculated based on the definition of the Obukhov length (eq. 2.14) fitting to pure logarithmic profiles for a neutral atmosphere:

$$u = \frac{u_*}{k} \ln \frac{z}{z_0} \,, \tag{2.25}$$

$$\theta - \theta_0 = \frac{\theta_*}{k} \ln \frac{z}{z_0} \,. \tag{2.26}$$

u_* is determined in the following manner. The applied procedure, which is widely used during the entire procedure, fits the paired data $\{x = \frac{1}{k} \ln \frac{z}{z_0}, y = u\}$ to the linear model, $y = ax$, by minimizing the Chi-square error statistics which is computed as the sum of squared errors divided by the standard deviations. The intercept of the line is forced to be zero because at height $z = z_0$ the wind speed theoretically becomes zero. The slope of the fitted line (a) then gives u_*. For the similar determination of θ_* the surface value θ_0 is also neccessary. The latter is determined using interval bisector technique for fast convergence. The technique fits many lines during the iteration for many different θ_0 using the method described above storing the Chi-square error statistics for each fit. Then the surface value will be the value with the smallest Chi-square error. θ_* is calculated in the same way as u_* since the temperature difference profile $(\theta - \theta_0)$ is already known. $L_{initial}$ is estimated substituting u_* and θ_* into eq. 2.14.

During stable conditions, $L_{initial}$ is estimated from the bulk Richardson number (Yagüe and Cano, 1993) using Businger's similarity function (Businger, 1971):

$$F(Ri) = \frac{9.4Ri - 0.74 + \sqrt{4.88Ri + 0.5476}}{9.5 - 44.18Ri} \tag{2.27}$$

and

$$L_{initial} = \frac{z_2 - z_1}{\ln \frac{z_2}{z_1} F(Ri)} \,. \tag{2.28}$$

Iteration is starting with the $L_{initial}$ value, using the least squares fit technique described above to obtain θ_0, u_* and θ_* using equations 2.8 and 2.9 to determine the x and y values for the line fitting (instead of eq. 2.25 and 2.26). Again, the intercepts of the fitted lines are forced to be zero, and the slopes of the lines determine u_* and θ_*. A new L is calculated in each step from the new u_* and θ_* values. As it was mentioned in the beginning of this chapter, for unstable conditions data measured by the lowest 3 levels are utilized for the fitting (10 m, 48 m and 82 m), and for stable conditions data measured by the two lowest levels are used to ensure that only data measured inside the surface layer is used.

The iterative method consists of comparing the new L with the previously calculated one. Iteration finishes when the difference between two consecutive L values is less then 1% of the current Obukhov length, or after 30 iteration steps.

During stable conditions the iteration can fail, due the strong stability. If this is the case, the analytical solution of Lee (1997) is used if the bulk Richardson number is less than 0.2. In other cases turbulence is supressed or tends to be intermittent, so the similarity theory is no longer applicable. The formulae of Lee is the following:

$$\frac{z}{L} = \frac{\frac{z}{z-z_0} \ln\left(\frac{z}{z_0}\right)\left[-2\frac{\beta}{R}Ri + 1 - \sqrt{1 + \frac{4\beta(1-R)Ri}{R^2}}\right]}{2\frac{\beta}{R}\left(\beta Ri - 1\right)} \,, \tag{2.29}$$

where the constants $\beta = 5.3$ and $R = 0.95$ are determined according to the similarity functions of Högström (1996) used here. z is the geometrical height between the two lowest measuring levels defined as $z = \sqrt{z_1 z_2}$.

In case of successful iteration or analytical solution, the water vapor dry air mixing ratio (q, given in g/kg dry air) and carbon dioxide dry air mixing ratio (c, given in ppm, which is equivalent with μmol/mol dry air) profiles are used to estimate q_* and c_* with the line fitting method described above using eq. 2.10.

Finally, the scales are converted to usual physical fluxes:

$$\tau = \rho u_*^2 \,, \tag{2.30}$$

$$H = -\rho c_{pd} \theta_* u_* \,, \tag{2.31}$$

$$LE = -\rho L_v \frac{1}{1000} q_* u_* \,, \tag{2.32}$$

$$F_{cp} = -\rho \frac{M_{CO_2}}{M_d} c_* u_* \,, \tag{2.33}$$

where τ is the momentum flux (or Reynolds' stress in kg m^{-1} s^{-2}), H is the sensible heat flux (in W m^{-2}), LE is the latent heat flux (the energy flux equivalent of the vertical mass transfer of water vapor in W m^{-2}), F_{cp} is the CO_2 flux (in mg m^{-2} s^{-1}), ρ is the density of air, c_{pd} is the specific heat of dry air, L_v is the latent heat of vaporization (in J kg^{-1}), M_{CO_2} is the molar weight of carbon dioxide and M_d is the molar weight of dry air (in kg mol^{-1}).

Since profile measurements are performed in every 8 or 10 minutes (see section 2.2.1), the fluxes calculated from each available individual measurement are averaged to 60 minutes.

Figure 2.8 shows one week of profile data together with some meteorological elements.

2.3 The direct flux measuring system

2.3.1 Introduction

As it was proposed by Baldocchi et al. (1996), direct and long term carbon dioxide flux measurmements are needed to clarify the role of the different ecosystems located under different climatic conditions in the global carbon cycle. Current advances in micrometeorology allow us to conduct long term uninterrupted turbulence measurements (AmeriFlux, EUROFLUX, AsiaFlux and others, see the FLUXNET website, 2001, e.g. Wofsy et al., 1993; Vermetten et al., 1994; Valentini et al., 1995, 1996, 2000; Grace et al., 1995, 1996; Black et al., 1996; Baldocchi et al., 1996, 1997; Grelle and Lindroth, 1996; Goulden et al., 1996; Greco and Baldocchi, 1996; Hensen et al., 1997; Grelle, 1997; Aurela et al., 1998; Hollinger et al., 1998; Lindroth et al., 1998; Saigusa et al., 1998; Anthoni et al., 1999; Yamamoto et al., 1999; Malhi et al., 1999; Yi et al., 2000; Baldocchi et al., 2000; Aubinet et al., 2000; Markkanen et al., 2001) even during conditions when the classical assumptions for turbulent flux measurements are not fulfilled (McMillen, 1988; Grelle and Lindroth, 1996; Moncrieff et al., 1997).

Therefore, a measuring system for the flux estimation by means of the eddy

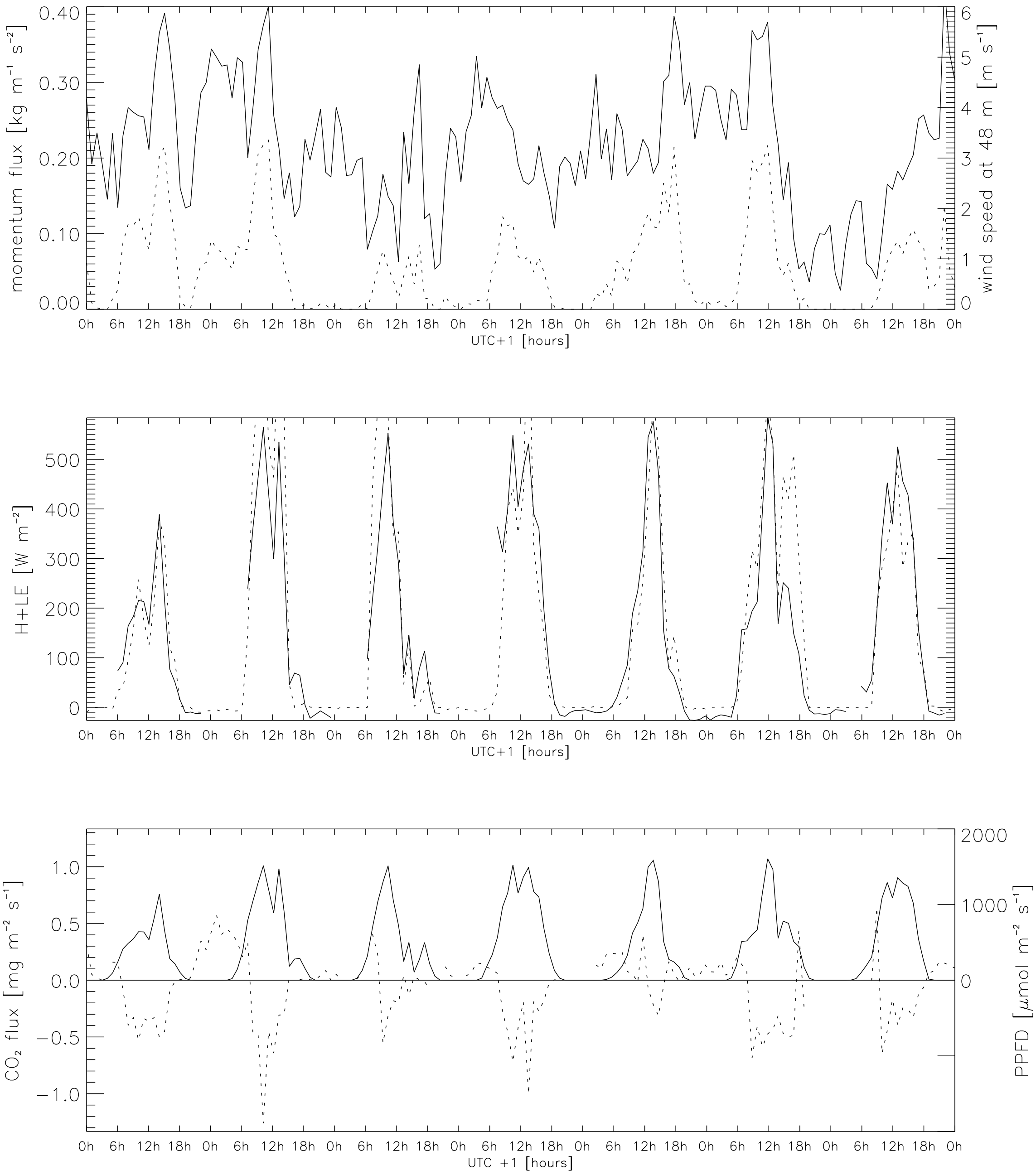

Figure 2.8: One week of profile flux data (11-17 July, 1997) together with some meteorological elements. Upper plot: average wind speed measured at 48 m (solid line) and the momentum flux (dashed line). Middle plot: The net radiation (solid line) and the sum of sensible and latent heat flux (dashed line). Lower plot: photosynthetically active photon flux density (PPFD, solid line), and the CO_2 flux (dashed line).

covariance (EC) method was also installed on the tower. The system was put into operation in April, 1997.

The height for the turbulence sensors was chosen to satisfy the few requirements: the measurement should be representative to a larger region (regional scale), so the sensors are supposed to be mounted as high as possible, but still low enough to be inside the surface layer during unstable conditions, which is approximated as the lower 10% of the height of the convective boundary layer (100-150 m). Because of further technical reasons the height was chosen to be 82 m.

The region and the method would let us determine fluxes representative to a single species (e.g. agricultural crops) using data selection based on source area models (Schmid, 1994, 1997), but the strategy applied is to determine net ecosystem exchange which is representative to the whole region with mixed vegetation. Thus the ensemble fluxes will reveal the carbon exchange of a region with mixed vegetation and therefore the net value gives us a chance to extend the validity of the calculations to a larger region, of course with critical evaluation.

2.3.2 The monitoring system

Measurements of the vertical flux of CO_2, H_2O, momentum and sensible heat by eddy covariance at 82 m above the ground was facilitated by mounting an ultrasonic anemometer (Gill Solent Enhanced), an aspirated thermocouple (50 cm from the anemometer) for fast-response temperature measurements, and an additional air sampling tube for CO_2 and H_2O measurements to the 4.4 m long instrument arm. The measuring system was developed and operated by László Haszpra (Hungarian Meteorological Service).

Measurements of CO_2 and H_2O are made at $\sim$4 Hz using a fast response IRGA (LI-COR model LI-6262). Air is pumped through the 115 m long sampling tube and the analyzer at about 15 l min^{-1}, producing a pressure drop of approximately 45 kPa. Pressure fluctuations generated by the pump are damped by means of a 6 l buffer volume. Immediately behind the sample cell of the analyzer we measure pressure (MKS Instruments model 122A barotron), temperature and relative humidity (Vaisala HMD20YB). The pressure and temperature data are used to correct the instrument response for variations in these parameters (see below). The humidity data are used to determine the calibration function for water vapor measurements by the LI-COR 6262 IRGA.

The CO_2 analyzer runs in relative mode. Dry, synthetic air with a CO_2 mixing ratio of 330-340 ppm is used as a reference gas (Messer Hungarogáz) during the measurements. The flow rate is 5-10 cm^3 min^{-1} through the reference cell of the IRGA. The analog output of the analyzer for CO_2 and H_2O, as well as the signals of the pressure and temperature/humidity sensors are digitalized by the common A/D-RS232 converter.

A separate data acquisition computer (486 PC with a 40 MHz CPU, 4 MByte RAM, 1 GByte HD) is used to read data from the fast-response instruments (sonic anemometer, thermocouple, and IRGA). The computer communicates with the instruments through two standard serial ports: COM1 receives the data from the sonic anemometer while the two A/D-RS232 devices are controlled via COM2. The data acquisition cycle is triggered by the signal from the sonic anemometer. After reception of a data package (horizontal and vertical wind speed, wind direction and error code) the computer requests data from the aspirated thermocouple, the CO_2/H_2O analyzer and its accessory sensors (pressure, temperature/humidity), and the CO_2 profile analyzer. The position of the multiport valve of the profile system is also determined, which allows synchronization between the two independent data acquisition computers. The data acquisition software is written in Turbo Pascal language and runs under DOS 5.0. The eddy covariance system produces data at a rate of about 600 MByte/month, and the data are stored on a CD-R without compression.

Data coverage from the beginning of the EC measurement (end of April, 1997) until the failure of the IRGA (which caused data loss from the beginnig of 2000) was around 85%. After data screening it reduced to 78%. The average data coverage for the FLUXnet community is 69% (Falge et al., 2001).

2.3.3 Calibration

The response of the IRGA is calibrated by comparison to ambient CO_2 and H_2O measurements from the slow-response sensors, similar to the method of Berger et al. (2001) (i.e. no calibration gases are used in the fast response system). A calibrated CO_2 measurement is typically obtained every 8 minutes at the 82 m level. Exact synchronization of the signals requires accounting for the time for air to pass through the sampling tubes of the profile and the eddy systems.

The lag time of the profile system is calculated from the measured flow rates and from *in situ* tests. The lag time for the profiling system was around 3 minutes.

It is very important to keep track of the lag times since these values are also used during the calculation of the lagged covariances, which appear to be very sensitive for the lag times in some cases. For the eddy covariance system two different lag time values are calculated for H_2O and CO_2 (Moncrieff et al., 1997) using a spectral method. First, the daily lag time values are calculated without any restrictions for the whole dataset. Then a polynomial is fitted to the long-term lag time series which is used to determine the actual time window where the lag time is supposed to occur. The time window used is 16 sec around the fitted value. Lagged covariances inside this window are used for the following procedure.

The usual method is to calculate the lag times for each averaging period to search for the time where the maximum correlation occurs (Fan et al., 1990). It appears however, that this is not always a plausible method. Figure 2.9 shows the normalized lagged covariances for one day. The solid lines in the lower part of the figure shows detectable peaks which correspond to the lag time for CO_2 during daytime. The nighttime sharper peaks in the upper part mark the same lag time as the daytime values, which means that the lag time is quite constant during one day, and it is possible to determine one average daily lag time value. It should be noted that this method is only applicable if the pump is expected to produce an approximately constant flow rate, which is the case in our system. Especially during nighttime when turbulence is suppressed or the turbulent transport is small, the lagged covariances do not always show detectable peaks. It can be seen in figure 2.9 that in some cases the maximum covariance occurs a few seconds away from the real lag time value. Moreover, as it is indicated by the arrow, sometimes the correct lag time occurs at the minimum covariance. As a consequence, individual lag times for CO_2 are determined by finding the maximum covariance inside a very small (1 s) time window around the daily average value. The small window ensures that the appropriate lag time will be determied even if the covariance has its minimum around the daily average.

The method described above for CO_2 is not always applicable for H_2O. The nighttime lag values are usually undetectable since latent heat flux is very small during this period (see fig. 2.9). The daytime (positive) covariances does not exhibit the same behaviour as CO_2 does in many cases, and it appears that

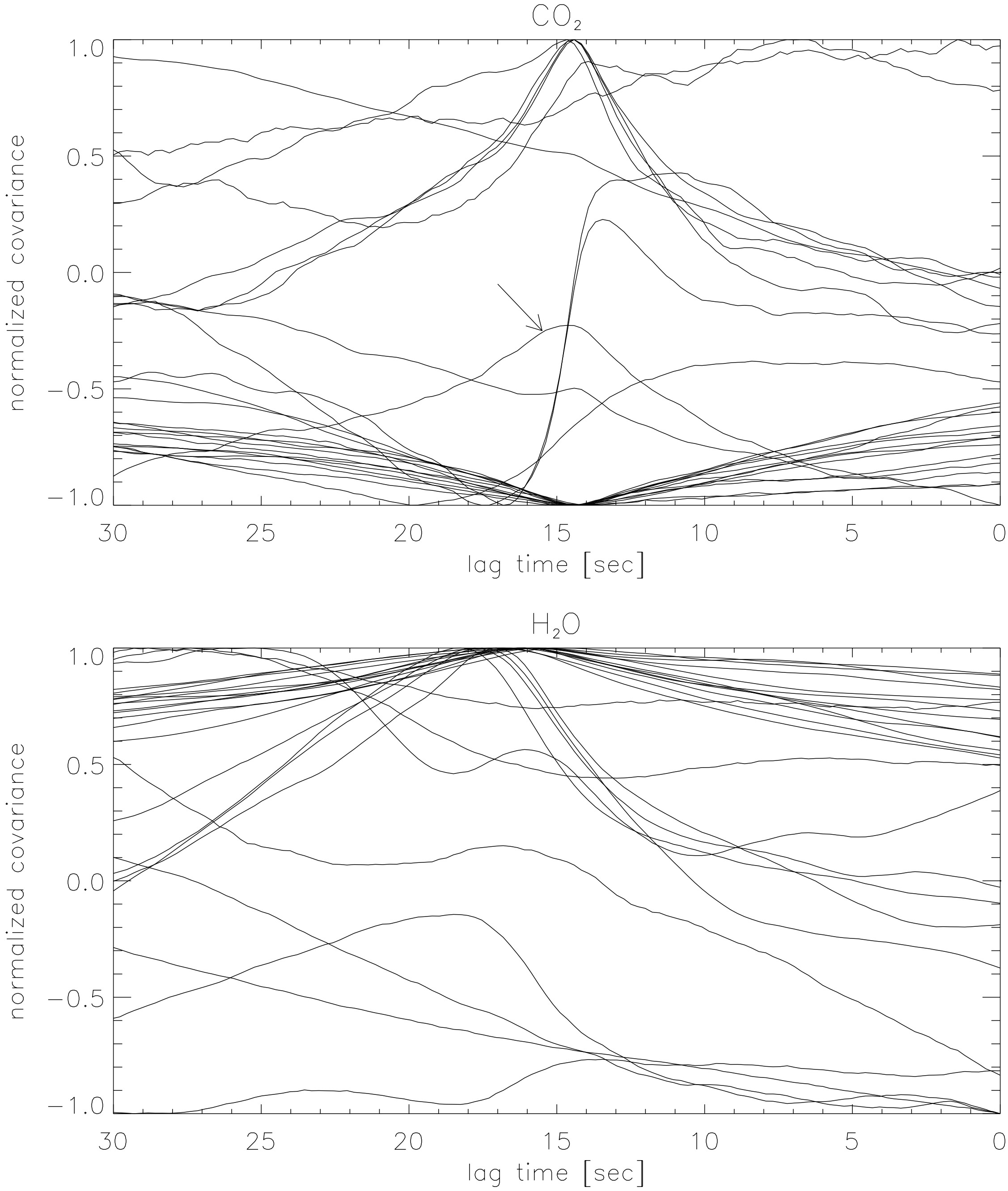

Figure 2.9: Normalized lagged covariances for carbon dioxide (upper plot) and water vapor (lower plot) as functions of the lag time for one day (23 June, 1998). Carbon dioxide flux is typically negative and largest (in absolute sense), while water vapor flux is positive and largest during daytime, hence the best detectable peaks are expected to occur during daytime. The lagged covariance function indicated by the arrow in the upper plot is an example to prove that in some cases the lag time does not occur at the maximum covariance while a detectable peak does occur.

during many days it is not possible to determine the average daily value. For this reason, based on long term experience, the lag times for H_2O are calculated as the lag time for CO_2 plus 2.5 sec. It should be noted that the day presented in figure 2.9 is an optimal day for the determination of the H_2O lag times.

The built-in clocks of the data acquisition computers (see sections 2.2.1 and 2.3.2) appeared to shift with respect to each other. This shift could be tracked since the eddy covariance system monitors the state of the multiport valve of the profile system, and the changes in the valve state are tied to specific time stamps of the profile computer.

Once the correct synchronization is performed, the calibration can take place. We use the following function for calibration (LI-COR, 1996):

$$f\left(V\frac{p_0}{p}\right)\frac{T}{T_0}+c_r=c\,, \tag{2.34}$$

where V is the voltage signal (CO_2 or H_2O) of the IRGA, p and T is the pressure and temperature inside the measuring cell, respectively, p_0 and T_0 are arbitrary reference values for temperature and pressure, which are used to normalize the pressure and temperature (T_0 = 273.15 K and p_0 = 1000 hPa is used here), c_r is the mole fraction of CO_2 or H_2O in the reference gas (zero for H_2O, 330-340 μmol mol^{-1} for CO_2) and c is the mole fraction of water vapor or carbon dioxide measured by the slow reference system. The analyzer is calibrated in terms of H_2O and CO_2 mole fraction as it is recommended by the manufacturer (McDermitt et al., 1993).

Eq. 2.34 can be rewritten as:

$$f\left(V\frac{p_0}{p}\right)=(c-c_r)\frac{T_0}{T}\,. \tag{2.35}$$

Linear regression is carried out between $(C-C_r)\,T_0/T$ and Vp_0/p to determine the slope and intercept of the response function, f. V, p and T are determined as 20 sec averages of the signals selected based on the synchronization of the data acquisition computers.

The detailed calibration procedure for H_2O and CO_2 are as follows. First, saturated water vapor pressure is calculated inside the measuring cell from data measured by the Vaisala sensor located immediately behind the measuring cell:

$$e_s = 6.108 \cdot 10^{\frac{7.5(T-273.15)}{235+T-273.15}}, \tag{2.36}$$

where e_s is given in hPa. Next, calibrated H_2O and CO_2 mole fraction is calculated as follows:

$$q = \frac{rh}{100}\frac{e_s}{p}1000\,, \tag{2.37}$$

$$c = \frac{c_{82}}{1 + \frac{q_d}{1000}} \tag{2.38}$$

with

$$q_d = q\left(1 - \frac{q}{1000}\right)\,, \tag{2.39}$$

where q is the mole fraction of water vapor (given in mmol mol^{-1}), c is the mole fraction of carbon dioxide (in μmol mol^{-1}), and q_d is the dry air mole fraction of water wapour (given in mmol/mol dry air), rh is the relative humidity that is also measured by the Vaisala sensor, c_{82} is the CO_2 mixing ratio at 82 m measured by the profiling system. It should be noted that since the air sampled by the profiling system is dried (see section 2.2.1), the resulting CO_2 data are expressed in terms of dry air mole fraction. Mole fraction, however, is defined as the mole number of the considered gas divided by the mole number of the complete gas mix (with water vapor), while dry air mole fraction is defined as the mole number of the gas divided by the mole number of the dry air. Equation 2.38 calculates "regular" mole fraction based on the dry air mole fraction measured by the slow system.

The next step is the application of the linear approximation for H_2O and CO_2 based on eq. 2.35:

$$m_q V_q \frac{p_0}{p} + b_q = q\frac{T_0}{T} \tag{2.40}$$

and

$$m_c V_c \frac{p_0}{p} + b_c = (c - c_r)\frac{T_0}{T} \tag{2.41}$$

where m_q, b_q, m_c and b_c are the slope and intercept of the lines determined by linear regression for water wapour and carbon dioxide, respectively.

Figure 2.10 shows the fit for a typical day. Since most of the variance is contained in the measured voltage signal it is extremely important to determine the correct slope of the fits (Berger et al., 2001). Using linear regression, occasional

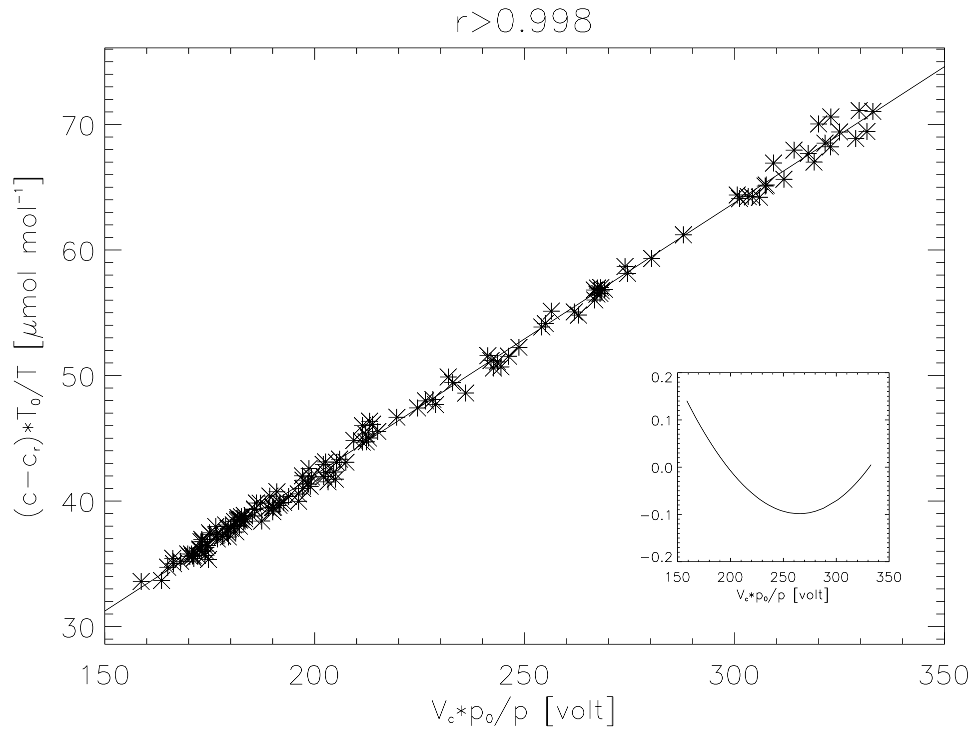

Figure 2.10: Typical daily calibration function for CO_2 (17 June, 1997). The correlation coefficient (r) was very close to unity. Inset graph: the difference between the 5th order polynomial supplied by the IRGA manufacturer and the linear approximation. As it is obvious from the figure, the linear approximation can be used instead of the 5th order polynomial.

outliers can result in a poor fit due to an undesired sensitivity to outlying data, thus they are removed interactively, and the resulting linear fits typically show very high correlation.

The manufacturer provides a fifth order polynomial calibration curve for the instrument (LI-COR, 1996), but the polynomial differs only slightly from linear in the range of interest (360-500 ppm) as shown by the inset graph in Fig. 2.10. Calibration values are determined for each 24 hours of measurement. The calibration factors are quite stable in time.

The calibration can be verified with plotting the daily CO_2 time series determined from the fast response system together with the CO_2 data at 82 m determined from the profiling system.

2.3.4 Data processing

Eddy covariance technique is used to calculate flux densities of momentum, sensible heat, water vapor and CO_2 by measuring the mean covariance between vertical velocity and the other quantity in question. The method is based on the Navier-Stokes equations of motion, after application of Reynolds' averaging procedure. The vertical flux density of one quantity with density ρ thus has the form: $F = \overline{w'\rho'}$. The advantage of the method is that the values inferred by the profile method (u_*, $\overline{w'\theta'}$ and $\overline{w's'}$, see section 2.2.3 for abbreviations) can be measured directly. Turbulent fluctuations are determined from the differences between the instantaneous and mean quantities.

Eddy covariance provides a more accurate way to determine vertical fluxes compared to the fluxes calculated by means of the semi-empirical similarity theory. It is extremely important to take care of the quality of the measurement and the data processing since errors (most seriously selective systematic errors) can cause serious bias in the integrated, long term net ecosystem exchange (Moncrieff et al., 1996). The main reason for the complicated data correction and quality control described below is to minimize the error term in the measurement.

2.3.4.1 Averaging time

The appropriate averaging time to be used can be determined by the use of an ogive function (Foken and Wichura, 1996). This function is defined as the cumulative integral of the cospectra beginning with the highest frequencies. The cospectra of scalar A and B is defined as follows: let F_A and F_B be the discrete Fourier transform of the simultaneously measured scalars A and B, respectively. Let $F_A = F_{Ar} + F_{Ai}$ and $F_B = F_{Br} + F_{Bi}$, where subscripts r and i denote real and imaginary parts of the discrete Fourier transform, respectively. The cospectrum is defined as

$$Co = F_{Ar}F_{Br} + F_{Ai}F_{Bi} \tag{2.42}$$

(Stull, 1988). It is important to note that the sum over frequency of all cospectral amplitudes, Co, equals the covariance between A and B. The ogive function has a form of

$$Og_{\overline{A'B'}} = \int_{\infty}^{n_0} Co_{\overline{A'B'}}(n)\, dn\ , \tag{2.43}$$

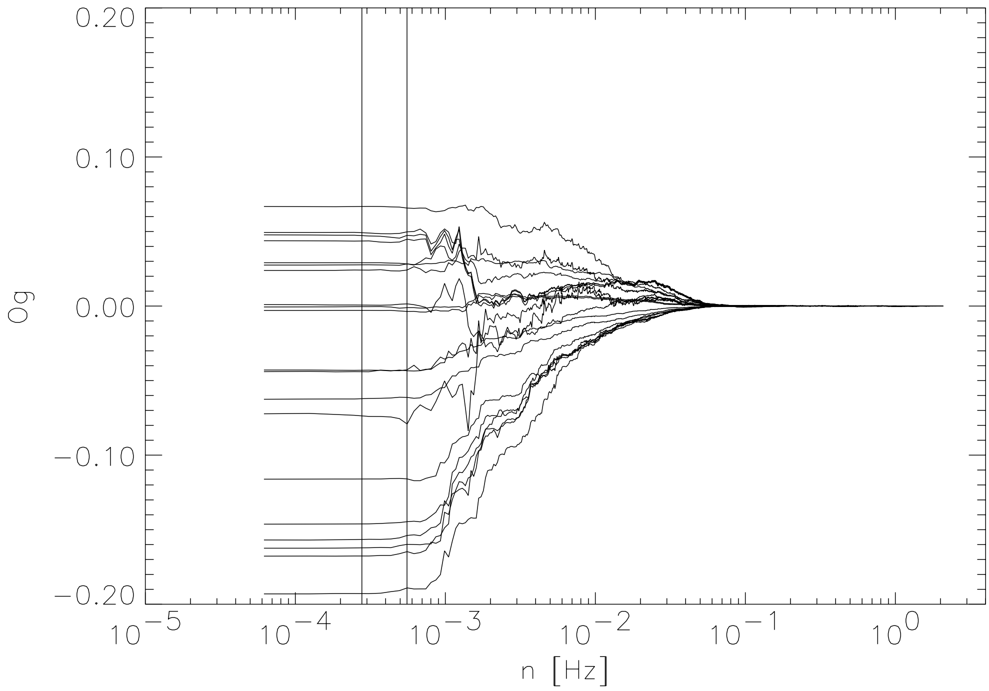

Figure 2.11: Carbon dioxide ogives (Og) based on 4.5 h periods, during 5 August, 1997. The vertical lines correspond to time periods of 1 and 0.5 h.

for any scalar flux $\overline{A'B'}$, where n denotes natural frequency and n_0 is the lowest frequency contributing to the integral. This ogive function converges to a constant value at a frequency which could be converted to the averaging time.

Figure 2.11 shows the ogive functions for one day based on continuous 4.5 hours long time series. It can be seen that 0.5 hours averaging time is neary appropriate, but for precision 60 minutes averaging time was chosen to determine turbulent fluxes. We should note that closer to the surface 30 min averaging time is widely used in micrometeorology. Since turbulent scales become larger if we move away from the surface, a longer averaging time is required to resolve the low frequency part of the fluctuations which contributes to the turbulent transport. Also, the ogives show that 4 Hz sampling frequency is more than enough to resolve the high frequency scales contributing to the turbulent transport at the height of the measurement.

2.3.4.2 Data preparation

For the calculation of the turbulent fluxes in question continuous 60 min time series are needed. Time series of wind speed are constructed directly from the sonic anemometer data (the computer stores information from the fast response sensors in 10 min long files). Time series of temperature fluctuations are constructed directly from the data measued by the aspirated thermocouple. As it was described in section 2.3.2, the data acquisition computer of the vertical flux monitoring system stores raw voltage data for CO_2 and H_2O together with physical quantities of pressure, temperature and humidity measured by the slow sensors immediately behind the sampling cell of the IRGA. Based on the calibration procedure described in section 2.3.3, the calibration constants for CO_2 and H_2O are utilized during this step.

After construction of the 60 min raw voltage time series, the voltage values are converted into physical quantities. Based on the equations and notations presented in the description of the calibration, water vapor mole fraction is calculated as follows:

$$q = \left(m_q V_q \frac{p_0}{p} + b_q \right) \frac{T}{T_0} \,. \tag{2.44}$$

Dry air mixing ratio of water vapor, r_q is calcualted as

$$r_q = \frac{q}{1 - \frac{q}{1000}} \frac{M_{H_2O}}{M_d} + c_{rq} \,, \tag{2.45}$$

where M_{H_2O} and M_d are the molecular weights of water vapor and dry air, respectively, and r_q is given in g H_2O/kg dry air.

The mole fraction of carbon dioxide can be calculated similarly:

$$c = \left(m_c V_c \frac{p_0}{p} + b_c \right) \frac{T}{T_0} + c_{rc} \,, \tag{2.46}$$

where c_{rc} is the mole fraction of CO_2 in the reference gas, and the result is given in μmol mol^{-1}. For the calculation of the dry air mixing ratio of carbon dioxide r_c, the mole fraction of water vapor has to be taken into account:

$$r_c = \frac{c}{1 - \frac{q}{10^3} - \frac{c}{10^6}} \frac{M_{CO_2}}{M_d} \,, \tag{2.47}$$

where r_c is given in mg CO_2/kg dry air. Division with 10^3 and 10^6 in the denominator is neccessary to calculate the mixing ratios in mol/mol, since q is given in mmol/mol and c is given in μmol/mol.

2.3.4.3 Wind vector rotation / mean vertical wind speed

Three dimensional wind vector rotation is applied to the sonic anemometer data following the method of Lee (1998). A general assumption for micrometeorological measurements is the zero mean vertical wind speed. Generally, zero mean average vertical wind speed is forced as part of the wind vector rotation routine (e.g. McMillen, 1988). Lee proposes that this may be a good assumption very close to the ground, but it is generally invalid at higher altitudes. The non-zero mean vertical velocity is caused by local thermal circulations, topographically modified flow, divergence in convective cell-like structures or synoptic scale subsidence. The non-zero mean vertical wind speed transports heat, water vapor and carbon dioxide across the plane of the actual measuring height, while this transport is undetectable by the eddy covariance system, which is based on the measurement of the fluctuating signals. Focusing on carbon dioxide, this transport can be severe during nighttime, when carbon dioxide usually accumulating below the inversion layer causing high vertical gradients of CO_2 near the ground. As an example, a mean vertical velocity of 5 cm s^{-1} at the measuring height causes -100 W m^2 equivalent energy flux for daytime (or an uncertainty of about 20% of the observed net radiation).

As it is stated in Lee (1999), it is not appropriate to use the mean vertical wind speed measured by the sonic anemometer because of the low signal level, the possible sensor tilt and the aerodynamic shadow of the sensor or the tower. As it is proposed by Lee, the true mean vertical velocity can be approximated from the following equation:

$$\widehat{w} = \overline{w} + a(\phi) + b(\phi)\,\widehat{u}, \tag{2.48}$$

where $\widehat{u}$ and $\widehat{w}$ are the measured mean horizontal and vertical velocities in the coordinate system defined by the instrument, respectively, $\overline{w}$ is the true mean vertical velocity, and a and b are the wind direction (ϕ) dependent coefficients. Since $\overline{w}$ behaves in a random fashion, the long term data can be used to evaluate a and b with least absolute deviation method. Lee (1999) recommends the least squares method, but the "robust" least absolute deviation method seems to be more appropriate, since the use of the Chi-square error statistics applied in the least squares method can result in a poor fit to the data due to an undesired sensitivity to outlying data.

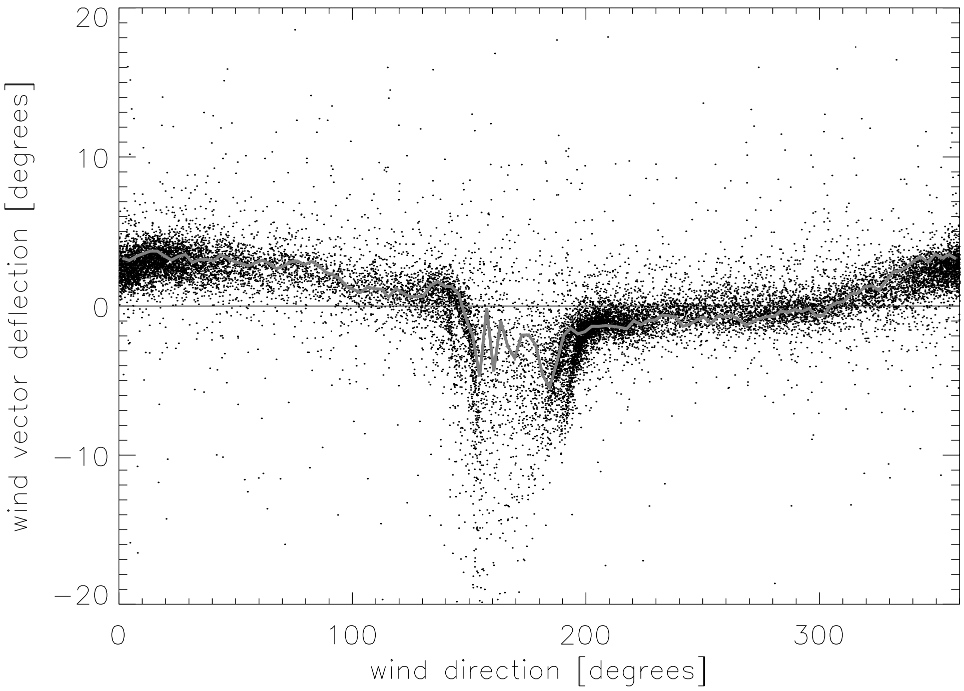

Figure 2.12: The wind direction dependent deflection of the hourly average wind speed during the whole measurement period. The solid grey line represents the angle of the average deflection determined for each 3^o intervals. The effect of the tower is clear between 140^o and 190^o.

Values of a and b are determined as functions of ϕ in 3^o intervals using data from a previous complete run on the existing database. Once the coefficients are determined, eq. 2.48 can be used to determine to calculate $\overline{w}$ for each run. Horizontal rotation is applied to the wind speed data such that $\overline{v}$ is forced to zero. Next, the coordinate system is rotated to ensure that the mean vertical wind speed is equal to the one calculated using eq. 2.48. The rotated wind data is used to calculate turbulent fluxes and other statistics. The true average vertical wind speed is finally stored for each hourly period. The standard deviation of the lateral wind speed fluctuations (that is v after coordinate system rotation) together with the wind direction are also stored in order to be able to calculate turbulent flux source areas in the future.

Figure 2.12 shows the deflection of the average three dimensional wind vector in the coordinate system defined by the instrument. The plot was constructed using all available EC data. The solid grey line represents the b values (see eq. 2.48) for each 3^o intervals calculated using the least absolute deviation method.

The effect of the tower body is clear from the figure between wind direction 140^o and 190^o. There is a sinusoidal behaviour outside this region which is caused by a slight tilt of the instrument. This tilt is compensated using the above method proposed by Lee (1998).

The application of the mean vertical velocity in the calculation of the net ecosystem exchange will be discussed later.

2.3.4.4 Trend removal

As it was mentioned earlier, turbulent fluxes are calculated from the fluctuations of the time series considered. Fluctuations are calculated as deviations from a specific mean value. There are several methods found in the literature to calculate mean values such as recursive digital filters, spectral high-pass filters, running mean or box-car averages and linear trend removal technique (McMillen, 1988; Denholm-Price and Rees, 1998). Some of the methods (e.g. recursive digital filtering) are used in real-time data processing systems. Since data processing takes place off-line in our case, a more sophisticated trend removal technique is possible.

Other advantage of trend removal is that the effect of a complex terrain or a slight non-stationarity can be addressed partially with this method (McMillen, 1988; Grelle and Lindroth, 1996; Moncrieff et al., 1997; Weidinger et al., 1999), while these problems can not be addressed easily in the flux-profile calculations.

Sensitivity tests had been performed to choose the most adequate trend removal technique. In the beginnig, moving average trend removal was applied since this is one of the most popular techniques. Based on the result of the sensitivity test derived from data of three randomly selected days, 1000 sec time window seemed to be appropriate for trend removal (three days may seem to be less than enough for the test, but we should note that sensitivity tests are heavily computational time consuming). 1000 sec is the upper limit of the time constants generally used in measuring systems located lower in the surface layer (McMillen, 1988). It is important to note that the moving average tred removal technique causes spectral energy to be redistributed in an undesirable fashion (see Fig. 3. in Denholm-Price and Rees, 1998), which needs further spectral corrections. The neccessary power spectal transfer function can be found in Kaimal et al. (1968).

As more powerful computers became available for data processing, a more

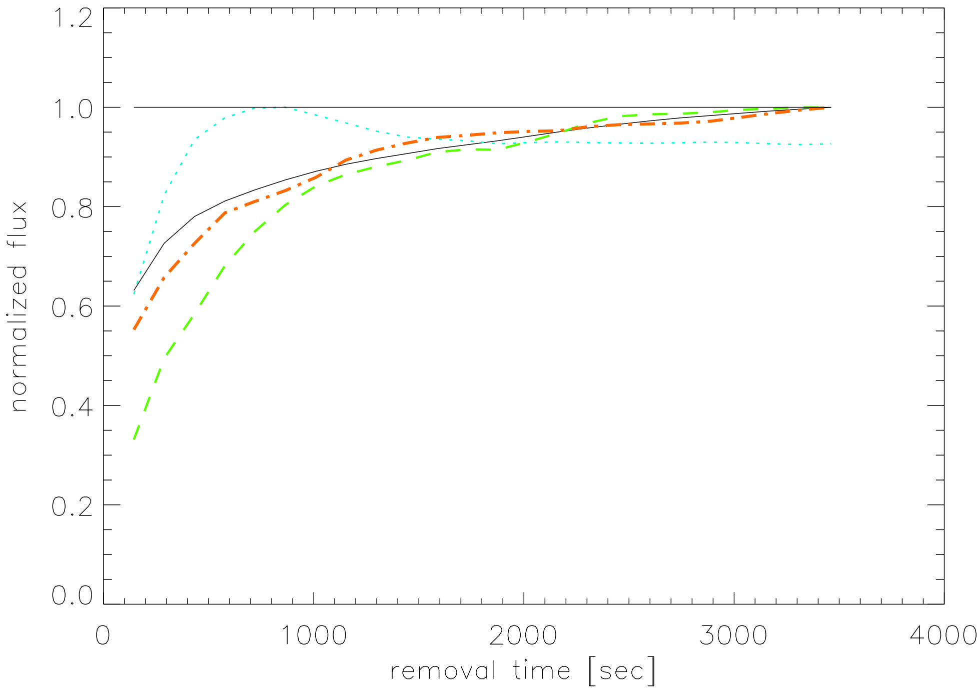

Figure 2.13: Dependence of the normalized mean covariances on the mean removal time applied during the moving average trend removal procedure. The figure represents average data of the daily averages for the 30 days selected. Solid line is the momentum flux, dotted line is the temperature flux, dashed line is the latent heat flux and dashed-dotted line is the carbon dioxide flux. The unusual behaviour of the temperature flux foreshadows the errors associated with the temperature fluctuation measurement.

mature sensitivity test was performed. Based on data of 30 randomly selected days it became clear that 1000 sec time window is too small to get accurate fluxes. Maximum covariances has been reached using data window of 60 min or longer (Figure 2.13), thus it seemed reasonable to change the trend removal method to a simpler linear trend removal method. This method also seemed to be the most appropriate for eddy flux measurements carried out on very high towers (K. Davis, pers. comm.).

This result is consistent with the large turbulent scales detected with the ogive functions, as it was mentioned in section 2.3.4.1. A shorter time window would cause removal of frequencies that contribute to the turbulent transport. As a result, a linear trend is removed from each 60 min interval of all data used for the eddy flux calculations (wind components, temperature, H_2O and CO_2) to get the fluctuations neccessary for the calculation of the turbulent fluxes.

2.3.4.5 Quality assurence

As part of the quality assurance procedure applied, data values outside 4σ are removed from each hourly time series before the trend removal is performed (Eugster et al., 1997). This despiking procedure uses the same linear trend removal to determine the standard deviation of the dataset. This ensures the homogeneity of the wind speed, temperature, water wapour mixing ratio and carbon dioxide mixing ratio data filtering out the extreme values caused by instrument error, precipitation, moisture or rime.

Spectral analysis is performed as a powerful tool for the quality check of the eddy covariance system and the measuring devices. The ideal turbulent signal has a well defined spectrum which can be approximated with each limited time series. The spectral analysis is performed with standard FFT routine (Stull, 1988; Matyasovszky, 1990).

Figure 2.14 shows the power spectra of horizontal wind speed, vertical wind speed, temperature, water vapor and carbon dioxide mixing ratio as an average of two hourly spectra measured between 12h and 14h UTC+1 in 24 July, 1999. The average horizontal wind speed was 9.5 m s^{-1}.

As natural frequency multiplied with the power spectra itself is plotted against natural frequency and both axes are logarithmic, the power spectra should ideally decrease linearly with a slope of -2/3 in the inertial subrange of the turbulent signal according to Kolmogorov's law (Kaimal et al., 1972). Also, the ideal shape of the power spectra is described in Kaimal et al. (1972). As it is described by Anderson and Verma (1984) and Ohtaki (1985), spectral similarity exists between the spectra of temperature, water vapor and carbon dioxide. This similarity means that the spectral and cospectral curves are similar in the ideal case.

It is evident from figure 2.14 that all power spectra behaves well except the spectra of the temperature fluctuations. As it was mentioned above in the context of the mean removal time calculations (section 2.3.4.4), the temperature fluctuations exhibited an unusual behaviour. Now the damaged power spectra gives the explanation: the thermocouple seems to act as a kind of a high-pass filter. While the inertial subrange follows the -2/3 slope ideally, the lower frequency signal (caused by the larger scale eddies) is damped between 0.001 and 0.1 Hz. This can be caused by the low heat capacity of the reference box of the thermocouple, which means that the box follows the temperature of the air filtering out the low

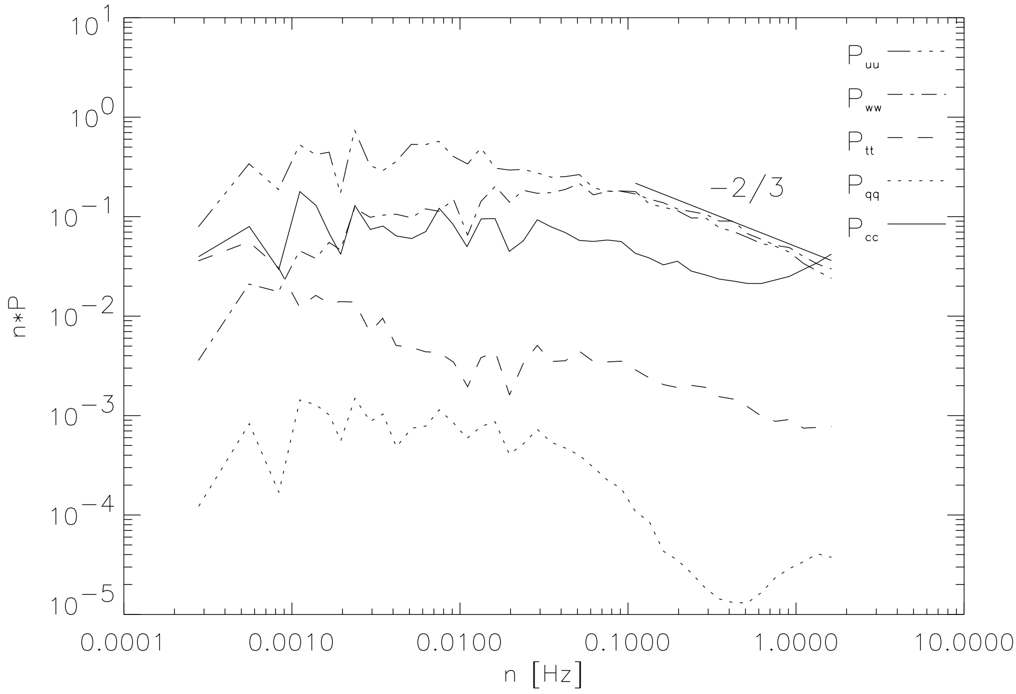

Figure 2.14: Average power spectra (P) of the measured data produced from two hourly spectra in 24 July, 1999 (12h-14h UTC+1). The mean wind speed was 9.5 m s^{-1}. According to Kolmogorov's law (Kaimal et al., 1972), the inertial subrange spectra must follow the -2/3 slope. As spectral similarity is supposed to exist between the power spectra of the temperature, water vapor and carbon dioxide, the temperature spectra is obviously damaged. There is some noise in the high frequency part of the signal measured by the IRGA as it is experienced by several LI-COR 6262 users (e.g. Grelle and Lindroth, 1996).

frequency temperature fluctuations that still contribute to the turbulent flux.

There is some noise in the inertial subrange spectra of water wapour and carbon dioxide at frequencies higher than 0.5 Hz. This noise has a random fashion and should not be correlated with the vertical wind speed. The same behaviour was observed by many scientists working with a LI-COR 6262 instrument (e.g. Grelle and Lindroth, 1996; Eugster et al., 1997).

The water vapor power spectra also exhibits some degradation in the inertial subrange, which is caused by attenuation of fluctuations and possibly by water condensation inside the air inlet tubes (B. Berger, pers. comm.). A methodology to reconstruct a damaged water vapor spectra can be found in Berger et al. (2001).

Figure 2.15 shows the cospectra of vertical wind speed fluctuations with hor-

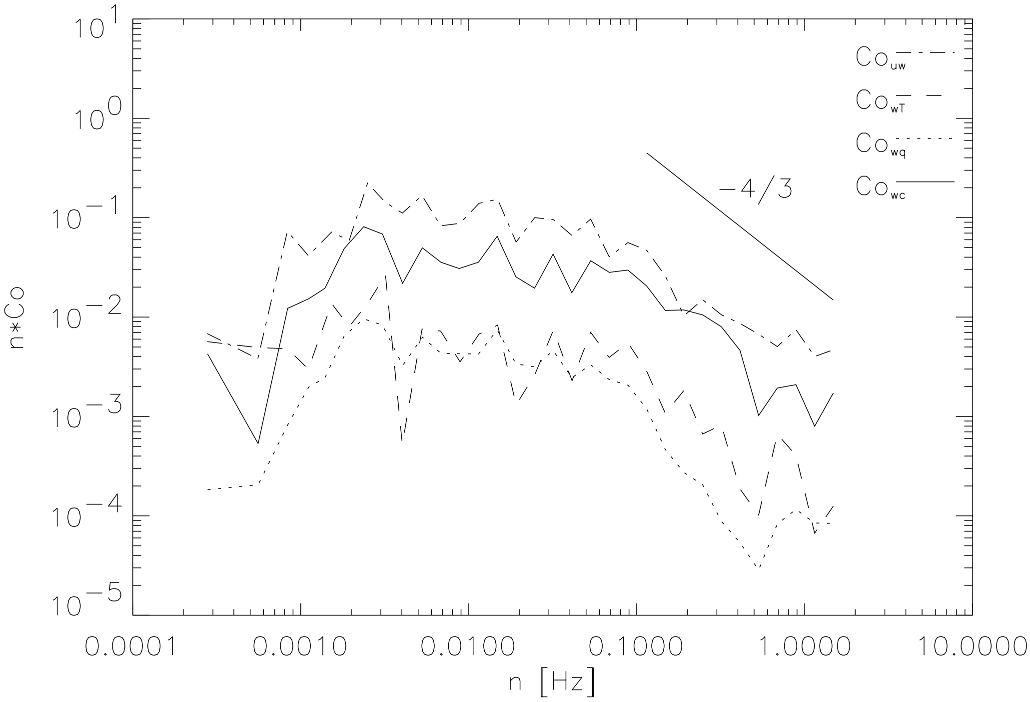

Figure 2.15: Average cospectra (Co) of the data produced from two hourly spectra in 24 July, 1999 (13h-15h UTC+1). The mean wind speed was 9.3 m s^{-1}. Ideally the inertial subrange spectra must follow the -4/3 slope (Kaimal et al., 1972). The temperature cospectra is evidently damaged. There is no apparent noise in the high frequency range of the IRGA signal cospectra which means that the noise apparent in the IRGA power spectra has a random nature which does not correlate with the vertical wind speed.

izontal wind speed, temperature, water vapor mixing ratio and carbon dioxide fluctuations. The plot is constructed as an average of two hourly cospectra measured in 24 July, 1999 between 13h and 15h, UTC+1. The average wind speed was 9.3 m s^{-1}.

Most of the cospectra exhibit correct behaviour, as they follow the -4/3 slope in the inertial subrange (Kaimal et al., 1972). The wT cospectra is clearly degraded, as it is expected from the power spectral plot. The degradation is most visible between 0.003 Hz and 0.03 Hz, where the cospectra actually crosses the water vapor cospectra caused by the degraded cospectral amplitude.

The water vapor cospectra drops faster than the expected -4/3 slope which means that there is a flux loss possibly caused by condensation in the tubes since the area under the cospetral curves are equal to the covariance (Stull, 1988). A part of the degradation is accounted for using the spectral correction routines described in the next subsection.

2.3.4.6 Final calculations

Turbulent fluxes are calculated from covariances of the despiked and detrended time series taking into account the delay time of signals determined during the calibration procedure outlined in section 2.3.3. Periods with incomplete sampling over the entire hourly period are not used for flux calculation. Raw covariances are converted into physical quantities using equations 2.30-2.33.

To determine the quality of the measurement, and to classify the data Foken and Wichura (1996) propose three tests: the instationarity test, the correlation test and the integral turbulent characteristics test. In our case the instationarity test of the hourly flux values is applied to qualify the data calculated. The quality flags (e.g., the percentage of instationarity) can be used in the determination of the net carbon balance of the region in such a way that flux values beyond a specific threshold instationarity are not used, resulting in less random error in the measurement. However, it should be noted that the effect of random error in the determination of the net carbon budget of the region is not severe if the time series available is long enough (Moncrieff et al., 1996).

Since the fluctuations of H_2O and CO_2 measured by the LI-COR 6262 are expressed in terms of mole fraction relative to dry air it is not necessary to perform the corrections for variations of the density of air (Webb et al., 1980; Grelle and Lindroth, 1996; Berger et al., 2001).

Additionally, Obukhov length is calculated from the turbulent characteristics and stored to provide stability information neccessary for the spectral corrections and for the flux source area analysis.

2.3.4.7 Post-processing: spectral corrections

It is not possible to construct a measuring system which detects all fluctuations with zero response time, and wich does not affect the measured signal itself. Moreover, introducing a closed-path gas analyzer to the system causes extra demands with regards to corrections. A part of these corrections — e.g. the utilization of the lag time — was already described.

Spectral corrections are supposed to be applied in order to account for the damping of fluctuations caused by the long air sample tubes, limited sensor response time, sensor line averaging and sensor separation, and sampling. One possible correction method is the application of a series of transfer functions defined for each correction term (Moore, 1986; Leuning and Moncrieff, 1990; Lenschow and Raupach, 1991; Massman, 1991; Leuning and King, 1992; Suyker and Verma, 1993; Moncrieff et al., 1997; Aubinet et al., 2000).

One other scheme which is quite frequently used in micrometeorology is the application of the spectral corrections based on the comparison of the (hopefully) ideally measured sensible heat cospectra (Co_{wT}, see e.g. 2.42 for the definition of cospectra), and the degraded water vapor and carbon dioxide cospectra (Högström et al., 1989; Grelle, 1997; Berger et al., 2001). The method is quite attractive, however it is not to apply to our system since the temperature signal is heavily degraded. Both method is based on the assumption of spectral similarity between temperature, H_2O and CO_2 (Anderson and Verma, 1984; Ohtaki, 1985).

The scheme of Moore (1986) is applied through the use of transfer functions for each correction term. The fractional error of the measured flux can be written as:

$$\frac{\Delta F_s}{F_s} = 1 - \frac{\int_0^\infty T_{ws}\left(n\right) Co_{ws}\left(n\right) dn}{\int_0^\infty Co_{ws}\left(n\right) dn} \, , \tag{2.49}$$

where $T_{ws}\left(n\right)$ is the convolution of all transfer functions associated with sensors of vertical wind speed and the scalar quantity in question, $Co_{ws}(n)$ is the cospectrum of the scalar flux F_s, and n is natural frequency.

To calculate $T_{ws}\left(n\right)$, we need to determine each individual transfer functions. In our system, corrections are applied in order to take into account the effect of the signal damping inside the air inlet tube, the limited time response of the IRGA, the sensor line averaging inside the IRGA's optical path, the sensor line averaging caused by the sonic anemometer, the sensor separation caused by the separation of the sensors (i.e. the separation of the air inlet and the sonic anemometer), and the effect of the discretized sampling of the continuously fluctuating flow field (Moore, 1986). These transfer functions are described in the followings.

a) Spectral attenuation

The signal damping (i.e. spectral attenuation) caused by the long air inlet tubes can be approximated if the type of the flow (laminar or turbulent) is known and the parameters of the tubing are measured (Leuning and Moncrieff, 1990; Massman, 1991; Leuning and King, 1992; Moncrieff et al., 1997; Suyker and

Verma, 1993). Caused by the change in the lag time of our eddy covariance system, the type of the flow is not constans in time, but dependent on the date. Massman (1991) provides transfer functions for both laminar and turbulent flow rates.

The general transfer function has the form of

$$T_t(n) = \exp\left(-4\pi^2 n^2 \Lambda L a u_t^{-2}\right), \tag{2.50}$$

where n is natural frequency, Λ is the attenuation coefficient (different for laminar and turbulent flow), L is the tube length (115 m in our case), a is the (internal) radius of the tube (a=0.00295 m) and u_t is the velocity of air inside the tube (calculated as L divided by the average lag time determined during the calibration procedure).

In case of *laminar* flow rate ($Re = u_t 2a/\nu_{air}$<2300, where the kinematic viscosity of air is calculated as $\nu_{air} = \left(0.0916\frac{t_{avg}}{1^oC} + 13.195\right) 10^{-6}$ m^2 s^{-1}, with the air temperature t_{avg} in Celsius), the tube attenuation coefficient can be written as (Philip, 1963):

$$\Lambda = 0.0104 \nu_{air} Re D^{-1} \tag{2.51}$$

where D is the molecular diffusivity of water vapor and carbon dioxide. These values are taken directly form Massman's web site: $D_{H_2O} = 0.2178{\cdot}10^{-4}$ m^2 s^{-1}, $D_{CO_2} = 0.1381{\cdot}10^{-4}$ m^2 s^{-1}. It should be noted that the transfer function for laminar flow calculated with inserting eq. 2.51 into eq. 2.50 is valid for the case when $2\pi n a^2 D^{-1} < 10$ and $L/a \gg 0.05\nu Re D^{-1}$. In our case, when the highest frequency to be considered is the Nyquist frequency (2.08 Hz), both criteria is fulfilled. Considering the first criteria, the expression equals to 8.235 at n=2.08 Hz. The second criteria is easily fulfilled since L/a equals to 38.983 while the right hand side equals to ∼120 with Re=2200. Consequently, the transfer function is valid for our system with laminar flow configuration.

In case of turbulent flow inside the sampling tube Massman (1991) provides values of Λ and minimum L/a values for different Reynolds numbers (Table 1. in Massman's paper). Practically, the attenuation coefficient is determined with interpolation using the data provided by Massman (1991) for any given Reynolds number.

Comparison of the transfer functions associated with laminar and turbulent flow shows that turbulent flow field inside the air inlet tube causes less severe signal damping compared to the laminar case (Lenschow and Raupach, 1991; Massman, 1991; Suyker and Verma, 1992), hence this configuration is the desirable in eddy covariance systems using long air inlet tubes.

b) Limited time response of the IRGA

The transfer function associated with the limited time response of the LI-COR 6262 IRGA (τ=0.1 sec, Moncrieff et al., 1997) has the following form (Moore, 1986; Moncrieff et al., 1997):

$$G(n) = \frac{1}{\sqrt{1 + (2\pi n\tau)^2}} , \tag{2.52}$$

where n is natural frequency, as usually.

c) Line averaging

If a sensor measures the turbulent flow field over a finite sampling path, the signal of turbulent eddies with size comparable with the sensor path is averaged. In order to take it into account transfer functions should be applied. This function has a different form for scalar and vector quantities (Moore, 1986).

In our system, the LI-COR 6262 IRGA has an optical path with a length of 15.2 cm. To take into account its line averaging effect, the following transfer function should be considered:

$$T_p(f_{p1}) = \frac{\sin^2(\pi f_{p1})}{(\pi f_{p1})^2} , \tag{2.53}$$

where $f_{p1} = np_1/U$ is the normalized frequency, where the averaging path is given by p_1 and the average horizontal wind speed is given by U. Note that eq. 2.53 is different from the general case (eq. 7. in Moore, 1986), because the flow inside the optical bench is parallel to the averaging path. This transfer function has a very slight contribution to the overall transfer function.

A different transfer function is applied to the sonic anemometer data which has a transducer head-to-head averaging path of 15 cm. According to Moore (1986), this function is as follows:

$$T_w(f_{p2}) = \frac{2}{\pi f_{p2}} \left(1 + \frac{\exp(-2\pi f_{p2})}{2} - \frac{3(1 - \exp(-2\pi f_{p2}))}{4\pi f_{p2}}\right) , \tag{2.54}$$

where $f_{p2} = np_2/U$ is again the normalized frequency, where the averaging path length of the GILL sonic anemometer given by p_2.

d) Sensor separation

The sensor separation can be hadled using the general transfer function for lateral and longitudinal sensor separation (Moore, 1986). The transfer function has the form of

$$T_{ss}\left(f_{ss}\right) = \exp\left(-9.9 f_{ss}^{1.5}\right) \ , \tag{2.55}$$

where $f_{ss} = n \cdot ss/U$, where the separation distance is given by ss (ss=0.8 m is used here).

e) Discretized sampling

The effect of the discretized sampling of the continuously fluctuating flow field using the analog to digital conversion can be approximated using the following equation (Moore, 1986):

$$T_a\left(n\right) = 1 + \left(\frac{n}{n_s - n}\right)^3 \ , \tag{2.56}$$

where n_s is the sampling frequency.

The whole data acquisition system's transfer function can be calculated utilizing all transfer functions described above (subscript s refers to CO_2 or H_2O):

$$T_{ws}\left(n\right) = T_a\left(n\right) T_t\left(n\right) G\left(n\right) T_{ss}\left(f_{ss}\right) \sqrt{T_p\left(f_{p1}\right) T_w\left(f_{p2}\right)} \ . \tag{2.57}$$

Note that the only difference between the whole system's transfer function for CO_2 and H_2O resides in the different signal damping inside the air inlet tubes described by the different transfer functions, which is caused by the different molecular diffusivity (D) values for water vapor and carbon dioxide in eq. 2.50 and 2.51.

In an earlier stage of the data processing moving averages trend removal technique was applied, which needed further spectral correction described by Kaimal et al. (1968). As it was described in section 2.3.4.4, linear trend removal is applied currently, which does not cause spectral modification of the turbulent characteristics.

Once the system's transfer function is determined, we have to obtain adequate cospectral models which can be applied in eq. 2.49 to estimate the loss in the system. The modified forms of model spectra of Kaimal et al. (1972) is used for this purpose (Moore, 1986, Moncrieff et al., 1997). These normalized model spectras describe the stability dependent behaviour of the atmospheric spectra and cospectra of wind speed, temperature or any other scalar. The integrals of the model cospectra are equal to unity, thus they can easily be modified to simulate the real atmospheric spectra of the parameter in question.

The model spectra definitions are based on the normalised frequency $f = n(z-d)/U$, where z is the measuring height above the zero plane displacement d, and U is the average horizontal wind speed. Normalization is neccessary since high wind speed causes the turbulent signal biased towards the higher frequency range accorning to Taylor's hypothesis (Stull, 1988).

The functional forms of the model spectra are as follows. During stable conditions it is written as

$$Co_{ws}(n) = \frac{1}{n}\frac{f}{A_{ws} + B_{ws} f^{2.1}}\,, \tag{2.58}$$

where

$$A_{ws} = 0.284\left[1 + 6.4\left(\frac{z-d}{L}\right)\right]^{0.75}\,, \tag{2.59}$$

and

$$B_{ws} = 2.34 A_{ws}^{-1.1} \tag{2.60}$$

(Moncrieff et al., 1997). Here L denotes the Obukhov length, and s is the scalar quantity (CO_2 or H_2O).

During unstable conditions the model spectras are as follows:

$$Co_{ws}(n) = \frac{1}{n}\frac{12.92 f}{(1+26.7f)^{1.375}}\,, \quad f < 0.54\,, \tag{2.61}$$

$$Co_{ws}(n) = \frac{1}{n}\frac{4.378 f}{(1+3.8f)^{2.4}}\,, \quad f \geq 0.54\,. \tag{2.62}$$

As it was mentioned at the end of subsection 2.3.4.6, Obukhov length is calculated in each hourly period to provide stability information for the model spectra calculations. Flux loss caused by the eddy covariance system is estimated substituting the model cospectra and the overall system transfer function into 2.49.

Since the manipulation described above are based on theoretical transfer func-

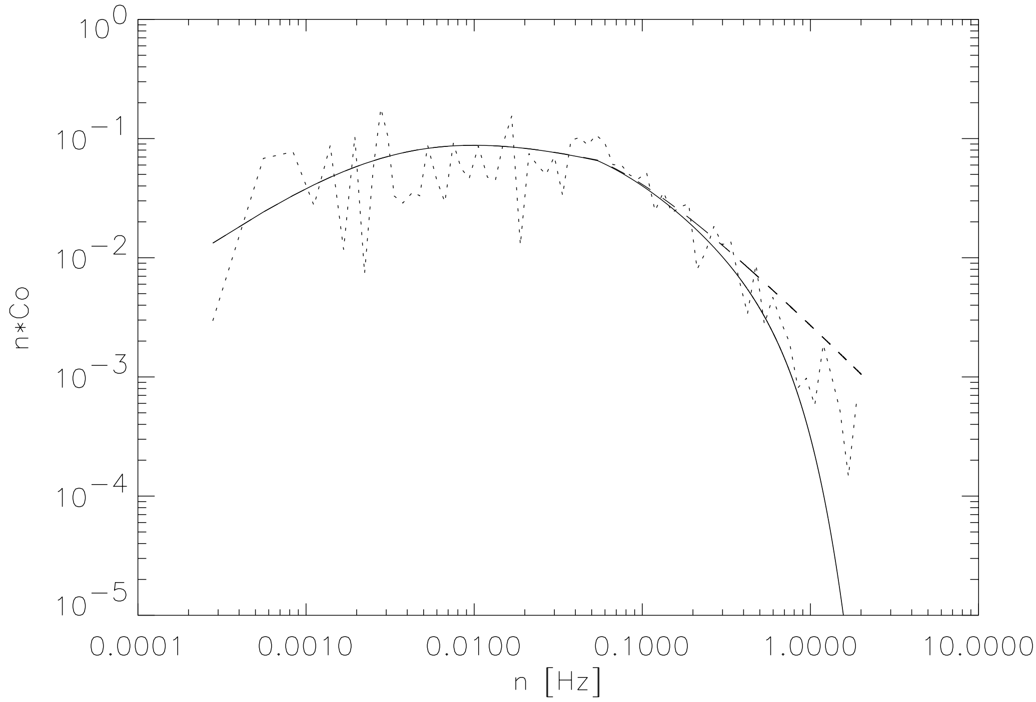

Figure 2.16: Theoretical (dashed line), measured (dotted line) and simulated cospectra (solid line) of carbon dioxide. The measured cospectra is an average of two hourly cospectra measured in 5 August, 1998 (10h-12h UTC+1). The mean wind speed was 8.2 m s^{-1}. The theoretical cospectra is calculated from eq. 2.61 and 2.62.

tions published in the literature, it is useful to prove that the cospectra behaves the same way as it is expected.

Figure 2.16 shows the cospectra of the vertical wind speed fluctuations with the carbon dioxide mixing ratio fluctuations measured in 5 August, 1998 between 10h and 12h UTC+1 together with the theoretical Kaimal cospectra for unstable situations, and the same cospectra multiplied by the total measuring system transfer function. The average horizontal wind speed was 8.2 m s^{-1}. The measured cospectra follows the simulated one well indicating that the theoretical transfer functions describe the behaviour of the system adequately. There is a slight deviation from the theoretical curve at the highest frequencies, but the contribution of the shortest wavelengths to the total flux is very little (e.g. the area under the curve at that specific interval is little).

Figure 2.17 shows the relative frequency distribution of the CO_2 flux loss calculated from the theoretical considerations. The histogram was created using

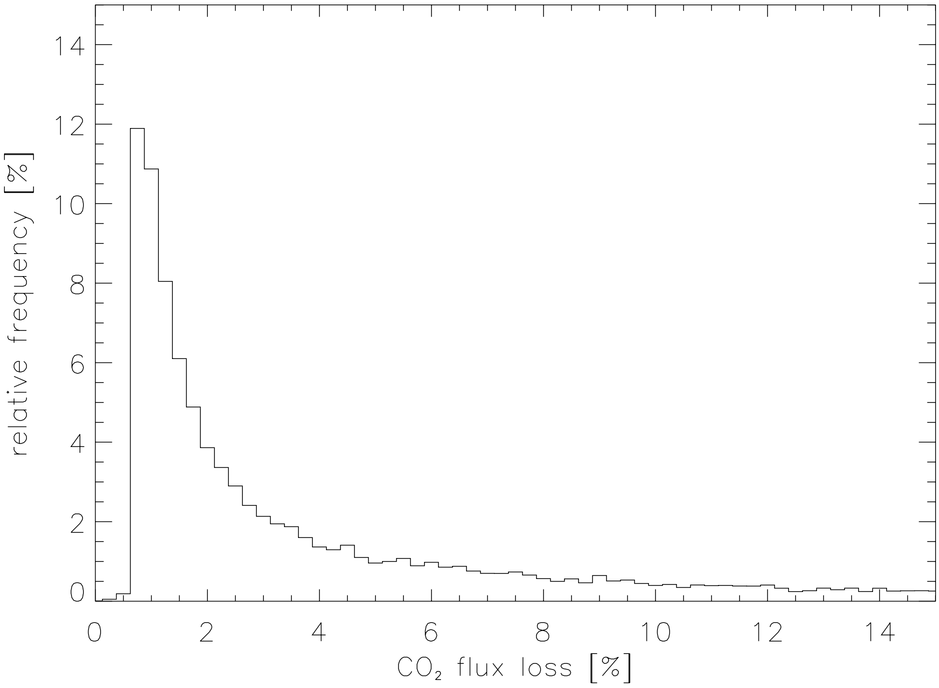

Figure 2.17: Relative frequency distribution of the CO_2 flux loss for the 82 m eddy covariance system.

all available data.

Average losses of the eddy covariance system are about 6.6% for CO_2 and 5.9% for H_2O. In 59% of the cases for H_2O and in 55% for CO_2 the loss is less than 3%. In 84% of the cases for H_2O and in 82% for CO_2 the loss is less than 10%. Flux loss is higher during stable conditions. Low values of the Obukhov length (L, defined by eq. 2.14) or high wind speed conditions (U), cause extra loss. For example, L=10 m and U=5 m s^{-1} causes 21.7% and 23.4% loss for H_2O and CO_2, respectively. In case of L=20 m and U=15 m s^{-1}, the loss is 26.4% for H_2O and 29.5% for CO_2.

As it was mentioned before, it appears that the water vapor signal suffers from excess spectral degradation compared to the theoretical spectral damping because of the long tubing of the system which causes extra loss of water vapor flux, hence needs more investigation, but this is out of scope of this work.

2.3.5 Summary

As a summary, the steps of the calibration and the data processing are as follows:

1. determination of the lag times
2. synchronization of the computers
3. calculation of the calibration functions
4. averaging time determination
5. conversion of voltage signal into physical quantities
6. wind vector rotation
7. trend removal
8. data screening
9. calculation of covariances
10. conversion into physical fluxes
11. instationarity test
12. spectral corrections

This is a routine method which is suggested to be used by other investigators who conduct long term, tower based eddy covariance measurements with similar instrumentation.

2.4 The Japanese system

The second eddy covariance system developed by the National Institute for Resources and Environment (NIRE, Tsukuba, Japan) was put into operation at the end of 1998, but because of technical difficulties, the system started to provide usable data in the beginning of March, 1999.

The new system was installed on a separate 10 m mast (which is also used in the concentration profiling system described in section 2.2.1) at 3 m height. Thus, it has a very limited flux source area (Schmid, 1994, 1997), which means that information gathered by the system is representative to a circle of a maximum radius of 300 m around the mast following the meteorological rule of thumb (Businger, 1986).

2.4.1 Equipment

The basic instruments of the Japanese system are another LI-COR LI-6262 fast response IRGA and a three dimensional fast response sonic anemometer-thermometer (Kaijo-Denki, model DA-600). Air inlet tubes were mounted at 10 m and 3 m to perform both concentration gradient and eddy covariance measurements. A programmable timer is used to switch between the air inlet tubes and the calibration gases. Different pumps are used to suck air from the measuring levels and the calibration gas tanks. The IRGA, its pumps (one for 10 m and one for 3 m), the timer and the calibration gases are located in a ventillated box near the 10 m mast allowing a very short air inlet tubing. Raw voltage data detected by the fast response sensors are collected and digitised by means of a TEAC datalogger at exact 5 Hz. The data are written to magneto-optical disks in binary format. The disks are brought to Budapest for data processing once a month.

Before 13 April, 1999 the system worked in two separate modes: it performed gradient measurements and eddy covariance measurements by turns. The data acquisition program allowed us to calculate 16 minute averages of gradient data and 16 minute averages of eddy covariance data (with 2 minutes overlapping). This measuring routine turned out inadequate since the ogive functions (see section 2.3.4.1) of the data did not converge during the 16 minute periods. For this reason, the measuring regime had been changed. The new measuring cycle consists of four 6 hour long periods, with each period begins with a 16 minute air sampling from the 10 m level (air inlet is installed near the existing 10 m inlet of the profiling system), with eddy covariance sampling during the rest of the 6 h period. The sampling of the 10 m level makes it possible to compare the profile system and the Japanese system.

Data coverage between 1 March 1999 and 18 December 2001 was 71%, after data screening it reduced to 65%.

2.4.2 Calibration

The LI-COR LI-6262 is calibrated against two standard gases with known concentrations (320 ppm and 420 ppm) once a day, short before midnight. This method is more common in the field of long term ecosystem carbon dioxide exchange studies than the one described in section 2.3.3. The advantage of using calibration gases is the avoidance of the complex calibration procedure described in section 2.3.3. The disadvantage is the interruption of the data collection during the calibration period. The analyzer runs in absolute mode.

Calibration starts at 23h 46min UTC+1, and finishes at midnight. The programmable timer switches between the standard gases in every 2 minutes so that each first minute is used to flush the sampling cell, while the signal measured during the second minute is integrated to determine the response of the instrument, to track the zero and span drift (LI-COR, 1996).

Factory calibration (fifth order polynomial for CO_2 and third order polynomial for H_2O) is applied to convert the raw voltage signal into mole fraction (LI-COR, 1996). Dry air mixing ratio is calculated in the same way as it is described in section 2.3.4.2 to avoid using the Webb-correction (Webb et al., 1980). Span and zero drifts are taken into account using a linear stretch of the time series based on the measured mixing ratios of the calibration gases. The validity of the linear approximation for the instrument in the range of interest is described in section 2.3.3.

2.4.3 Data processing

The data processing technique is very similar to that described in section 2.3.4.

Based on ogive tests described in section 2.3.4.1 it was found that 30 min averaging time is appropriate to determine turbulent fluxes considering the height of the measurements (Foken and Wichura, 1996).

Spectral analysis is performed to check the quality of the measured data.

Figure 2.18 shows the power spectra of horizontal wind speed, vertical wind speed, temperature, water vapor and carbon dioxide mixing ratio as an average of two half hourly spectra measured between 10h and 11h UTC+1 in 19 June, 1999 at 3 m height. The average horizontal wind speed was 3.3 m s^{-1}. The plot was chosen to be typical for the whole measurement.

Compared with the power spectra of the 82 m EC system (figure 2.14), it is apparent that the temperature spectra is correct here, and all power spectra behaves well expect the spectra of the IRGA. The spectra of water vapor and carbon dioxide falls faster in the inertial subrange than the ideal -2/3 slope which is caused by the signal damping inside the tube, the sensor line averaging and the limited response time of the instruments. This effect causes more severe

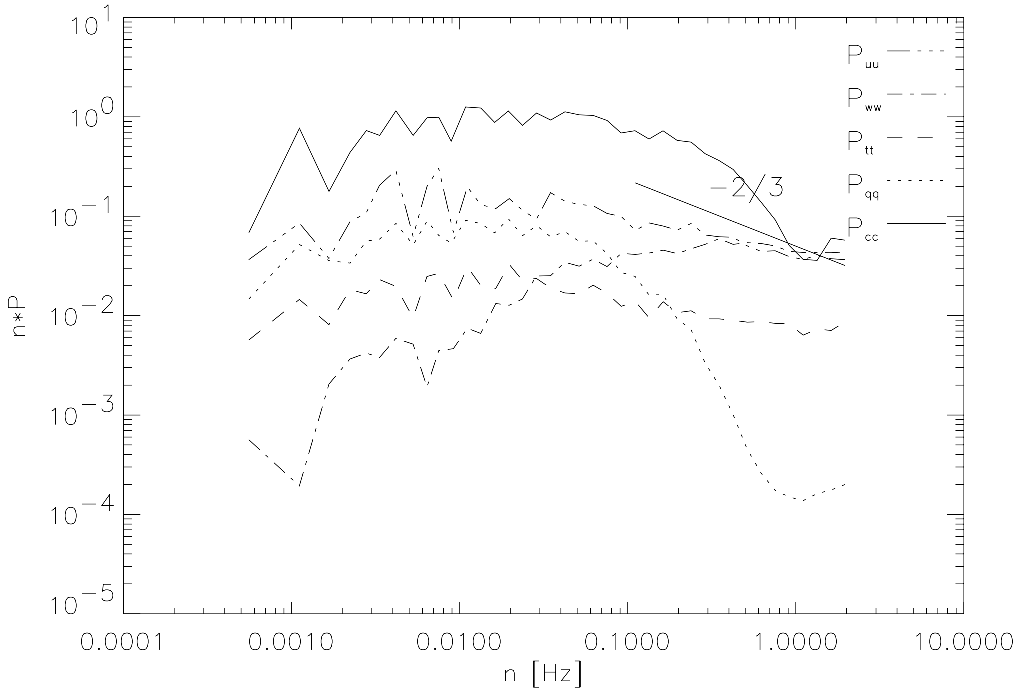

Figure 2.18: Average power spectra (P) of the measured data produced from two half hourly power spectra in 19 June, 1999 (10h-11h UTC+1). The mean wind speed was 3.3 m s^{-1}.

signal loss than at the EC system at 82 m. The increased signal loss is partly a consequence of the laminar flow configuration inside the tubes (the tube length is 10 m, the lag time is around 3 sec, and the inner diameter of the tube is 6 mm). As it was stated before (section 2.3.4.7), turbulent flow field inside the air inlet tube causes less severe signal damping compared to the laminar case (Lenschow and Raupach, 1991; Massman, 1991; Suyker and Verma, 1993).

There is some high frequency noise in the signal of the LI-COR which was also present in the other EC system. That noise is supposed to be random as it was stated before (section 2.3.4.5) and is not correlated with the vertical wind speed.

Figure 2.19 shows the cospectra of vertical wind speed fluctuations with horizontal wind speed, temperature, water vapor mixing ratio and carbon dioxide fluctuations. The plot is constructed as an average of two half hourly cospectra measured in 19 June, 1999 between 10h and 11h, UTC+1. The average wind speed was 3.3 m s^{-1}.

The cospectra of vertical wind speed with the horizontal wind speed behaves

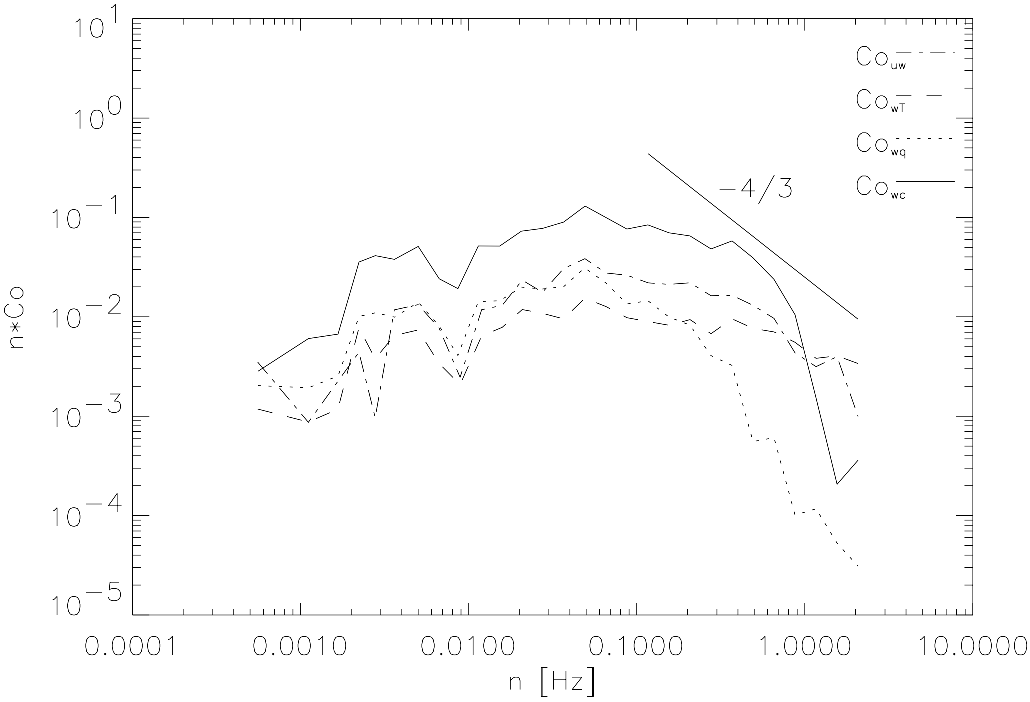

Figure 2.19: Average cospectra (Co) of the data produced from two half hourly spectra in 19 June, 1999 (10h-11h UTC+1). The mean wind speed was 3.3 m s^{-1}.

ideally in the inertial subrange as it follows the -4/3 slope. The temperature-vertical wind speed cospectra exhibits a slight deviation from the ideal shape in the inertial subrange. The cospectra of water vapor and carbon dioxide drops considerably faster than the ideal slope. This behaviour was expected from the power spectras. The degradation is accounted for using spectral correction routines similar to the one described in section 2.3.4.7. It is also evident from the figure comparing with Fig. 2.15 that the size of the eddies that contribute to the turbulent transport is smaller at this height than at higher elevation in the atmospheric boundary layer. Since spectral degradation occurs in the high frequency range of the cospectra, it is expected to cause more severe signal loss than in the case of the 82 m EC system.

Spikes are removed from the time series during data processing (data values outside $\pm 5\sigma$ are removed). The treshold value is somewhat higher than the one used for the 82 m system, since the low elevation favours high frequency eddies. Experience shows that in some cases, when wind blows from the direction of the nearby road, exhaust gas of overpassing cars may cause short extreme spikes in the carbon dioxide concentration time series which could cause severe computational error if not accounted for. Other instrument noise apparent in the wind speed data and sonic temperature data, caused by rime or liquid water, is also removed. Short before the malfunction of the Kaijo-Denki sonic anemometer at the beginning of 2001, the system produced extremely noisy data, mostly present in the sonic temperature time series. During the same period, the internal temperature and pressure sensor of the IRGA also produced defective data, and the water vapor signal was also damaged. However, it was still possible to calculate carbon dioxide fluxes, without the pressure and temperature correction (see eq. 2.44 and eq. 2.46). The quality of the data is reduced during this period, which should be kept on mind during data interpretation.

Three dimensional wind vector rotation is applied to the sonic anemometer data to ensure that the mean vertical velocity equals to zero (McMillen, 1988). The method is mainly used to account for the shadow effect of the sonic head. No significant real average vertical wind speed is expected to occur at this height (Lee, 1998).

A linear trend is removed from each half hourly (or 16 min long, before 13 April, 1999) time series to calculate the fluctuating time series.

Lag times are determined during the data processing using spectral technique. The lag times are considerably smaller in this case since the air inlet tube is much shorter here.

Turbulent fluxes are calculated from covariances of the despiked and detrended time series taking into account the delay time of the signals. Raw covariances are converted into physical quantities using equations 2.30-2.33.

Spectral corrections are applied to account for the damping of the signal inside the tube, the sensor line averaging, the limited response time of the anemometer and the IRGA, and the analogue-to-digital conversion. The methodology of the correction is described in subsection 2.3.4.7. The neccessary parameters are as follows: the separation distance between the air inlet and the anemometer is 23 cm, the response time of the Kaijo-Denki sonic anemometer is 0.1 sec, the response time of the LI-6262 is 0.1 sec, the path length of the anemometer is 20 cm, the length of the teflon tube is 10 m and the inner diameter is 6 mm.

Figure 2.20 shows the cospetra of the vertical wind speed fluctuations with the carbon dioxide mixing ratio fluctuations measured in 20 June, 1999 between 10h and 11h UTC+1 together with the theoretical Kaimal cospectra for unsta-

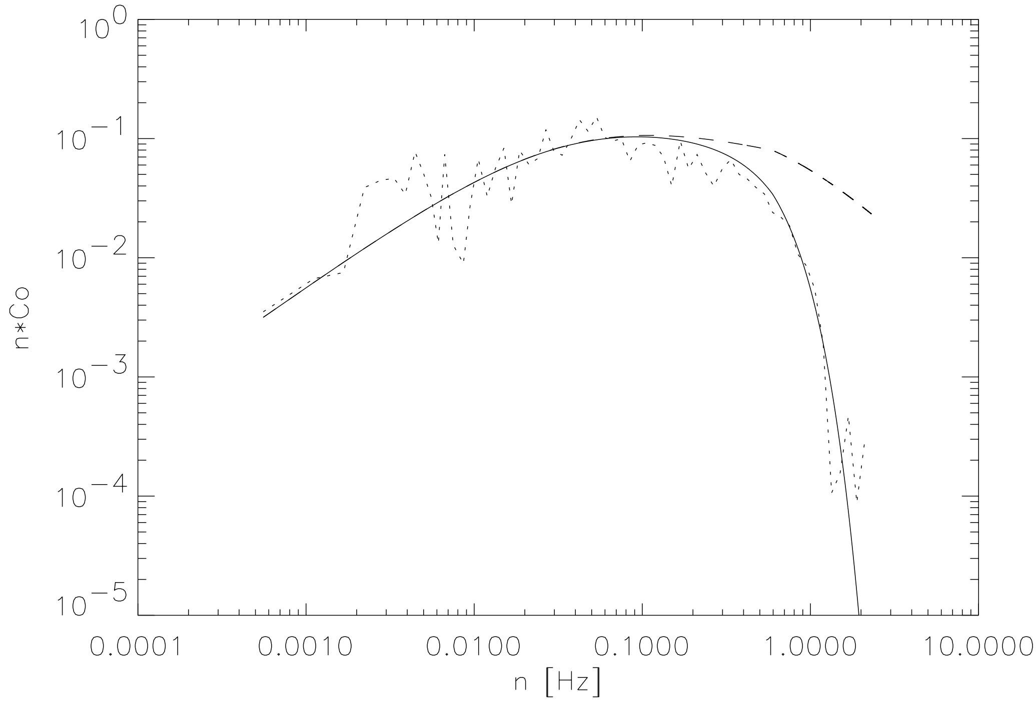

Figure 2.20: Theoretical (dashed line), measured (dotted line) and simulated cospectra (solid line) of carbon dioxide. The measured cospectra is an average of two half hourly cospectra measured in 19 June, 1999 (10h-11h UTC+1). The mean wind speed was 3.3 m s^{-1}.

ble situations, and the same cospectra multiplied by the total measuring system transfer function. The average horizontal wind speed was 3.3 m s^{-1}. The measured cospectra follows the simulated one well indicating that the theoretical transfer functions describe the behaviour of the system adequately. This result also supports the validity of the spectral corrections applied to the EC system at 82 m, where the validity of the correction is less confirmed visually.

Figure 2.21 shows the relative frequency distribution of the CO_2 flux loss calculated from the theoretical considerations. The histogram was cproduced using all available data.

Average losses of the eddy covariance system are about 23.1% for CO_2 and 20.4% for H_2O. In 75.1% of the cases for H_2O and in 79.7% for CO_2 the loss is between 10% and 30%.

Additionally, Obukhov length is calculated from the turbulent characteristics and stored to provide stability information neccessary for the spectral corrections and for the flux source area analysis.

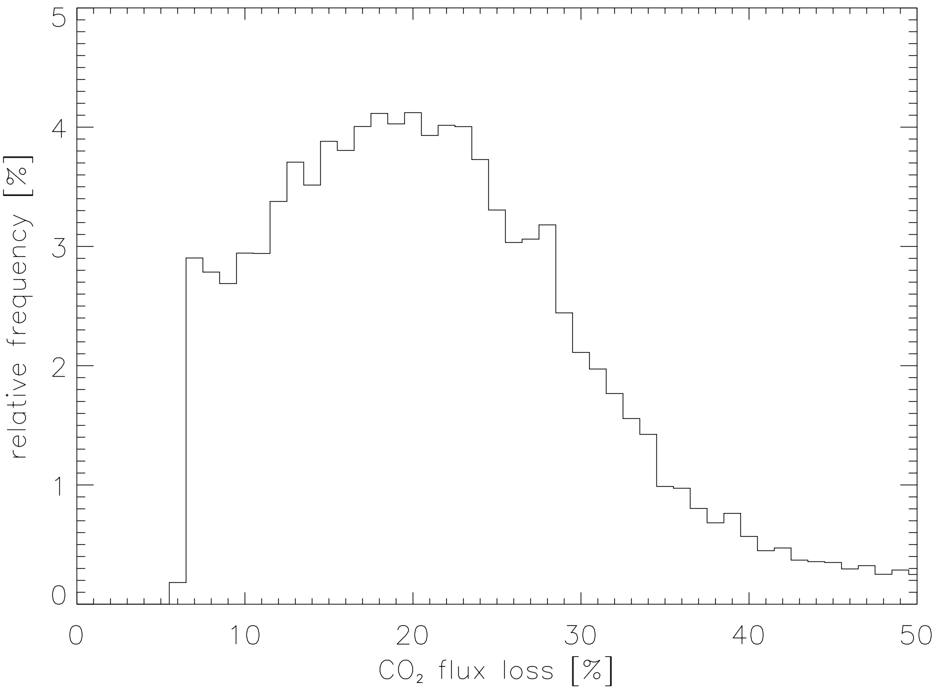

Figure 2.21: Relative frequency distribution of the CO_2 flux loss for the 3 m eddy covariance system.

2.4.4 Summary

In summary, the steps in calibration and data processing are as follows:

1. determination of the averaging time
2. conversion of voltage signals into physical quantities
3. span and zero correction
4. data screening
5. wind vector rotation
6. trend removal
7. determination of the lag times
8. calculation of lagged covariances
9. conversion into physical fluxes
10. spectral corrections

Chapter 3

Results

This chapter presents the results of the dissertation. The results are built upon the CO_2 flux and concentration values determined following the methodology of the previous chapter. Description will be given about the measured concentration data in section 3.1. The calculation methodology of Net Ecosystem Exchange (NEE) and the related conclusions will be described in section 3.2. Comparison and critical evaluation of the measured fluxes will be presented in section 3.3. The response of the carbon exchange process to the environmental conditions will be evaluated in section 3.4. Seasonal and interannual variability of NEE will be described in section 3.5 for the 82 m (large scale) system and for the 3 m (local) system. Error assessment will be presented in section 3.6.

3.1 Concentration profiles

Haszpra (1999a) presents time series and average vertical gradients of CO_2 mixing ratios at the site, and a comparison of CO_2 data from the Hegyhátsál tower with data from the WMO/GAW K-puszta site in central Hungary.

The weekly flask samples collected for analysis by NOAA/CMDL provide an independent check on the calibration of our CO_2 mixing ratio measurements. The relationship between flask measurements and simultaneous in-situ data (with a few outliers rejected) does not differ significantly from 1:1 (slope = 0.945, residual standard deviation = 2.2 ppm, n = 104, data not shown). The large RSD reflects the high degree of temporal variability of CO_2 mixing ratios at our site and the difficulty of matching the flask and in-situ data exactly in time. The data are

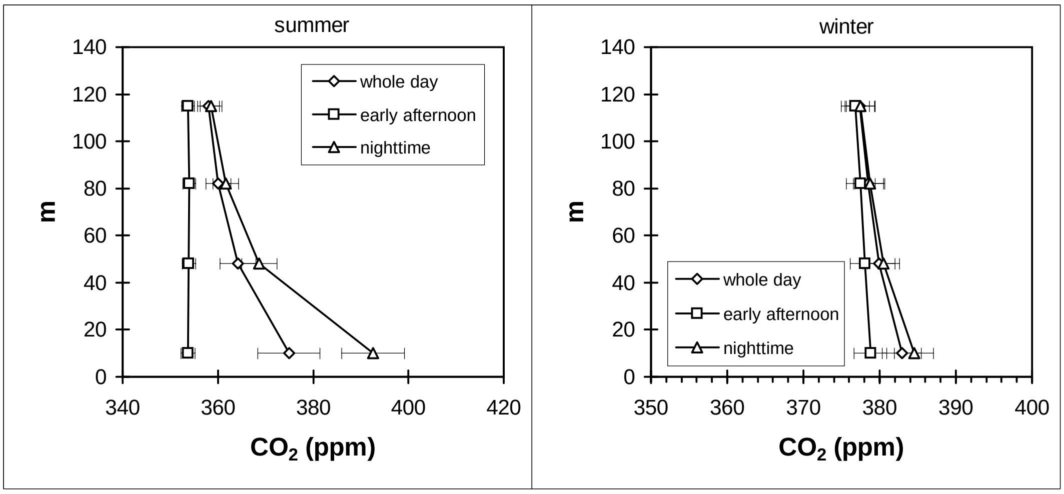

Figure 3.1: Vertical profiles of carbon dioxide mixing ratio in different seasons and in different time of the day at Hegyhátsál (error bar = $\sigma/4$) (The figure is taken from Haszpra, 1999a).

available on the Internet via anonymous FTP (NOAA CMDL ftp site, 2001).

The long term, high precision concentration profiles give insight into the biochemical processes of the vegetation. High CO_2 concentration accumulates close to the surface during nighttime in the growing season due to respiration, which is flushed out to the upper atmosphere during the morning transition period, when the nighttime inversion breaks up (Figure 3 in Haszpra, 1999a). This behaviour must appear in the measured vertical fluxes.

Figure 3.1 shows the vertical profiles of carbon dioxide in winter and summer, in different time of the day. The summertime plot demonstrates the accumulation of CO_2 during night, and the carbon uptake of the vegetation during daytime (CO_2 concentration is lowest near the ground during daytime). The wintertime plot indicates the effect of accumulated carbon dioxide during the dormant season when respiration and soil CO_2 efflux are the main determinatives of the carbon balance.

Since the objective of the present study is different from the above, no further details are presented here about the profiles, but simply refer to Haszpra (1999a).

Figure 3.2 shows the comparison of the CO_2 concentration values measured by the profiling system at 10 m and the concentration values measured during the profile (or concentration) measuring periods of the Japanese system. The plot was

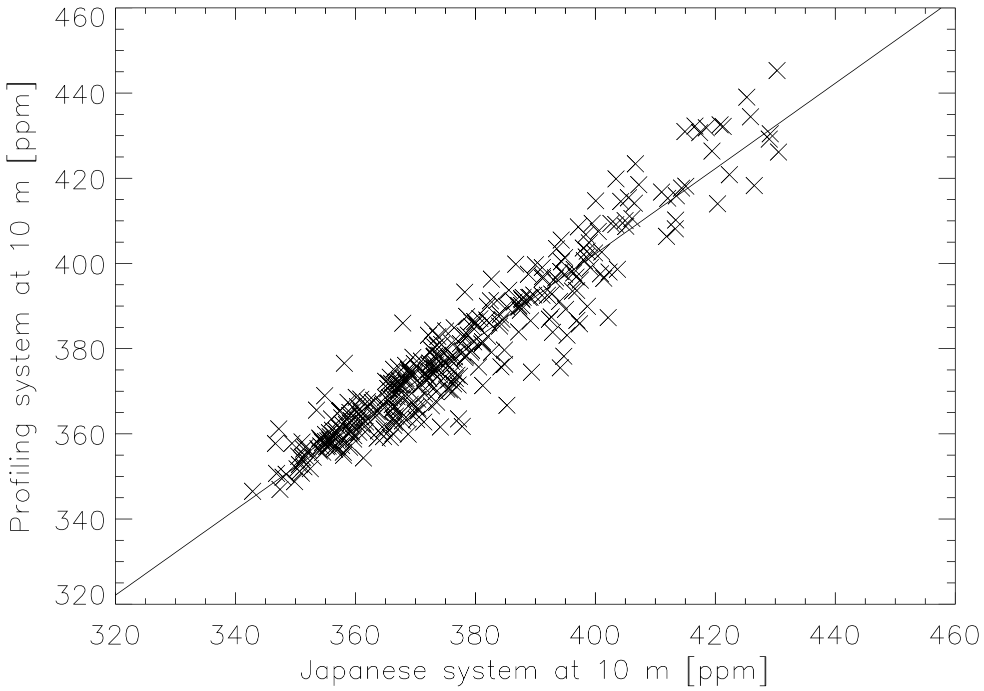

Figure 3.2: Comparison of the carbon dioxide concentration data in ppm measured by the Japanese system and the profiling system at 10 m. Number of samples: 377. The equation of the linear regression: $y = 1.00154x + 1.63$, $r = 0.954$.

produced using all available data from the Japanese system. The corresponding values were chosen such that the time difference between the time stamp of the Japanese data relative to the profiling data was less than 8 minutes. The Japanese data were averaged for 15 min intervals. The plot was produced excluding some extreme differences, most probably caused by poor synchronization between the timer of the Japanese eddy covariance system and the internal clock of the profile data acquisition computer and by unusual instrument drift (as it was described in section 2.4.2, the Japanese system is calibrated for the whole day based on the calibration conducted short before midnight, while the profiling system is continuously accounted for instrument drift — see section 2.2.1).

The slope of the linear regression is 1.00154, and the intercept is 1.63, r=0.954. This indicates that the measured values are well correlated.

3.2 The net ecosystem exchange

3.2.1 Theory

The basic aim of this long term carbon dioxide flux study is the determination of the net CO_2 budget of the vegetation. If one conducts a measurement higher in the atmospheric boundary layer, the vertical fluxes detected by the instruments are measures of the fluxes crossing the horizontal plane of the measuring height. According to the definition (Stull, 1988), the surface layer is the part of the atmospheric boundary layer where the vertical fluxes and stress varying within 10%. The change of the flux with height is called flux divergence. Flux divergence comes from the storage of the vertically transported scalars (e.g. temperature, water vapor, carbon dioxide, etc.) in the air.

Considering a daytime situation, when the surface layer is generally well mixed due to shear and buoyancy induced turbulence, the storage varies very little with height. This is not the case during nighttime, when inversion builds up, and the scalars may be trapped below the inversion layer. If the EC measuring height lies above the top of the inversion, the system may detect zero vertical flux, while there is a significant scalar flux at the surface (e.g. Grace et al., 1996).

Based on this reasoning, eddy covariance data alone is not appropriate to calculate the net carbon dioxide flux of the region (called Net Ecosystem Exchange, briefly NEE) because of the severe underestimation of the nocturnal CO_2 efflux. This systhematic underestimation causes huge errors in the long term integrated carbon dioxide budget (Moncrieff et al., 1996). The EC flux estimates NEE well only during daytime and nighttime windy conditions, when the lower part of the boundary layer is well mixed (Grelle, 1997).

As a consequence, it is important to take into account the effect of the storage to perform accurate NEE measurements. As it is stated by Baldocchi et al. (2000), most of the scientists concerned with long term NEE measurements utilize the storage to determinate the net budget of a region.

NEE of a scalar c can be calculated based on the conservation equation in the $x-z$ plane, ignoring the molecular term (Lee, 1998):

$$\frac{\partial c}{\partial t} + \frac{\partial (uc)}{\partial x} + \frac{\partial (wc)}{\partial z} = S \, . \tag{3.1}$$

Here axis x is aligned with the average wind direction, and axis z is aligned perpendicular to the local terrain. S is the source term, u and w are the velocity components in the x and z directions, respectively. After Reynolds decomposition and averaging, the equation leads to:

$$\frac{\partial \overline{c}}{\partial t} + \frac{\partial \overline{u'c'}}{\partial x} + \overline{u}\frac{\partial \overline{c}}{\partial x} + \overline{c}\frac{\partial \overline{u}}{\partial x} + \frac{\partial \overline{w'c'}}{\partial z} + \frac{\partial \left(\overline{w}\,\overline{c}\right)}{\partial z} = S\,. \tag{3.2}$$

Air is assumed to be incompressible so that

$$\frac{\partial \overline{u}}{\partial x} = -\frac{\partial \overline{w}}{\partial z} \simeq -\frac{\overline{w_r}}{z_r}\,, \tag{3.3}$$

where $\overline{w_r}$ is the mean vertical velocity at the measuring height (z_r). Assuming zero divergence of the horizontal eddy flux (term 2 on the left hand side of eq. 3.2 equals 0) and zero horizontal advection (term 3 equals 0) and utilizing eq. 3.3, the integration of eq. 3.2 with respect to z yields:

$$NEE \equiv \int_0^{z_r} S\,dz + \left(\overline{w'c'}\right)|_{z=0} = \int_0^{z_r} \frac{\partial \overline{c}}{\partial t} dz + \left(\overline{w'c'}\right)_r + \overline{w_r}\left(\overline{c_r} - \langle\overline{c}\rangle\right)\,, \tag{3.4}$$

where subscript r denotes the quantity at height z_r, and $\langle\overline{c}\rangle$ is the average concentration between the ground and this height. It should be noted that the above model assumes zero horizontal advection, which is not neccessarily satisfied (Lee, 1998; Finnigan, 1999; Baldocchi et al., 2000; Yi et al., 2000) but very hard to measure accurately.

Traditionally, NEE is determined as the sum of the CO_2 storage change below the observational level (F_s, term 1 in the right hand side of eq 3.4) and the eddy flux at the measuring height (F_c, term 2 in the right hand side). Since mean vertical wind speed ($\overline{w_r}$) was supposed to be zero, term 3 in the right hand side of eq. 3.4 is zero in this approach.

In recent years it has been recognized that the nighttime NEE estimates during low wind speed conditions are somewhat lower than during well-mixed conditions (Lee, 1998; Malhi et al., 1999; Baldocchi et al., 2000; Yi et al., 2000). This discrepancy has led to the suggestion that eddy covariance is “missing” some of the nocturnal CO_2 flux, which can cause a selective systhematic error in the integrated net carbon balance of the biosphere (Moncrieff et al., 1996) resulting in a severely biased NEE estimate.

In order to account for this phenomena, Lee (1998) proposed a new method to calculate NEE, which includes a non-zero mass flow term (term 3 in the right hand side of eq. 3.4). This term describes the vertical advection of mass caused by a non-zero mean vertical velocity, $\overline{w_r}$ (the method for the calculation of this vertical velocity was described in section 2.3.4.3).

The method became controversial recently (Finnigan, 1999; Yi et al., 2000; Baldocchi et al., 2000). The basic problem with the correction proposed by Lee (1998) that it handles the problem of advection in a simple one dimensional framework while the local circulations or larger scale atmospheric transport motions are three dimensional phenomena, with a generally complicated flow system. The vertical advection correction handles only a part of the error associated with the advection. As it is suggested by Finnigan (1999), the advection should not be treated in a one dimensional framework as it is proposed by Lee (1998), but surprisingly, "the advection correction proposed by Lee ... appears to improve energy and carbon budget closure at some sites." (Finnigan, 1999).

Yi et al. (2000) proposes a method for the investigation of the effect of horizontal advection based on multilevel eddy covariance measurements carried out on a very tall tower.

On the other hand, it is neccessary to mention that there are still arguments that there is no problem with the nighttime NEE estimates, but that the problem lies with the respired CO_2 residing very close to, or remaining within, the soil surface and thus not being adequately captured by the storage change measurements (Malhi et al., 1999). Another possibility is that there is a reduction in the outgoing soil CO_2 flux during nonturbulent conditions because of reduced pressure pumping of air out of soil pore spaces (Malhi et al., 1999).

3.2.2 Application

As it is described in the previous section, the NEE calculation requires accurate carbon dioxide storage calculations (Fan et al., 1990) from the concentration profiles. This is generally calculated using a finite difference approach of term 1 in the right hand side of equation 3.4:

$$\int_0^{z_r} \frac{\partial \overline{c}}{\partial t} dz = \frac{d}{dt} \int_0^{z_r} \overline{c} dz = \frac{\Delta \left(\sum c_z \Delta z \right)}{\Delta t} \tag{3.5}$$

Usually, the profiles are calculated using simple linear interpolation between levels, where the concentration below the lowest level is considered to be constant (K. Davis, pers. comm.).

Similarity theory (see section 2.2.3) provides a good framework for the NEE calculations in another way. A more accurate storage calculation is performed by fitting the concentration data to obtain the concentration profile using an appropriate similarity function.

In our case the rate of change of the CO_2 storage below the measuring level is calculated as follows:

1. First, the carbon dioxide profile data are interpolated for each hourly boundary datum using a cubic spline function (Horváth and Práger, 1985) (concentration data are available generally in each 8-10 minutes, which is not neccessarily coincides with the beginning of the hours). As a result, two complete profiles are obtained for the beginning and for the end of a specific 60 min period.

2. A theoretical logarithmic CO_2 profile is constructed for the two profiles based on the closest available stability parameter (L), friction velocity (u_*) and scalar scaling parameter (s_*) using eq. 2.10.

3. Since the measured CO_2 profile values are considered to be exact, the theoretical logarithmic profiles are modified to fit the measured data. Linear interpolation is used between 82 m and 48 m, since the deviation of the linear profile from the logarithmic profile is slight here. Below 48 m, the logarithmic profile is forced to fit the measured values at 48 m and 10 m. This is accomplished by shifting and stretching the ideal profile to fit the data.

Comparison with the rate of change of storage calculated using the linear method shows small difference, but it is well known that slight systhematic errors may grow to cause considerable bias in the integrated net flux (Moncrieff et al., 1996).

As it was described in section 2.3.4.3, real mean vertical wind speed is calcualted for our site as part of the wind vector rotation routine. This value can be utilized to calculate the vertical mass flow term for each hourly interval (Lee, 1998) as it is performed by e.g. Baldocchi et al. (2000). However, it was found that this method should *not* be used for our site. The reason is that during nighttime the 82 m level gets out of the inversion layer and completely decouples from the ground. In such a situation, the onset of a non-zero mean vertical velocity clearly can *not* advect the whole, 82 m thick air column, but only the upper part of it, which lies above the inversion with considerably lower CO_2 concentration. This results in a clearly different mass flow term compared to the one estimated from the 3rd term in eq. 3.4. In fact, inclusion of term 3 in the right hand side of eq. 3.4 into the calculation of NEE yields ecologically incorrect results: it causes extremely high or low (depends on the day and hour) respiratory rates during nighttime.

If the measuring level lies inside the inversion, the mass flow correction may be more plausible, but the most recent investigations propose that the correction must be treated with caution, as it was described in section 3.2 (Finnigan, 1999; Yi et al., 2000). During daytime, when the lower boundary layer is well-mixed, term 3 in eq. 3.4 $\simeq 0$ because of the slight difference between the CO_2 concentration at 82 m and the average CO_2 concentration of the air layer below 82 m.

Summarizing the above, NEE is calculated as the sum of the eddy flux measured at 82 m plus the rate of change of CO_2 storage below 82 m for the large scale system (NEE$=F_c + F_s$). For the Japanese system at 3 m, the eddy flux is considered to be equal to NEE because of the slight storage change below. The interpretation of the flux data calculated by means of the similarity theory is descibed in the next section.

3.3 Comparison of the calculated fluxes

Direct comparison of surface fluxes computed from flux-profile relationships and by using eddy covariance, or from the two eddy covariance systems is complicated for non-homogeneous surfaces because the region of the surface (footprint and source area, Schmid, 1994, 1997) influencing each estimation may be different.

Horst (1999) shows that the source areas associated with fluxes measured by application of similarity theory and the eddy covariance technique should be approximately equal if the eddy covariance measurement is made at the effective measuring height that is defined as the arithmetic mean of the elevations of the highest and lowest profile measurements for stable stratification, or the geometric mean for unstable stratification (Horst, 1999). In our case the effective measuring height of the profile system is 28.6 m during unstable and 29 m during stable conditions. Thus, the profile method and the two eddy covariance system (82 m and 3 m) always represent different source areas in the mosaic-type terrain (see

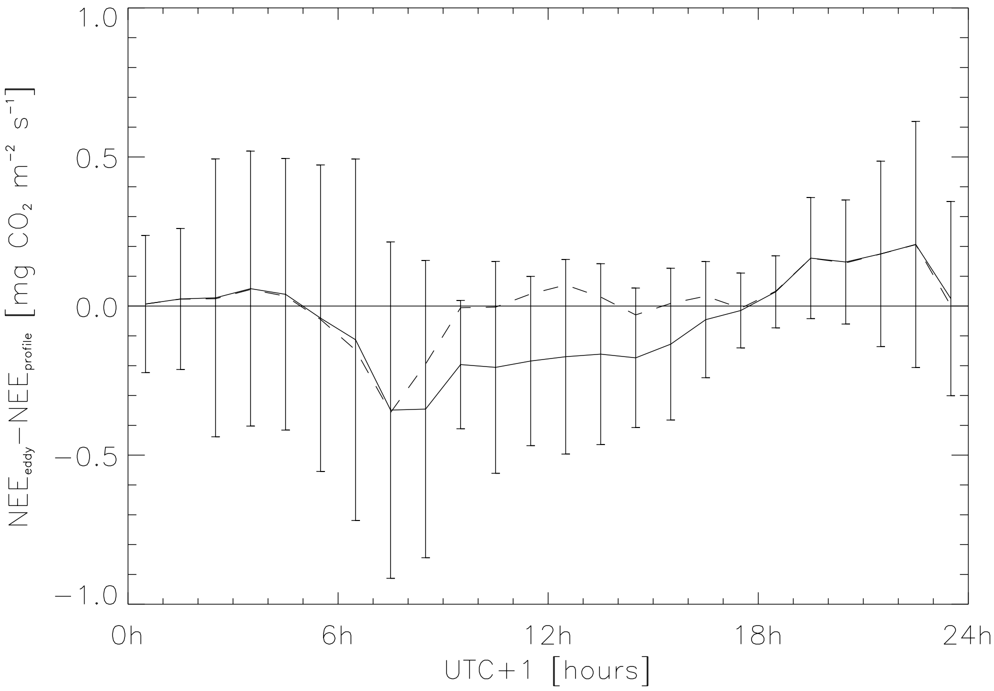

Figure 3.3: Average daily difference of NEE calculated from the 82 m EC system and from the similarity theory for July, 1997-1999 (solid line, ±standard deviation is also plotted), and the average daily difference of the EC-based NEE and the profile NEE calculated from the modified, site specific similarity function (dashed line).

fig. 2.3). This may cause differences among the NEE values measued by the three systems.

Furthermore, fluxes determined by eddy covariance are expected to be reliable even during slightly non-steady conditions, whereas the validity of the flux-profile relationship is questionable for such conditions. Computational problems occur during highly stable conditions due to the failure of convergence in the iterative calculation method using the flux-profile relationship causing lack of flux data during many nights. Intermittent turbulence at night also causes uncertainties. The error correction routines outlined in section 2.2.2 are also a possible source of error due to the uncertainties in the temperature reconstruction routine.

The net ecosystem exchange calculated from the first eddy covariance system can be used to estimate the error term in the similarity theory calculation. In our case, the mean daily cycle of the deviation of the profile fluxes from NEE is calculated for each month using the data from all available years (Fig. 3.3, solid

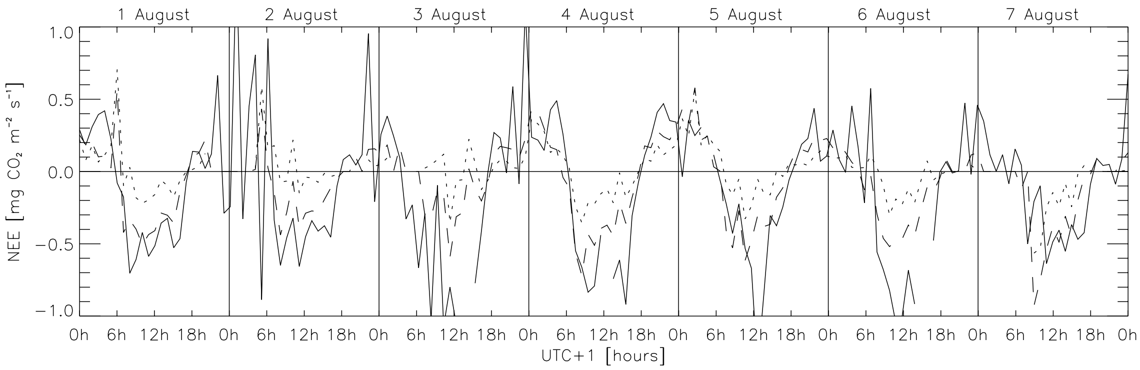

Figure 3.4: Comparison of NEE measured by the two methods, and the effect of the correction on the profile method for one week (1-7 August, 1998). Solid line: NEE; dotted line: original, unmodified profile CO_2 flux; dashed line: modified profile CO_2 flux.

line). The data comparison shows that there is a systematic underestimation of NEE calculated from the profile method during daytime, and a smaller systematic overestimation during nighttime. There is an emphasized underestimation during the morning transition period. Construction of a new, site specific similarity function for CO_2 based on the existing NEE data, following the method of e.g., Högström (1988), gave better results, but the problem of the morning transition period was not solved (Fig. 3.3, dashed line). This problem can be eliminated if the calculated monthly average daily deviations are simply added to the daily profile CO_2 flux data calculated from the similarity theory.

Figure 3.4 compares the NEE calculated from the profile data by means of the surface layer similarity theory and from the direct flux measurements by means of the eddy covariance technique at 82 m for a continuous 7 day period between 1 August and 7 August, 1998. During this period daily mean temperature ranged between 19^{o}C and 26^{o}C, and there was no precipitation. A cold frontal overpass occured between the 3rd and 5th of August, causing partial cloudiness during the 4th and 5th of August.

The figure shows the raw, unmodified profile fluxes (dotted line) vs. NEE (solid line), and the modified similarity fluxes (dashed line). The matching of the data is significantly improved with the method applied.

In summary, flux estimates based solely on the theoretical flux-profile relationships from similarity theory do not provide accurate, long-term carbon budget estimates due to both random and systematic errors, and site specific factors.

Since selective-systematic errors can change even the sign of the long-term net carbon dioxide budget of a region (Moncrieff et al., 1996), these errors can cause significant bias in the overall regional net source/sink estimation. In spite of this weaknesses of the profile flux dataset, it is useful for filling the data gaps that inevitably occur during long-term eddy covariance measurements. The application of the "tweaked" profile fluxes in the estimation of the net carbon balance of the region is described below.

Comparison of the eddy covariance based NEE measured at 3 m and 82 m is not straightforward. The 82 m NEE is a measure of the overall behaviour of the surrounding forest patches, cultivated areas, vineyards, settlements, etc. The flux source area is clearly changing day-by-day, and during each specific day, so there is no reason to tie the results to any specific biome type (C_3 or C_4 crops, trees, etc.). In contrast, the 3 m system has a very limited source area (the surrounding 300 m radius circle according to the micrometeorological rule-of-thumb (Businger, 1986)). Thus, the area "sensed" by the instruments is more definite.

Keeping all the above in mind, we may compare the NEE measured by the two, independent system.

Figure 3.5 shows a comparison of the calculated monthly mean daily NEE cycles measured by the 82 m system and the 3 m system for six months in 1999. The monthly averages are calculated directly from the measured NEE data, not utilizing any gap filling routine for missing data.

The figure shows that the vegetation around the TV transmitter tower (mainly grassland) starts to act as a sink of CO_2 earlier compared to the average behaviour of the vegetation in a larger scale (arable land and forest patches). In March 1999 the 82 m system detected a net loss of CO_2 from the biosphere to the atmosphere, while the small scale system detected a net gain of CO_2. This may be caused by the early activity of the grassland around the tower site. The nighttime respiration rates are very similar at this part of the year. During April, the monthly net budget changed sign as it is measured by the 82 m system, but the daytime photosynthetic rates are still lower here compared to the 3 m system. This difference persists during May, when the maximum value of the 3 m NEE is about 0.85 mg CO_2 m^{-2} s^{-1} (19.3 μmol m^{-2} s^{-1}) but only 0.7 mg CO_2 m^{-2} s^{-1} (15.9 μmol m^{-2} s^{-1}) for the 82 m system. The nighttime respiration measured by the 3 m system starts to exceed the 82 m respiration.

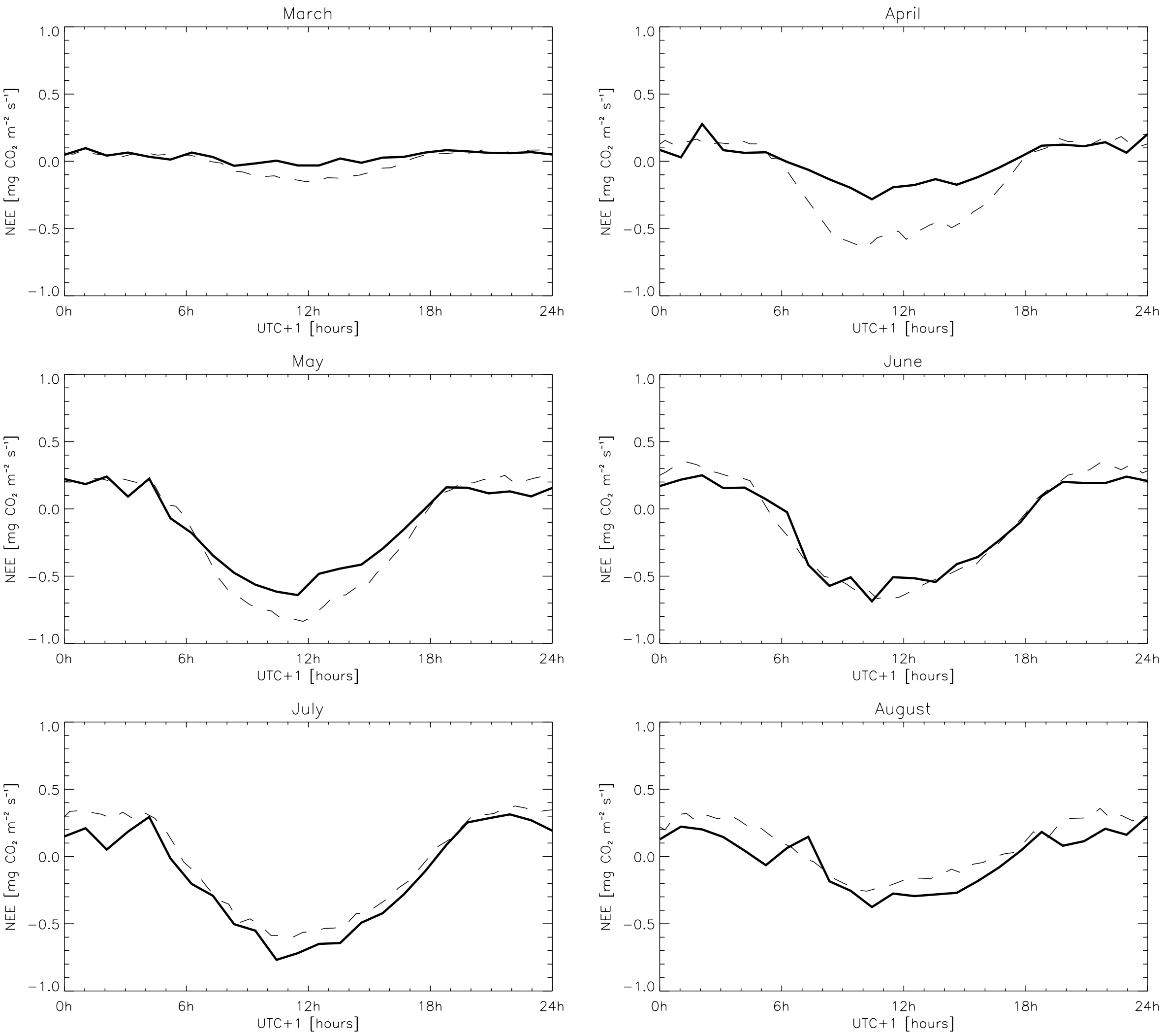

Figure 3.5: Comparison of the ensemble averages of daily NEE measured by the 82 m EC and the 3 m EC system for 6 months during 1999. Solid line: NEE at 82 m; dashed line: NEE at 3 m.

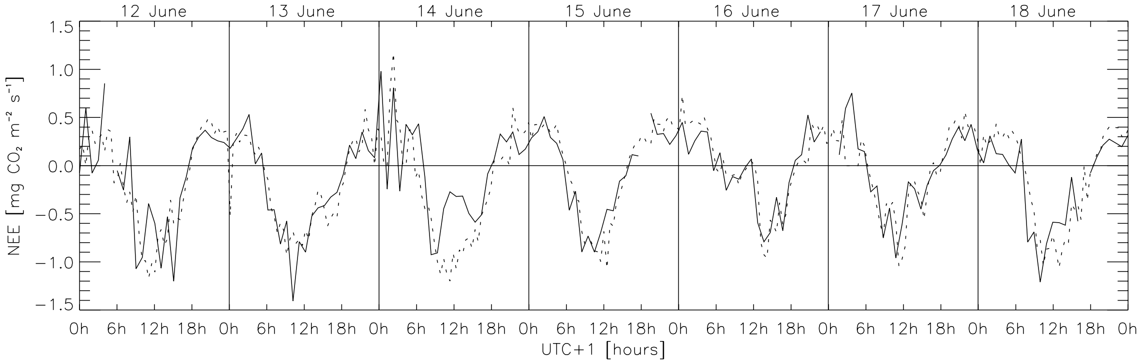

Figure 3.6: Comparison of NEE measured by the 82 m and the 3 m EC system for one week during the growing season of 1999. Solid line: NEE measuret at 82 m; dotted line: NEE at 3 m.

In June, the daytime NEE are approximately the same for the two scale reaching almost 0.7 mg CO_2 m^{-2} s^{-1} (15.9 μmol m^{-2} s^{-1}) around noon. This is lower than the 3 m average value in May. The 3 m respiratory rates are higher that the 82 m rates. As we will see it later, this difference restricts the carbon balance of the tower's surroundings. Daytime 82 m NEE exceeds the 3 m value in July, while the respiration remains higher for 3 m. The large scale average NEE reaches 0.8 mg CO_2 m^{-2} s^{-1} (18.2 μmol m^{-2} s^{-1}) during daytime. August exhibits similar behaviour as June, with a considerably lower daytime carbon uptake rate (less than 0.4 mg CO_2 m^{-2} s^{-1} (9.1 μmol m^{-2} s^{-1})). This lower value is caused by changes in the environmental conditions (see later).

The comparison demonstrates the effect of the different flux source areas on the ensemble monthly cycles of NEE as measured by the two measuring system.

Figure 3.6 shows the comparison of a weekly NEE time series measured by the 82 m and the 3 m system between 12 June and 18 June, 1999. During this period daily mean temperature ranged between 16^{o}C and 18^{o}C. 1.2 mm precipitation fell in 15 June and 6.9 mm during 17 June. There was no frontal activity except during 12 June, but the sky was frequently covered by clouds during the whole period.

The daily courses of NEE are very similar in many cases in spite of the different source areas, but there are some differences that are attributed to the different scale (e.g. during 14 June).

NEE peaks at about noon for both system and can exceed 1.4 mg CO_2 m^{-2} s^{-1} (31.8 μmol m^{-2} s^{-1}) for the 82 m system (the absolute maximum for the whole measurement is around 1.5 mg CO_2 m^{-2} s^{-1} (34.1 μmol m^{-2} s^{-1})), and about 1.2 mg CO_2 m^{-2} s^{-1} (27.3 μmol m^{-2} s^{-1}) for the 3 m system. During May, when NEE at 3 m is the largest, its maximum reaches the maximum of NEE at 82 m. The nighttime respiration at 3 m is somewhat larger than for 82 m as it is expexted from the monthly averages.

Other feature of the plot is a phenomenon that is experienced several times during the growing season: during nighttime the vegetation might appear to be a sink for a few hourly periods, and these periods are connected with very high, rapidly changing outgoing NEE in the neighbouring intervals (between 0-6 h in 14 June). This might be caused by intermittent turbulent processes that flushes the accumulated CO_2 out of lower air layer. The sink behaviour during nighttime is ecologically incorrect, but can be explained by the rapid change of the storage: if a flush-out event occurs, the CO_2 storage of the air layer below 82 m indicates CO_2 uptake of the vegetation. If the change of the storage term is not compensated by a strong apparent eddy flux at 82 m, or if this flux is detected later (which means that it reaches the 82 m level later), NEE indicates CO_2 uptake by the vegetation. If this is the case, a peak is expected later during the night, which is of course caused by the restored normal storage change and the previously flushed CO_2. These peaks are visible in the figure. It should be noted, that this phenomena does not cause bias in the net daily CO_2 ecosystem exchange since all neccesary terms are measured, although not in the same time (i.e. the peaks compensate each other). Horizontal advection might also play important role in the above phenomena (Yi et al., 2000).

All of the above raise the need for a flux footprint/source area model to investigate the area of representativeness for the EC-based systems. Due to the complexity of the problem (Schmid, 1994, 1997; Horst, 1994, 1999), there is no appropriate model available for practical purpose. The mini-FSAM model of Schmid (1994) is a promising, tiny, easy to use flux source area model, but as it is admitted by the same author (Schmid, 1997), it became clear that the earlier calculations had contained mistakes, thus the model should not be used for source area calculations in any way. A possible future aim of the current project is the development of a model which can be used in practice to determine the area of representativeness for the measurements as a routine task.

3.4 Environmental forces

Based on the long term measurement data, we can investigate the response of the measured NEE to the environmental factors. The main variables controlling the behaviour of the vegetation is the incoming photosynthetically active photon flux density (PPFD), temperature, soil mositure and vapor pressure deficit (VPD, defined as the difference between the saturated water vapor pressure and the actual water vapor pressure at a given temperature in the atmosphere).

PPFD is the most immediate environmental control on photosynthesis (Malhi et al., 1999). The major influence of temperature on net carbon balance is through its effects on rates of both autotrophic and heterotrophic respirations (Malhi et al., 1999). Since we can not distinguish between these two types, we may only describe the net effect of respiration. Vapor pressure deficit controls stomatal closure, thus it has a direct effect on the rate of photosynthesis. High VPD causes stomatal closure, decreasing photosynthesis (Anthoni et al., 1999). Lack of soil moisture also reduces carbon uptake by causing stomatal closure, but also affects soil carbon and nutrient release by restricting microbial decomposition (Malhi et al., 1999).

PPFD, VPD and air temperature are currently measured by our system. Soil moisture measurement will be installed in the near future at Hegyhátsál.

Figure 3.7 shows the temporal course of the daily aggregated environmental variables controlling the carbon budget of the vegetation for 1997, 1998 and 1999 (i.e. for the whole 82 m EC measurement period, so far[1]).

Based on the PPFD and NEE time series, it is possible to construct the light response function of NEE for the different months during the growing season. This can be used for modelling purposes.

Figure 3.8 shows the NEE-PPFD function for August, 1997-1999. Data was measured between 8 h and 19 h UTC+1. Number of samples = 788. NEE was classified by the measured VPD. The figure shows that on average, higher VPD causes slight decrease (in absolute meaning) of NEE, as it is expected from the theory. The fitted equation is a Michaelis-Menten type rectangular hyperbola (Valentini et al., 1996; Markkanen et al., 2001). The NEE-PPFD function has the following form (solid line in figure 3.8):

[1]The heart of the measuring system - the LI-COR 62-62 IRGA - has broken down in the beginning of 2000 and was out of operation until February, 2001.

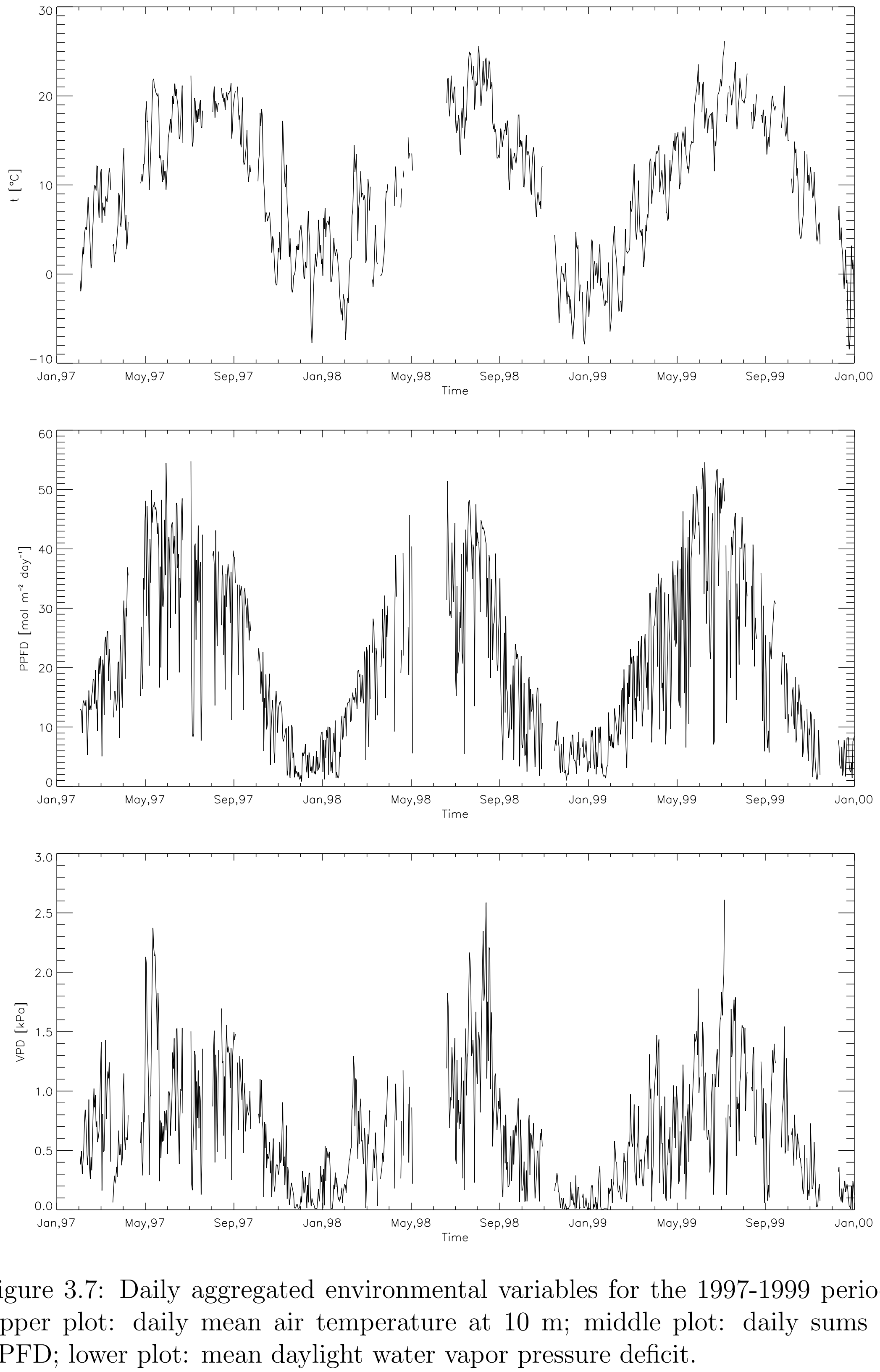

Figure 3.7: Daily aggregated environmental variables for the 1997-1999 period. Upper plot: daily mean air temperature at 10 m; middle plot: daily sums of PPFD; lower plot: mean daylight water vapor pressure deficit.

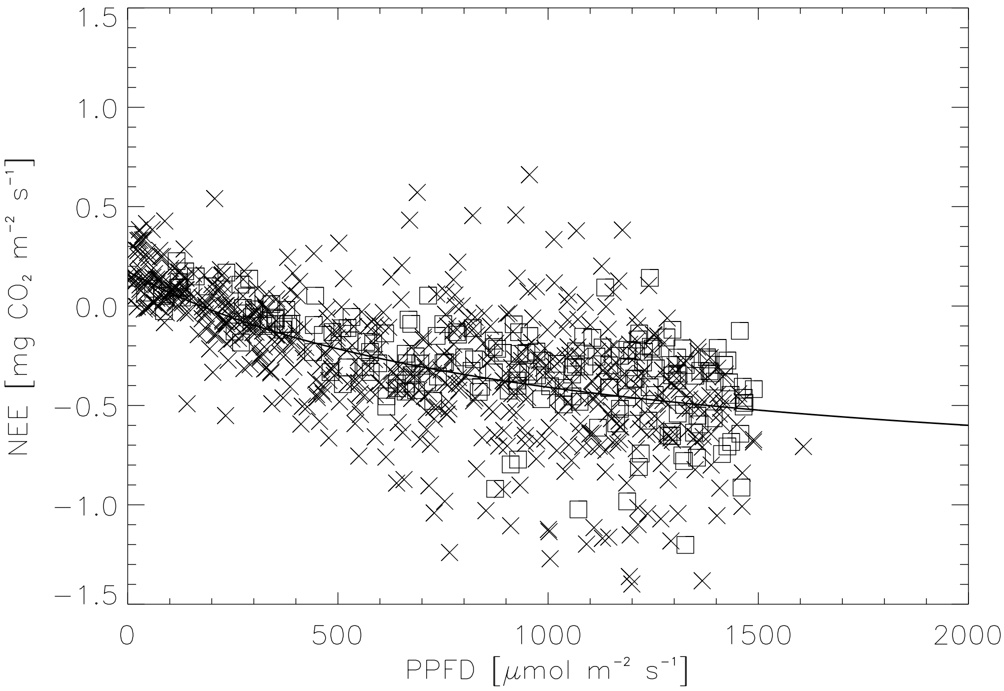

Figure 3.8: Light response curve of NEE based on all available data for August, 1997-1999. NEE calculated between 8 h and 19 h UTC+1 are plotted against PPFD. Number of samples: 788. X sign: NEE with VPD<1.5 kPa; square sign: NEE with VPD≥1.5 kPa. Negative NEE indicates CO_2 uptake by the vegetation. The functional form of the solid line is eq. 3.6.

$$NEE = a\frac{PPFD}{PPFD + b} + c \tag{3.6}$$

where $a = -1.154$ mg m^{-2} s^{-1}, $b = 980.961$ μmol m^{-2} s^{-1}, $c = 0.174$ mg m^{-2} s^{-1} for August, PPFD is given in μmol m^{-2} s^{-1}, and NEE is in mg CO_2 m^{-2} s^{-1}. Light response curve of NEE is estimated for each month during the growing season (March-October) using all available data from 1997, 1998 and 1999. The coefficients of the NEE-PPFD function is shown in table 3.1.

Investigation of nighttime NEE as a function of air temperature showed that it is not reasonable to calculate NEE-t response function for each month separately because of the large scatter of the observed data (Greco and Baldocchi, 1996; Valentini et al., 1996). Instead of this, one curve is fitted to all data measured during the growing season.

Figure 3.9 shows the NEE-air temperature function (air temperature measured at 10 m is used) during nighttime for March-August, 1997-1999. Number

	a [mg m^{-2} s^{-1}]	b [μmol m^{-2} s^{-1}]	c [mg m^{-2} s^{-1}]	n
March	-0.246	73.525	0.192	350
April	-0.492	244.387	0.184	340
May	-1.201	663.331	0.246	493
June	-1.302	600.823	0.324	636
July	-1.389	799.208	0.259	374
August	-1.154	980.961	0.174	788
September	-0.622	226.867	0.194	497
October	-0.482	63.649	0.299	318

Table 3.1: Coefficients of the NEE-PPFD response function during the growing season estimated for the 1997-1999 period. The general form of the function is eq. 3.6. The number of hourly samples (n) used for the fitting is also shown.

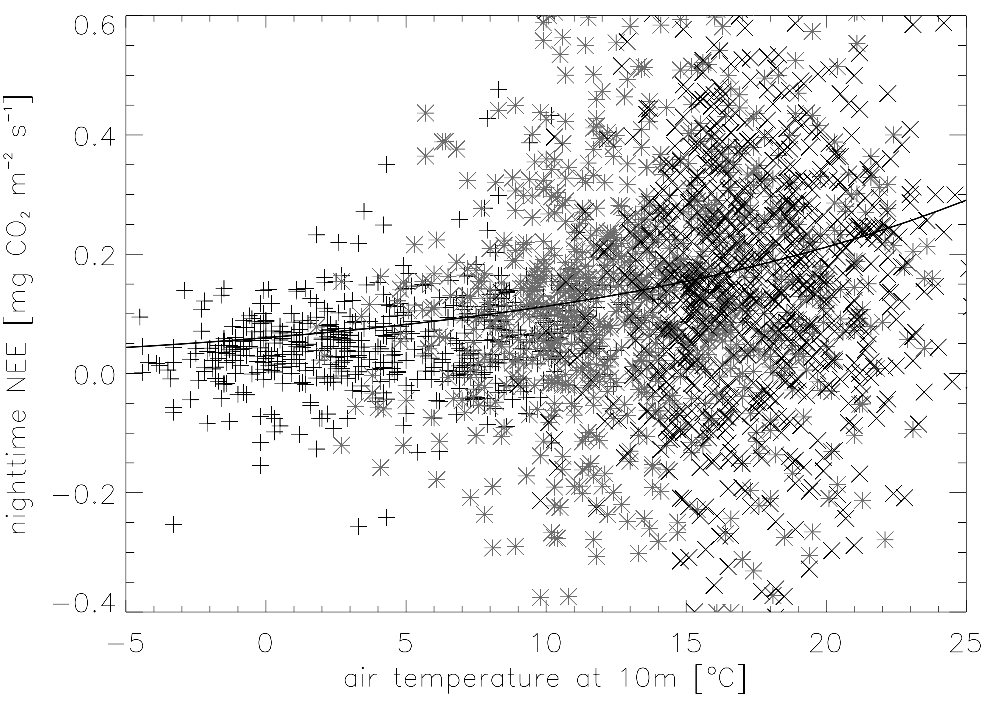

Figure 3.9: Relationship between NEE and air temperature at 10 m during nighttime. NEE measured between March-August is plotted from all available years (1997-1999). Plus sign: data measured during March; grey asterisk: data from April-June; X sign: data from July and August. (September and October is not plotted for clarity). All data defines a single curve, although very high scatter is observed.

of samples used for fitting = 3356 (includes data from March-October, 1997-1999; September-October data is not plotted but used for fitting). Nighttime period before day of year (DOY) 100 and after DOY 260 is defined as the period between 18 h and 5 h UTC+1, and the period from 20 h till 3 h between DOY 100 and DOY 260. The fitted curve has the following form:

$$NEE = x \exp\left(y \cdot t_{10}\right) \tag{3.7}$$

where $x = 0.06$ and $y = 0.063$ (the linear correlation coefficient is only 0.21) and t_{10}, the air temperature at 10 m, is given in Celsius. The Q_{10} coefficient (i.e. the ratio of the rate of respiration at one temperature to that at a temperature 10 degrees lower) is 1.88.

Outside the March-October period, another NEE-t_{10} function is constructed using both daytime and nighttime data using data from all available years. The coefficients of the fitted curve are $x = 0.041$ and $y = 0.014$ (data not shown). This curve shows good agreement with the previous one in the -5 - 0^oC interval. This curve is supposed to be used for NEE modelling purposes both for daytime and nighttime in this period as a function of air temperature.

The same procedure is performed for the Japanese system. Air temperature measured by the Kaijo-Denki anemometer/thermometer at 3 m was used to determine the NEE-t_3 relationship during nighttime. PPFD measured by the profile system was used to fit the NEE-PPFD curves in the same way as it is done in the case of the 82 m system.

Coefficients of the light response curve are presented in table 3.2 for the growing period of 1999 (except October, when no PPFD data was available).

During the vegetative period, one NEE-t_3 curve is constructed similarly to the 82 m system. Since air temperature at 3 m is measured by the system, the ensemble temperature response curve is estimated from all available data from 1999 and 2000. The coefficients of this ensemble curve are $x = 0.066$ and $y = 0.08$, to be used with eq. 3.7 for months between March and October. The Q_{10} coefficient is 2.23 here. This is higher than that estimated for 82 m for the same period mainly caused by the higher respiration rates of the vegetation (see fig. 3.5) that is sensed by the 3 m system (source area, see section 3.3) during nighttime.

	a [mg m^{-2} s^{-1}]	b [μmol m^{-2} s^{-1}]	c [mg m^{-2} s^{-1}]	n
March	-0.386	63.833	0.244	823
April	-1.403	603.01	0.209	1167
May	-1.329	446.365	0.316	1338
June	-1.507	636.586	0.34	621
July	-1.303	451.294	0.389	650
August	-0.815	612.294	0.234	1016
September	-0.525	258.952	0.204	666
October	-0.378	330.391	0.084	209

Table 3.2: Coefficients of the NEE-PPFD function during the growing season of 1999-2000 for the 3 m system. The general form of the function is eq. 3.6. The number of half hourly samples (n) used for fitting is also shown.

For months between November and February, the exponential function defined by $x = 0.035$ and $y = 0.04$ should be used both for daytime and nighttime.

3.5 Seasonal and interannual variability of net ecosystem exchange

The previous sections described the methodology to calculate hourly NEE data for both the 82 m (large scale) system and the 3 m (local scale) system. The profile "tweaking" methodology together with the empirical NEE-PPFD and NEE-t functions are powerful tools to estimate NEE when a direct measurement of NEE is not available. The final step towards the calculation of annual carbon dioxide exchange is the integration of the hourly data.

3.5.1 Net ecosystem exchange, gross primary production and total ecosystem respiration

3.5.1.1 The large scale system

As it was stated before, data gaps occur inevitably during long term ecosystem studies due to instrument malfunction or other factors (e.g. calibration periods, data storage problems, human factor, etc.). The profile method turned out to be inadequate for long term NEE calculation but useful for filling the data gaps.

Yearly net carbon dioxide exchange can be inferred from the monthly averages of NEE (Moncrieff et al., 1996), or from the daily sums of CO_2 exchange between the atmosphere and the biosphere. The latter method requires NEE information for each day of year. To complete this task, a data gap filling procedure must be developed (Falge et al., 2001) as an important step towards a defensible NEE study.

In our case, the first guess for each day is the monthly average daily NEE cycle calculated directly from the measured NEE (eddy flux at 82 m + rate of change of CO_2 storage below, i.e. $F_c + F_s$). All further step modifies this daily cycle where the improved estimate is available, leaving the rest of the cycle intact.

The second estimate is the modelled NEE calculated from the NEE-PPFD function during daytime (if PPFD is known), and from the NEE-t_{10} function during nighttime (if t_{10} is known).

The third estimate is the modified profile CO_2 flux described in section 3.3.

The fourth estimate is only applied in cases when F_c is available, but there is no F_s available. If this is the case, the monthly average daily F_s cycle is used to estimate the current storage term.

The fifth — and best — estimate is the measured NEE ($=F_c + F_s$). It was described in section 2.3.4.6 that the percentage of instationarity is calculated for each hourly period to test the quality of the measurement (Foken and Wichura, 1996). During the fifth step NEE values measured during periods with instationarity exceeding 30% are rejected.

Many authors use the empirical light-response function and the NEE-temperature function to fill data gaps (e.g. Valentini et al., 1996; Anthoni et al., 1999) at their site. Our approach is to use the semi-empirical similarity theory for this purpose, since it relies on a dynamic method compared to the empirical, statistics-based environmental forces method. As it was seen in section 3.4, the nighttime NEE-t function exhibits large scatter (e.g. Greco and Baldocchi, 1996; Valentini et al., 1996), which means that estimates based on the empirical NEE-t function may provide inaccurate estimates.

Having all neccessary measured data, and having a methodology to fill measurement gaps, we are capable to present the long term NEE time series for the two measuring system.

Figure 3.10 shows the temporal variation of the daily net CO_2 exchange during 1997, 1998 and 1999 as a function of time. Since direct flux measurements started at the end of April 1997, monthly average daily cycles were not available for

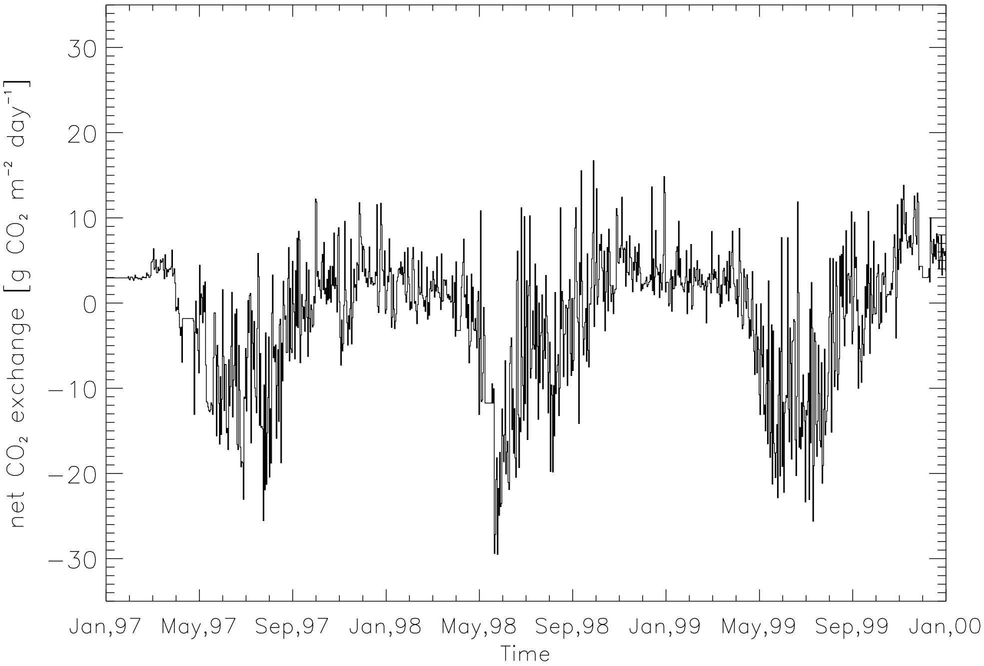

Figure 3.10: Annual and interannual variation of the daily net CO_2 exchange in 1997, 1998 and 1999 for the large scale system. Negative values indicate CO_2 uptake by the biosphere.

January-April. The neccessary daily cycles are calculated as the average of the 1998 and 1999 monthly values from January to April. Further steps of the gap filling is performed as it was described earlier in this section. The neccessay empirical environmental functions are presented in section 3.4.

Seasonality is evident in Fig. 3.10. CO_2 uptake exceeded 25 g CO_2 m^{-2} day^{-1} on some days during the growing season in some cases. However, there were also days when the biosphere lost carbon to the atmosphere. Wintertime NEE remains considerably larger than zero indicating active respiration even during the coldest days.

Figure 3.11 shows the cumulative carbon exchange for the 1997, 1998 and 1999 based on the presented data.

The calculations show that during 1997 CO_2 NEE was -491 g CO_2 m^{-2} year^{-1} (-134 g C m^{-2} year^{-1}), during 1998, -537 g CO_2 m^{-2} year^{-1} (-146 g C m^{-2} year^{-1}) and during 1999, -337 g CO_2 m^{-2} year^{-1} (-92 g C m^{-2} year^{-1}). It means that during the 3 year period of 1997-1999 the region sequestered 372 g C m^{-2}.

The dynamics of these fluxes can be better understood by breaking them down into subcomponents. NEE is defined as the sum of gross primary produc-

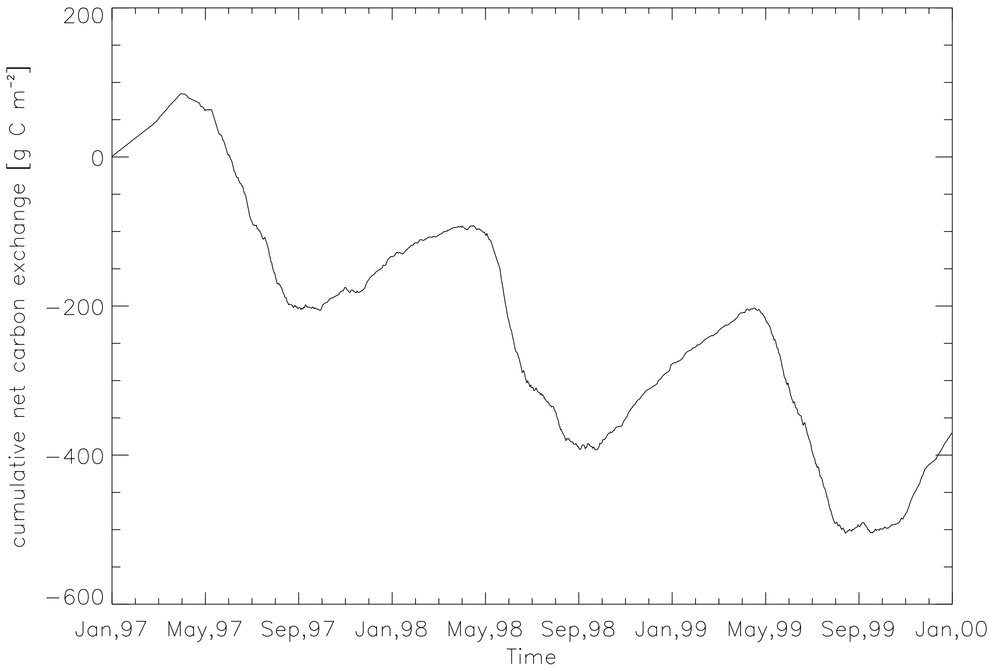

Figure 3.11: Cumulative carbon exchange for 1997, 1998 and 1999 for the large scale system.

tion (GPP) and total ecosystem respiration (R_t). R_t is defined as the sum of autotrophic respiration (R_a) and heterotrophic respiration (R_h), but this decomposition needs the measurement of at least one of the two components. As it is not performed at our site because of the large diversity of species, we only investigate GPP and R_t. Neither net primary production (NPP=NEE-R_h) nor soil carbon flux estimate is possible for the same reason. This is generally possible in sites with homogeneous vegetation and appropriate measuring devices (e.g. using the cuvette or chamber method).

GPP and R_t is calculated using the NEE-t_{10} relationship determined in section 3.4. Daily respiration is calculated from the nighttime NEE (which is actual respiration) and the modelled daytime respiration (missing temperature data is estimated from the monthly average daily course of temperature). GPP is calculated as NEE-R_t.

Figure 3.12 shows the annual and interannual cycle of NEE, R_t and GPP for 3 years between 1997 and 1999. Variability is present in the ecosystem respiration, but the interannual variability of NEE is mainly caused by differences in GPP (i.e. photosynthesys).

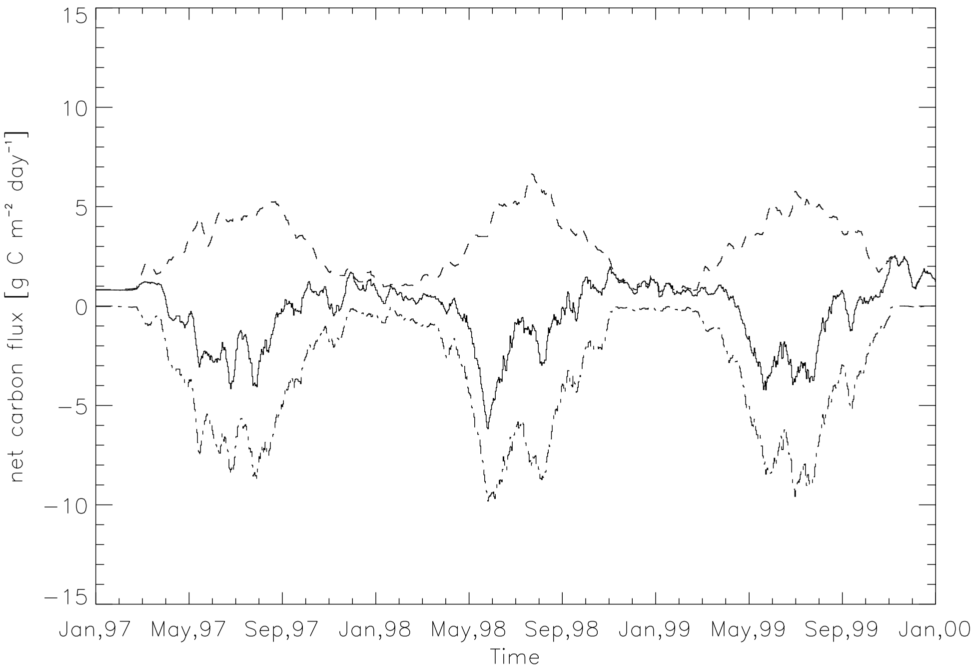

Figure 3.12: Annual variation of carbon NEE, GPP and R_t for the 1997-1999 period. Data are smoothed with boxcar average of 10 days for clarity. Solid line: carbon NEE: dashed line: R_t; dash dot line: GPP. Negative value indicate carbon uptake by the ecosystem.

Maximum values of NEE are around 4 g C m^{-2} day^{-1} in 1997 and 1999, but reach 6 g C m^{-2} day^{-1} in 1998. Maximum rates of GPP are less than 9 g C m^{-2} day^{-1} in 1997 but almost reach 10 g C m^{-2} day^{-1} in 1998 and 1999. The maximum respiration occurs in 1998.

Table 3.3 summarizes the calculated NEE and its subcomponents for each year from 1997 to 1999.

	NEE [g C m^{-2} year^{-1}]	GPP [g C m^{-2} year^{-1}]	R_t [g C m^{-2} year^{-1}]
1997	-134	-1151	1017
1998	-146	-1215	1069
1999	-92	-1155	1063

Table 3.3: Yearly sums of carbon NEE, GPP and R_t for 1997, 1998 and 1999.

3.5.1.2 The local scale system

Since the Japanese system started to provide data in March 1999, the missing data at the beginning of the year was filled using the empirical NEE-t function.

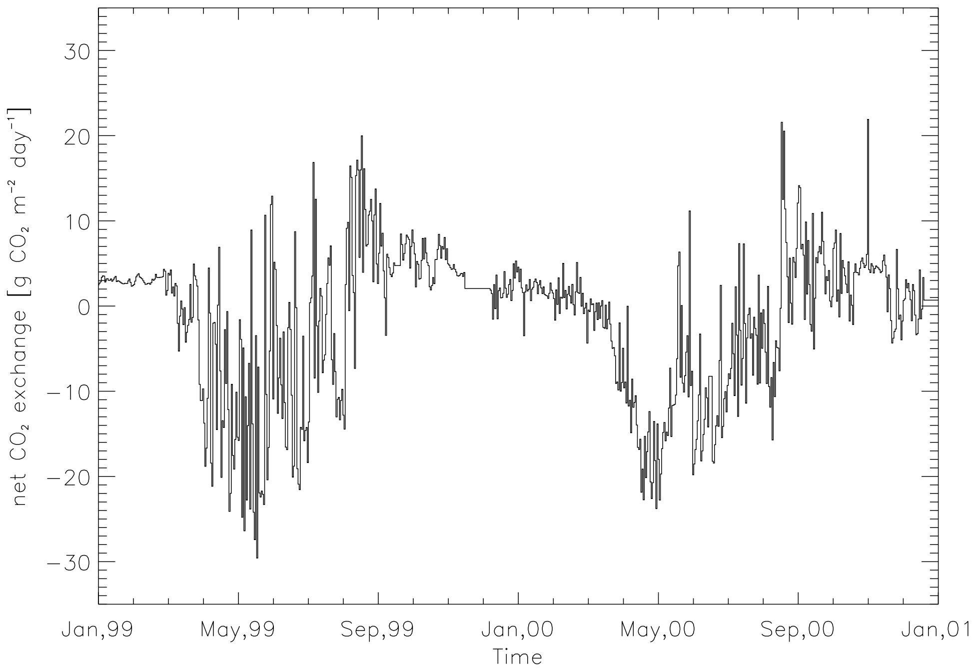

Figure 3.13: Daily net CO_2 exchange between the biosphere and the atmosphere as a function of time for the 3 m system during 1999 and 2000. The flat part is a consequence of the monthly average cycles used for data gap filling.

During the growing period, the empirical NEE-PPFD function was used to patch the missing daytime data. Unfortunately, there were two months during 2000 when no data was measured at all due to data acquisition failure (June and July). During this period, the empirical NEE-PPFD and NEE-t relationships were used to fill data gaps.

Figure 3.13 shows the temporal variation of daily net CO_2 exchange during 1999 and 2000 as a function of time. The figure is comparable with the measured net values of the 82 m system (fig. 3.10).

Figure 3.14 shows the temporal cycle of carbon NEE, R_t and GPP for the local, 3 m system. The most striking feature of the plot compared to fig. 3.12 is the enhanced rates of photosynthesis and ecosystem respiration. Yearly cycles in 1999 (the only year when both measuring system was operative) are similar both in NEE, GPP and respiration. Maximum daily NEE sums were higher as measured by the 82 m system.

Other interesting feature is the negative NEE during November and December, 2000. This is caused by an unusual warm period which supported carbon sequestration by the small scale vegetation.

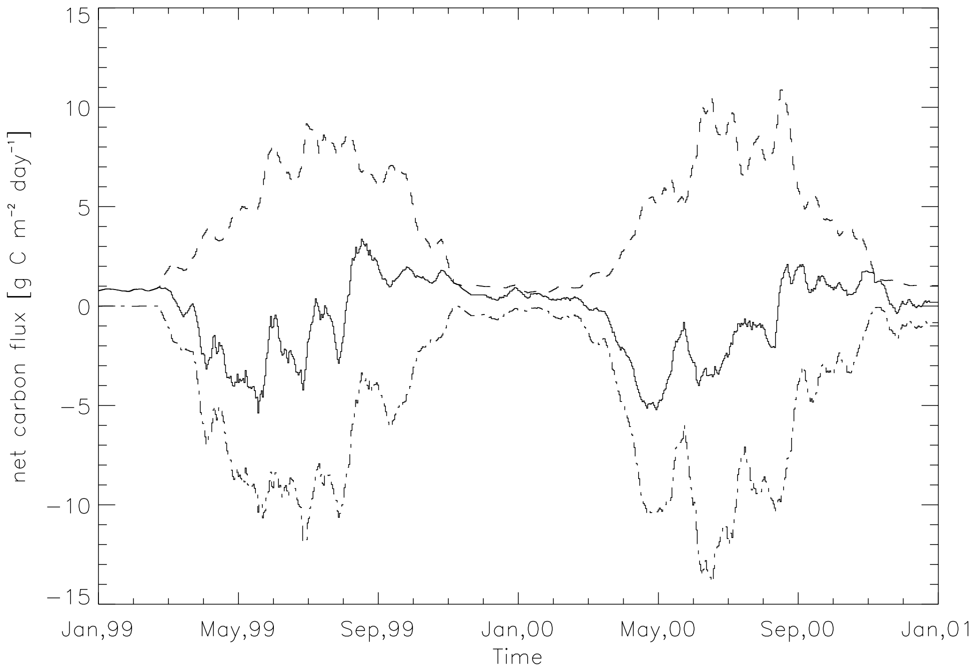

Figure 3.14: Annual variation of carbon NEE, GPP and R_t for 1999 and 2000 measured by the local, 3 m system. Data are smoothed with boxcar average of 10 days for clarity. Solid line: carbon NEE: dashed line: R_t; dash dot line: GPP. Negative value indicate carbon uptake by the ecosystem.

Finally, yearly sums of carbon NEE, GPP and R_t presented in table 3.4. There is a huge difference between carbon NEE calculated during 1999 and 2000. NEE measured in 1999 by the 82 m system and the 3 m system are very close. Since there are no more years available yet to compare yearly sums for the two systems, we may not conclude that the two systems measure the same NEE. Further data are needed to clarify the behaviour of the local scale during 2000.

	NEE [g C m^{-2} year^{-1}]	GPP [g C m^{-2} year^{-1}]	R_t [g C m^{-2} year^{-1}]
1999	-86	-1555	1469
2000	-247	-1773	1526

Table 3.4: Annual sums of carbon NEE, GPP and R_t for 1999 and 2000 at 3 m.

3.5.2 Climatic responses

It is evident from the above yearly budgets that the ecosystem is very sensitive to changes in the environmental conditions (Malhi et al., 1999). The balance between GPP and R_t is responsible for the observed variability of NEE. If GPP or R_t changes, both affects NEE and may lead to a situation when NEE even changes sign. That means that the region should turn to be a net source of CO_2 to the atmosphere. A warming climate in the Carpathian Basin may enhance ecosystem respiration in an exponential fashion (see eq. 3.7). If it is not compensated with GPP (e.g. because of drought which causes high VPD and low soil water content leading to reduced photosynthesis), NEE becomes positive. If this happens, this behaviour may act as a positive feedback to global warming.

Calculating monthly sums of NEE, GPP and R_t, we may try to find relationship between the monthly mean climat variability and the variability in the measured carbon fluxes.

Mean annual air temperature was 9.1^{o}C in 1997, 9.6^{o}C in 1998 and 9.6^{o}C in 1999. Annual precipitation was 695.3 mm in 1997, 844.4 mm in 1998 and 784.9 mm in 1999. As it was described in table 3.3, total respiration in 1997 was lower than in the other years, while it was about the same for 1998 and 1999. This can be explained by the lower annual average temperature (see eq. 3.7). Mean air temperature was about the same in 1998 and 1999, which resulted in very similar respiration rates.

In order to gain more insight into the processes governing the carbon balance, we can investigate the relation between the monthly sums of NEE, R_t and GPP, and the environmental forces.

Figure 3.15 shows (from top to bottom) the monthly sums of NEE, R_t, GPP (negative values represent carbon uptake by the vegetation), and PPFD, the monthly average temperature and the monthly sums of precipitation as measured by a nearby meteorological station (Szentgotthárd; the overplotted solid line is the normal values between 1961 and 1990 for both plots), and the monthly average daytime vapor pressure deficit for 1997, 1998 and 1999.

We may deduce more linkage between the variability of the carbon fluxes in monthly scale from figure 3.15.

Vapor pressure deficit does not seem to affect photosynthesis essentially. This is demonstrated with July and August 1998. VPD during August was considerably higher than during July, but rates of GPP was equal, which led to very similar rates of GPP. As we saw it before in fig. 3.8, photosynthesis is only affected by higher VPD values (VPD>1.5 kPa), but not in every cases. VPD may affect GPP in a daily or weekly scale, but it doesn't seem to govern GPP in

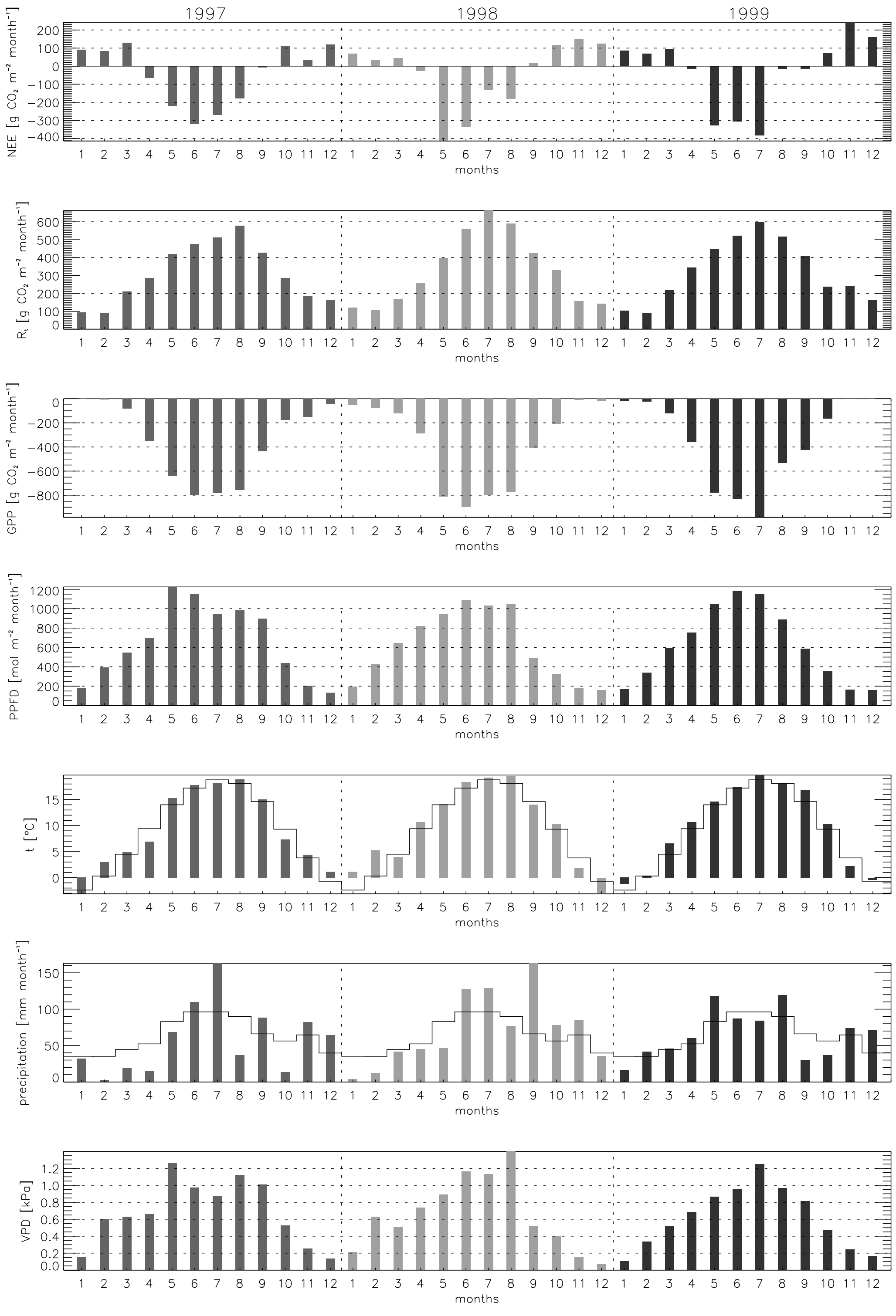

Figure 3.15: Monthly sums of NEE, R_t, GPP and PPFD, monthly average temperatures, monthy sums of precipitation and monthly average daytime VPD during 1997, 1998 and 1999. See text for details.

monthly or annual time scale.

Extreme events may be explained by other linkages. Since variability of NEE is expected to be derived by its subcomponents, we seek relationships between the climate forces and GPP and R_t. GPP is expected to be controlled by the monthly sums of PPFD. R_t is mainly derived by temperature, but soil CO_2 efflux may also be important. The following case studies reflect the climate responses of the biosphere.

In August 1999 NEE was unusually low. This is caused by the lower rates of PPFD which is resulted in lower GPP (compared to other years). Low PPFD is tied to the excess precipitation (cloudiness). In contrast, during July 1999 NEE was quite large. This is caused by the high rates of GPP compared to GPP measured during July 1997 and 1998.

High respiration sum occured during July 1998. This is caused by above average precipitation during average temperature conditions which supports microbial respiration in the soil. In contrast, during July 1997 above average precipitation occured together with below average temperature. This results in normal respiration rates.

High NEE occured during May 1998 which is caused by reduced respiration. This can be explained by the occurence of average temperature (during July 1997 and 1999 temperature was above average) and normal GPP.

We should note that not every extreme monthly event can be explained by such reasoning.

All of the above confirms the complexity of linkages between NEE and the environmental factors. The sensitivity of carbon sequestering ability of the region is also evident from the data. Further measurements are needed to confirm the observed linkages and to find others, and to provide forecasts about the carbon balance of the region under a changing climate (IPCC website, 2001).

3.6 Error assessment

The final question that should be addressed here is the accuracy of the measurement. Because of the large amount of data and the nature of the measuring system, countless error sources should be handled to conduct an accurate, reliable long-term measurement and finally to find a NEE value that is considered to be “defensible”. It was emphasised previously that great effort has been done to assure measurement quality.

Berger et al. (2001) estimates the uncertainty in the eddy flux measurements by a system very similar to ours to be around 2-4%. The possible error sources are: uncertainty in the calibration (average coefficients are used for voltage conversion during days with missing profile data), spectral degradation (which is correctable), and the random nature of turbulence. Storage change calculations are needed to compute NEE accurately (see section 3.2). It is hard to estimate the error in the storage change calculations because of the several influencing factors, but we may estimate the overall random error of NEE to be around 20%, as it is generally assumed for EC measurements (Foken and Wichura, 1996).

Energy balance closure test is applied by several authors (Greco and Baldocchi, 1996; Valentini et al., 1996; Baldocchi et al., 1997; Yamamoto et al., 1999; etc.) to test the validity of the EC measurement.

Since soil heat flux measurements are not yet realized at the site, it is estimated to be 10% of the net radiation. Using this approximation, the closure is about 63% (H+LE=0.63(R_n-G)-12 W m^{-2}, where R_n is net radiation and G is the soil heat flux; r=0.62, n=4282) for the 82 m system. Earlier we have demonstrated that a part of the closure imbalance is caused by the inadequate spectral response of the temperature fluctuation sensor (see section 2.3.4.5). However, this effect can not be responsible alone for the energy closure imbalance.

The closure is about 77% for the 3 m system (H+LE=0.77(R_n-G)-31.5 W m^{-2}, r=0.93, n=3256).

Possible causes of incomplete energy balance closure are errors in the spatial characterization of net radiation sensor (Schmid, 1997), advection and spatial variability of albedo and outgoing radiation (Anthoni et al., 1999). Furthermore, onset of a true mean vertical velocity may cause incomplete closure (Lee, 1998). As it was mentioned earlier, a mean vertical velocity of 5 cm s^{-1} at the EC measurement height may produce 100 W m^{-2} energy balance deficit.

In a recent paper of Anthoni et al. (1999) concludes that "it is very difficult to judge the validity of eddy covariance measurements in open-canopy ecosystems by testing the energy budget closure". Consequently, an incomplete energy balance does not neccessarily mean failure in the scalar fluxes.

Moncrieff et al. (1996) demonstrates the importance of random and systematic errors that may occur during long term ecosystem studies. The basic problem is trivial: if we fail to detect a part of the fluxes *systematically* (more precisely, selective-systematically), this may result in a huge error in the estimation of the net budget.

The effect of random errors (e.g. nonstationarity, random instrument noise, intermittency, etc.) disappears if the data set consists of several days of data (Moncrieff et al., 1996; Grelle, 1997). Since our measurement covers several days, furthermore a part of the random errors are filtered out (nonstationarity), we only need to focus on systematic errors (see figure 5 in Moncrieff et al., 1996 on page 236). We should note that a varying flux footprint generally causes a random error, but our system was basically built over a heterogeneous landscape, which means that variability in the flux footprint is expected and allowed.

Based on this reasoning, we may try to evaluate the possible selective systematic errors in the measurement.

Advection is an important phenomenon which can cause selective systematic errors (Yi et al., 2000; Moncrieff et al., 1996). Yi et al. (2000) estimates the effect of the advection from a multilevel EC system to a 30 m (virtual) tower to be around 10%. Recently, Lee (1998) proposed a one dimensional method to account for advection, as it was described in section 3.2. The method is successfully applied to a couple of sites (e.g. Baldocchi et al., 2000; Paw U. et al., 2000). As we saw it before in section 3.2.2, application of Lee's correction to our site provided ecologically incorrect results, and it is not used. The advection should not be treated in a one dimensional framework as it is proposed by Lee (1999), but surprisingly, "the advection correction proposed by Lee ... appears to improve energy and carbon budget closure at some sites." (Finnigan, 1999).

Advection may cause selective systematic (nighttime) underestimation of NEE according to many authors (Grace et al., 1996; Greco and Baldocchi, 1996; Baldocchi et al., 2000; Paw U. et al., 2000, Markkanen et al., 2001).

Following the method of Grace et al. (1996), we can investigate whether nighttime flux loss occurs at our site or not (Markkanen et al., 2001).

Figure 3.16 shows nighttime values of NEE and its subcomponents (eddy flux at 82 m and storage term) as a function of wind speed at the lowest level (10 m). The figure suggests that there is no "lost flux" during nighttime caused by advection (NEE does not decline at low wind speeds). The behaviour of the subcomponents is consistent: at low wind speed (when inversion builds up), the eddy flux is close to zero, i.e. no respired CO_2 reaches the eddy level but remains trapped below the 82 m level. This assumes an air layer where the

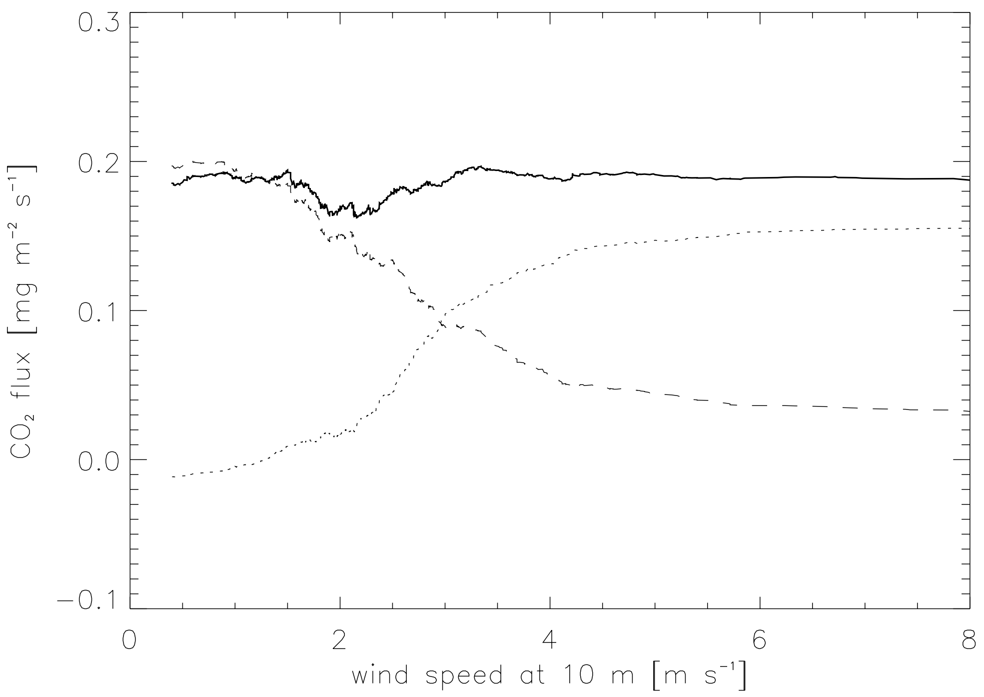

Figure 3.16: NEE, eddy flux and the storage term as a function of wind speed at 10 m during nighttime (data are ordered and smoothed with a boxcar of 500 data points) for June, July and August from all available years. Wind speed values below 0.4 m s^{-1} was ignored because of the small number of samle points. Dashed line; storage term; dotted line: eddy flux at 82 m; solid line: NEE. Nighttime is defined as the period between 20 h and 3 h UTC+1.

CO_2 concentration is gradually growing, that must appear in the rate of change of storage. Clearly, as the figure shows, the storage term is responsible for the whole NEE at the lowest wind speeds. As nighttime wind speed increasing, eddy flux becomes a more and more significant term in NEE while the importance of the storage term is decreasing. At wind speeds about 3 m s^{-1} the importance of the two term is in equal. At wind speeds higher than 4 m s^{-1} the largest part of NEE is represented by the eddy flux term, which means that the lower air layer is well mixed by shear induced turbulence.

The close match between NEE values at low and high wind speeds provides confidence that nocturnal NEE measurements are reliable (Grace et al., 1996), thus advection does not seem to cause systematic error in the measurement (but may cause random errors). This may be caused by the fact that the terrain around the tower site is quite level.

Following a night with high amount of CO_2 accumulated in the lower air

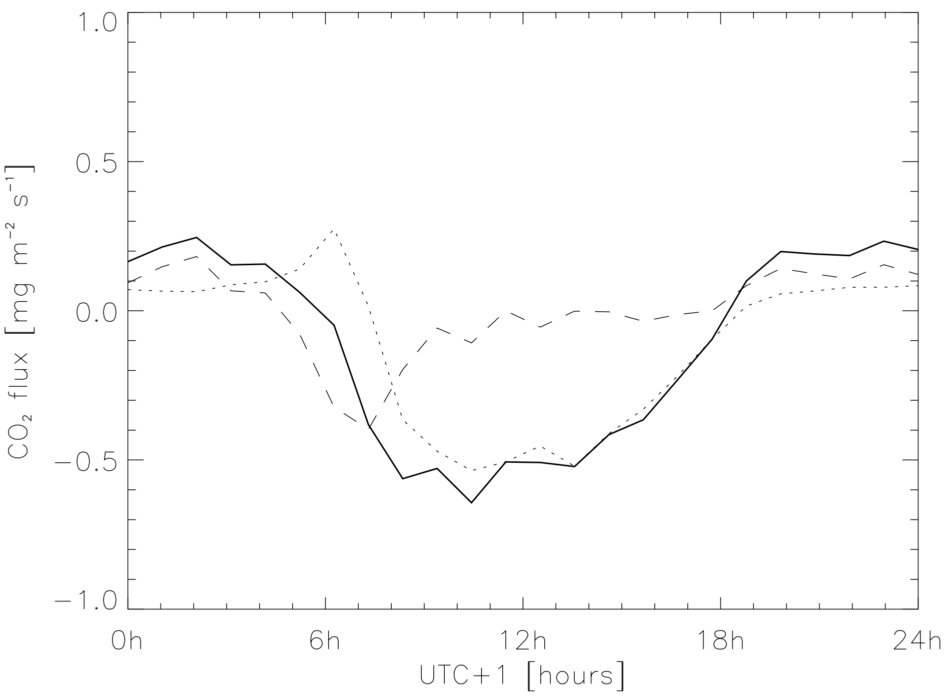

Figure 3.17: Monthly ensemble daily cycles of NEE, eddy flux and the storage term measured during June, 1999. Solid line: NEE; dotted line: storage term; dashed line: eddy flux at 82 m. Negative values denote CO_2 uptake by the vegetation.

layer, during the morning transition this CO_2 may flush out to the upper air layers. This phenomena is observed by e.g. Yi et al. (2000), Grace et al. (1996) and Moncrieff et al. (1996), but there are sites where this phenomena is rare (e.g. Anthoni et al., 1999). Considering our site, it is not possible that the vegetation may take up this accumulated CO_2 during the morning breakup of the inversion layer, thus it may appear both in the eddy flux measured at 82 m and at the storage term.

Figure 3.17 shows the monthly mean daily cycle of net ecosystem CO_2 exchange, the eddy flux measured at 82 m and the rate of change of storage term as measured during August 1999. The large peak in the eddy flux really present, but it is compensated by the storage term leading an ecologically acceptable daily NEE course.

Consequently, our NEE measurement can be considered reliable, and not contaminated by selective systematic errors (Moncrieff et al., 1996) caused by advection or underestimation of nighttime respiratory rates. This is also valid for the local, 3 m system. The main reason of this may be the good choice of the measuring site.

We should note that more complicated problems occur with measurements conducted in forested environments (e.g. Grelle, 1997; Anthoni et al., 1999; Yamamoto et al., 1999; Baldocchi et al., 2000; Paw U. et al, 2000; Yi et al., 2000). The problem is even more complicated if the terrain is not flat (Bladocchi et al., 2000; Yamamoto et al., 1999).

It is generally accepted that the long term precision of eddy covariance flux measurements is ±5-10% and the confidence interval about an annual estimate of NEE is ±30 g C m^{-2} $year^{-1}$ (Running et al., 1999).

Chapter 4

Conclusions

In the present dissertation an on-going program was described being carried out in Hungary to investigate the role of the temperate continental region in the global carbon cycle. Three closely linked measuring systems were described, which are operated near the village Hegyhátsál. The equipment is installed on a 117 m tall, free-standing TV and radio transmitter tower, and near the ground in close proximity of the tower.

One of the measuring systems is designed to measure the vertical profile of carbon dioxide mixing ratio and other meteorological elements. Design of the measuring system allows to calculate vertical fluxes of carbon dioxide by means of the classic, semi-empirical Monin-Obukhov similarity theory.

Another measuring system is designed to measure directly the vertical transport of carbon dioxide at 82 m height. The so-called eddy covariance technique is used which is the most common and reliable way currently available to determine the turbulent transport of carbon dioxide (and other scalars). The measurements made at 82 m are representative to an extedned, 8-10 km radius circle around the tower.

The installation of the second direct flux measuring system at 3 m provided the possibility to determine the carbon budget of the tower's surroundings. This measurement has a very limited flux footprint hence the results are representative only to the vegetation surrounded by the tower.

Despite the very different source area of the two measuring system, the local scale system may help to detect possible systhematic errors in the larger scale measurement (e.g. underestimation of the nighttime fluxes, intermittency, etc.)

because of its small distance from the ground. During 1999 when both measuring system was in operation, yearly Net Ecosystem Exchange measured by the two systems was approximately equal. Even though the two spatial scales are very different, it may indicate that the measuring system at 82 m works well notwithstanding the different approach and possible further error sources (e.g. storage).

It has been found that the region acts as a net sink of carbon dioxide in an annual scale, but the amount of sequestered carbon dioxide is variable in time due to changes in the environmental conditions. The ecosystem sequestered 92-146 g C m^{-2} $year^{-1}$ (0.92-1.46 t C ha^{-1} $year^{-1}$, or 3.37-5.35 t CO_2 ha^{-1} $year^{-1}$, depending on the year). In 2000 the local system recorded extremely high carbon sequestration. Unfortunately, this high value cannot be confirmed due to the malfunction of the regional scale system.

Table 4.1 shows the result of year-long NEE studies conducted over very different ecosystems. Our result (i.e. NEE, not Gross Primary Production or total ecosystem respiration!) is comparable with results from boreal environment, temperate croplands (Falge et al., 2001) or in some cases with results from temperate deciduous forests or even with NEE measured at tropical rain forests (Grace et al., 1995).

As the carbon balance of the measured region is very sensitive to respiration, it was found that the region may switch from being a carbon source to a sink as climate change proceeds (Malhi et al., 1999; IPCC website, 2001).

It is extremely important to conduct long term, direct carbon dioxide exchange measurements to quantify the carbon budget of the vegetation and to estimate the effect of the global climate change (Baldocchi et al., 1996). Our current knowledge is insufficient to close the global carbon cycle, and to estimate the future of the biosphere under changing climatic conditions (Malhi et al., 1999).

No perfect method exists to quantify the behaviour of the biosphere because of methodological difficulties. There is also uncertainty in the estimation of the soil carbon stocks. One important future task is the investigation of the soil carbon fluxes (Malhi et al., 1999) to constrain the soil carbon content. The upscaling of the local, sometimes site-specific measurements also causes uncertainty. Our approach was to try to avoid the upscaling problem by developing a measuring system which is designated to be representative for the regional scale with mixed, patch-like vegetation. Our approach fits the trend of micrometeorological mea-

Author	vegetation type	NEE [gC $m^{-2}year^{-1}$]
Malhi et al., 1999	boreal forest	-70
Lindroth et al., 1998	boreal forest	-70 - -220
Markkanen et al., 2001	boreal pine forest	-191 - -262
Black et al., 1996	boreal hazel nut/aspen	-130
Malhi et al., 1999	temperate forest	-585
Goulden et al., 1996	mixed temperate deciduous	-140 - -280
Valentini et al., 1996	temperate beech	-472
Yamamoto et al., 1999	deciduous forest (birch, oak)	-180
Greco and Baldocchi, 1996	deciduous forest	-525
Falge et al., 2001	corn (temperate region)	-467
Falge et al., 2001	wheat (temperate region)	-183
Falge et al., 2001	tallgrass prairie	-318
Malhi et al., 1999	tropical forest	-590
Grace et al., 1995	tropical forest	-100

Table 4.1: Comparison of year-long NEE measurements.

surements, which is the relocation of the measuring sites from flat, homogeneous (ideal) terrains to heterogeneous, sometimes sloping terrains which are characteristic of the real world (Baldocchi et al., 2000). This new approach raises many new problems associated with the change in the dynamics of the atmospheric motions (e.g. changes in the roughness, humidity, albedo, vegetation type, possible onset of local circulations, advection, etc.), thus much more attention must be paid to ensure that the results of the measurements are reliable, and reflect the real dynamics of the region. Detailed overview was given in this work considering as many problems as possible to assure data quality.

The region was not expected to act as a strong sink compared to forests, but its current carbon sequestring role is not insignificant and should be considered in any integrated, continent-scale carbon balance study.

There is no current agreement in the localization of the "missing sink" (Malhi et al., 1999). Different research groups detected different places for the sink (e.g. North America or Siberia after Fan et al. (1998) or Bousquet et al (1999), respectively). There are very few studies that approaches consistency with the current, ground-based results.This is mainly caused by methodological problems (Malhi et al., 1999). Delevopment must be done in this field to be able to utilize the ground-based data to constrain the models that describe the global carbon cycle.

In summary, our current knowledge of the carbon cycle is deeper than it used to be 10-20 years ago, but still, a great deal of work is needed to gain better insight into the biochemical and meteorological processes that govern the carbon balance of the biosphere and the CO_2 content of the atmosphere.

Acknowledgements

I am very grateful to Dr. László Haszpra, the principal investigator and organizer of the whole project. Without his super effort the whole project could not have been established. Thanks for the discussions and for the help with regards the data, the data processing, the interpretation of the data, the calculations, etc. I would like to thank the Department of Meteorology for the computing support and for the chance to stay at the Department working on my Ph.D. dissertation. Special thanks to Dr. Judit Bartholy for her motivation and for her advices. I am also very grateful to my supervisor, Dr. Tamás Weidinger for his support.

Special thanks to Dr. Ken Davis for the IDL code he provided and kick-started me in the work, and also for the hospitality in Minneapolis/St. Paul. Thanks to Dr. Brad Berger for his technical help and also for his hospitality. Thanks for the valuable discussions in the USA and in Hungary.

Special thanks to the CO_2 group in Japan, for the extremely kind hospitality of Dr. Yamamoto, for the discussions with Dr. Saigusa and Dr. Kondo. Thanks for sending me very important papers in various topics.

Special thanks to John Kert for the valuable technical english usage corrections.

I'm very garteful to my family, and to my girlfriend for her support, patience and motivation.

Use of the tower and transmitter building is kindly provided by Antenna Hungária Corporation. The project was supported by the U.S.-Hungarian Scientific and Technological Joint Fund (J. F. no. 162 [1992-1995] and J. F. no. 504 [1996-1999]), by the Hungarian National Scientific Research Fund (OTKA T7282 [1993-1996], OTKA T23811 [1997-2000], OTKA F026642 [1998-2001], OTKA T32440 [2001-2004]), by the Hungarian Higher Education Support Program (FKFP-0168/1997), by the Agency of Industrial Science and Technology (Japan), and by the Bilateral Intergovernmental S&T Cooperation (OMFB, Hungary).

Bibliography

[1] Anderson, D. E., Verma, S. B., 1984: Turbulence spectra of CO_2, water vapor, temperature and wind velocity fluctuations over a crop surface. *Boundary-Layer Meteorology*, **33**: 1-14.

[2] Anthoni, P. M., Law, B. E., Unsworth, M. H., 1999: Carbon and water vapor exchange of an open-canopied ponderosa pine ecosystem. *Agricultual and Forest Meteorology*, **95**: 151-168.

[3] Aubinet, M., Grelle, A., Ibrom, A., Rannik, Ü., Moncrieff,J., Foken, T., Kowalski, A. S., Martin, P. H., Berbigier, P., Bernhofer, Ch., Clement, R., Elbers, J., Granier, A., Grünwald, T., Morgenstern, K., Pilegaard, K., Rebmann, C., Snijders, W., Valentini, R., Vesala, T., 2000: Estimates of the annualnet carbon and water exchange of forests: the EUROFLUX methodology. *Adv. Ecol. Res.,* **30**: 113-175.

[4] Aurela, M., Touvinen, J-P., Laurila, T., 1998: Carbon dioxide exchange in a subarctic peatland ecosystem in northern Europe measured by the eddy covariance technique. *Journal of Geophysical Research*, **103D**: 11289-11301.

[5] Bakwin, P. S., Tans, P. P., Zhao, C. L., Ussler III, W., Quesnell, E., 1995: Measurement of carbon dioxide on a very tall tower. *Tellus*, **47B**: 535-549.

[6] Bakwin, P. S., Tans, P. P., Hurst, D. F., Zhao, C., 1998: Measurements of carbon dioxide on very tall towers: Results of the NOAA/CMDL program. *Tellus*, **50B**: 401-415.

[7] Baldocchi, D., Finnigan, J., Wilson, K., Paw U, K. T., Falge, E., 2000: On measuring net ecosystem carbon exchange over tall vegetation on complex terrain. *Boundary-Layer Meteorology*, **96**: 257-291.

[8] Baldocchi, D., Vogel, C. A., Hall, B., 1997: Seasonal variation of carbon dioxide exchange rates above and below a boreal jack pine forest. *Agricultural and Forest Meteorology*, **83**: 147-170.

[9] Baldocchi, D., Valentini, R., Running, S., Oechel, W., Dahlman, R., 1996: Strategies for measuring and modelling carbin dioxide and water vapour fluxes over terrestrial ecosystems. *Global Change Biology*, **2**: 159-168.

[10] Barcza, Z., Weidinger, T., Haszpra, L., 1996: Carbon dioxide concentration measurement in Hungary. *XXI. General Assembly of the European Geophysical Society,* The Hague, Netherlands, 6-10 May, 1996. Supplement issue Annales Geophysicae, Vol. 14, C462.

[11] Barcza, Z., Weidinger, T., Haszpra, L., 1997: Regional CO_2 flux measurements in Hungary. *Extended Abstracts, Fifth International Carbon Dioxide Conference*, Cairns, Australia, 8-12 September, 1997: 38.

[12] Barcza, Z., Haszpra, L., Iványi, Zs., Kondo, H., Saigusa, N., Yamamoto, S., 1999: Carbon dioxide flux monitoring over mixed agricultural terrain in Hungary. *XXIV. General Assembly of the European Geophysical Society,* The Hague, Netherlands, 19-23 April, 1999. Supplement issue Annales Geophysicae, Part 2. Vol. 1, C443.

[13] Barnola, J. M., Anklin, M., Porcheron, J., Raynaud, D., Schwander, J., Stauffer, B., 1995: CO_2 evolution during the last millennium as recorded by Antarctic and Greenland ice. *Tellus*, **47B**: 264-272.

[14] Bartholy, J., Matyasovszky, I., Weidinger, T., 2001: Regional climat change in Hungary: a survey and a stochastic downscaling method. *Időjárás*, **105**: 1-17.

[15] Benoit, R., 1977: On the integral of the surface layer profile-gradient functions. *Journal of Applied Meteorology,* **16**: 859-860.

[16] Berger, B. W., Davis, K. J., Bakwin, P. S., Yi, C., Zhao, C., 2001: Long-term carbon dioxide fluxes from a very tall tower in a northern forest: Flux measurement methodology. J. Atmospheric and Oceanic Technology, 18: 529-542.

[17] Black, T. A., Den Hartog, G., Neumann, H. H., Blanken, P. D., Yang, P. C., Russell, C., Nesic, Z., Lee, X., Chen, S. G., Staebler, R., Novak, M. D., 1996: Annual cycles of water vapour and carbon dioxide fluxes in and above a boreal aspen forest. *Global Change Biology*, **2**: 219-229.

[18] Bolin, B., Degens, E. T., Duvigneaud, P., Kempe, S., 1977: The global biogeochemical carbon cycle. In: The global carbon cycle. SCOPE 13 (edited by Bolin, B., Degens, E. T., Kempe, S. and Ketner, P.). John Wiley & Sons, Chichester - New York - Brisbane - Toronto.

[19] Bousquet, P., Ciais, P., Peylin, P., Ramonet, M., Monfray, P., 1999: Inverse modelling of annual atmospheric CO_2 sources and sinks. Part 1: Method and control inversion. *Journal of Geophysical Research*, in press.

[20] Businger, J. A., Wyngaard, J. C., Izumi, Y., Bradley, E. F., 1971: Flux-Profile Relationships in the atmospheric surface layer. *Journal of Atmospheric Sciences*, **28**: 181-189.

[21] Businger, J. A., 1986: Evaluation of the accuracy with which dry deposition can be measured with current micrometeorological techniques. *Journal of Climate and Applied Meteorology* **25**: 1100-1124.

[22] Carbon Dioxide Information Analysis Center website, Oak Ridge National Laboratory, 2001. `http://cdiac.esd.ornl.gov`

[23] Ciais, P., Tans, P. P., Trolier, M., White, J. W. C., Francey, R. J., 1995a: A large northern hemispheric terrestrial CO_2 sink indicated by the $^{13}C/^{12}C$ ratio of atmospheric CO_2. *Science*, **269**: 1098-1102.

[24] Ciais, P., Tans, P. P., White, J. W. C., Trolier, M., Francey, R. J., Berry, J. A., Randall, D. R., Sellers, P. J., Collatz, J. G., Schimel, D. S., 1995b: Partitioning of ocean and land uptake of CO_2 as inferred by ^{13}C measurements from the NOAA/CMDL global air sampling network. *Journal of Geophysical Research*, **100D**: 5051-5070.

[25] Conway, T. J., Tans, P. P., Waterman, L. S., Thoning, K. W., Kitzis, D. R., Masarie, K. A., Zhang, N., 1994: Evidence for interannual variability of

the carbon cycle from the National Oceanic and Atmospheric Administration/Climate Monitoring and Diagnostics Laboratory Global Air Sampling Network. *Journal of Geophysical Research*, **99D**: 22831-22855.

[26] Denholm-Price, J. C. W., Rees, J. M., 1998: A practical example of low-frequency trend removal. *Boundary-Layer Meteorology,* **86**: 181-187.

[27] Denning, A. S., Fung, I. Y., Randall, D., 1995: Latitudinal gradient of atmospheric CO_2 due to seasonal exchange with land biota. *Nature,* **376**: 240-243.

[28] Dixon, R. K., Brown, S., Houghton, R. A., Solomon, A. M., Trexler, M. C., Wisniewski, J., 1994: Carbon pools and flux of global forest ecosystems. *Science*, **263**: 185-190.

[29] Enting, I. G. and Mansbridge, J. V., 1991: Latitudinal distribution of sources and sinks of CO_2: results of an inversion study. *Tellus*, **43B**, 156-170.

[30] Dyer, A. J., Hicks, B. B., 1970: Flux-gradient relationships in the constant flux layer. *Quart. J. Roy. Met. Soc.*, **96**: 715-721.

[31] Enting, I. G., Mansbridge, J. V., 1991: Latitudinal distribution of sources and sinks of CO_2: results of an inversion study. *Tellus*, **43B**: 156-170.

[32] Etheridge, D. M., Steele, L. P., Langenfelds, R. L., Francey, R. J., Barnola, J. M., Morgan, V. I., 1996: Natural and anthropogenic changes in atmospheric CO_2 over the last 1000 years from air in Antarctic ice and firn. *Journal of Geophysical Research*, **101D**: 4115-4128.

[33] Eugster, W., McFadden, J. P., Chapin, F. S., 1997: A comparative approach to regional variation in surface fluxes using mobile eddy correlation towers. *Boundary-Layer Meteorology*, **85**: 293-307.

[34] Falge, E., Baldocchi., D., Olson, R., Anthoni, P., Aubinet, M., Bernhofer, C., Burba, G., Ceulemans, R., Clement, R., Dolman, H., Granier, A., Gross, P., Grünwald, T., Hollinger, D., Jensen, N.-O., Katul, G., Keronen, P., Kowalski, A., Lai, C. T., Law, B. E., Meyers, T., Moncrieff, J., Moors, E., Munger, J. W., Pilegaard, K., Rannik, Ü., Rebmann, C., Suyker, A.,

Tenhunen, J., Tu, K., Verma, S., Vesala, T., Wilson, K., Wofsy, S., 2001: Gap filling strategies for defensible annual sums of net ecosystem exchange. *Agricultural and Forest Meteorology,* **107**: 43-69.

[35] Fan, S., Gloor, M., Mahlman, J.,Pacala, S., Sarmiento, J., Takahashi, T., Tans, P., 1998: A large terrestrial carbon sink in North America implied by atmospheric and oceanic carbon dioxide data and models. *Science*, **282**: 442-446.

[36] Fan, S. M.,Wofsy, S. C., Bakwin, P. S., Jacob, D. J., Fitzjarrald, D. R., 1990: Atmosphere-biosphere exchange of CO_2 and O_3 in the central Amazon Forest. *Journal of Geophysical Research*, **95**: 16851-16864.

[37] Finnigan, J., 1999: A comment on the paper by Lee (1998): "On micrometeorological observations of surface-air exchange over tall vegetation". *Agricultural and Forest Meteorology*, **97**: 55-64.

[38] FLUXNET website, 2001. `http://daacl.esd.ornl.gov/FLUXNET`

[39] Foken, Th., Skeib, G., 1983: Profile measurements in the atmospheric near-surface layer and the use of suitable universal function for the determination of the turbulent energy exchange. *Boundary-Layer Meteorology*, **25**: 55-62.

[40] Foken, Th., Wichura, B., 1996: Tools for quality assessment of surface-based flux measurements. *Agricultural and Forest Meteorology*, **78**: 83-105.

[41] Fung, I. Y., Tucker, C. J., Prentice, K. C., 1987: Application of advanced very high resolution radiometer vegetation index to study atmosphere-biosphere exchange of CO_2. *Journal of Geophysical Research*, **92D**: 2999-3015.

[42] Goulden, M. L., Munger, J. W., Fan, S-M., Daube, B. C., Wofsy, S. C., 1996: Exchange of carbon dioxide by a deciduous forest: Response to interannual climate variability. *Science*, **271**: 1576-1578.

[43] Grace, J., Lloyd, J., McIntyre, J., Miranda, A., Meir, P., Miranda, H., Moncrieff, J., Massheder, J., Wright, I., Gash, J., 1995: Fluxes of carbon dioxide and water vapour over an undisturbed tropical forest in south-west Amazonia. *Global Change Biology*, **1**: 1-12.

[44] Grace, J., Malhi, Y., Lloyd, J., McIntyre, J., Miranda, A., Meir, P., Miranda, H., 1996: The use of eddy covariance to infer the net carbon dioxide uptake of Brazilian rain forest. *Global Change Biology*, **2**: 209-217.

[45] Grace, J. website. `http://www.ierm.ed.ac.uk/people/academic/grace.html`

[46] Greco, S., Baldocchi, D. D., 1996: Seasonal variations of CO_2 and water vapour exchange rates over a temperate deciduoud forest., *Global Change Biology*, **2**: 183-197.

[47] Grelle, A., Lindroth, A., 1996: Eddy-correlation system for long-term monitoring of fluxes of heat, water vapour and CO_2. *Global Change Biology*, **3**: 297-307.

[48] Grelle, A., 1997. *Long-term water and carbon dioxide fluxes from a boreal forest.* Doctoral thesis. Swedish University of Agricultural Sciences, Uppsala, 1997.

[49] Haszpra, L., 1995: Carbon dioxide concentration measurements at a rural site in Hungary. *Tellus*, **47B**: 17-22.

[50] Haszpra, L., 1999a: On the representativeness of carbon dioxide measurements. *Journal of Geophysical Research*, 1**04D**: 26953-26960.

[51] Haszpra, L., 1999b: Measurements of atmospheric carbon dioxide at a low elevation rural site in Central Europe. *Időjárás*, **103**: 93-106.

[52] Haszpra, L., Barcza, Z., 2001: A magyarországi légkör/bioszféra szén-dioxid fluxus mérések eredményei. F*izikai Szemle*, **2001/2**: 50-52.

[53] Haszpra, L., Barcza, Z., Bakwin, P. S., Berger, B. W., Davis, K. J., Weidinger, T. 2001: Measuring system for the long-term monitoring of biosphere/atmosphere exchange of carbon dioxide. *Journal of Geophysical Research,* **106D**: 3057-3070.

[54] Hensen, A., van den Bulk, W. C. M., Vermeulen, A. T., Wyers, G. P., 1997: *CO_2 exchange between grassland and the atmosphere.* Netherlands Energy Research Foundation, ECN-C-97-032.

[55] Hesshaimer, V., Heiman, M., Levin, I., 1994: Radiocarbon evidence for a smaller oceanic carbon dioxide sink than previously believed. *Nature*, **370**: 201-203.

[56] Hollinger, D. Y., Kelliher, F. M., Schulze E.-D., Bauer G., Arneth, A., Byers J. N., Hunt, J. E., McSeveny, T. M., Kobak, K. I., Milukova, I., Sogatchev, A., Tatarinov, F., Varlargin, A., Ziegler, W., Vygodskaya, N. N., 1998: Forest-atmosphere carbon dioxide exchange in eastern Siberia. *Agricultural And Forest Meteorology*, **90**: 291-306.

[57] Horst, T. W., Weil, J. C., 1994: How far is far enough?: The fetch requirements for micrometeorological measurement of surface fluxes. *J. of Atmospheric and Oceanic Technology*, **11**: 1018-1025.

[58] Horst, T. W., 1999: The footprint for estimation of atmosphere-surface exchange fluxes by profile techniques. *Boundary-Layer Meteorology*, **90**: 171-188.

[59] Horváth, Á., Práger, T., 1985: The dynamics of squall lines and their predictability. *Időjárás*, **89**: 141-160.

[60] Högström, U., 1988: Non-dimensional wind and temperature profiles in the atmospheric surface layer: a re-evaluation. *Boundary-Layer Meteorology*, **42**: 55-78.

[61] Högström, U., Bergström, H., Smedman, A.-S., Halldin, S., Lindroth, A., 1989: Turbulent exchange above a pine forest, I: fluxes and gradients. *Boundary-Layer Meteorology*, **49**: 197-217.

[62] Högström, U., 1996: Review of some basic characteristics of the atmospheric surface layer. *Boundary-Layer Meteorology*, **78**: 215-246.

[63] IPCC website, 2001. `http://www.IPCC.ch`

[64] IPCC, 1996: Climate change 1995: *The science of climate change* (edited by Houghton, J. T., Meira Filho, L. G., Callander, B. A., Harris, N., Kattenberg, A., Maskell, K.). University Press, Cambridge.

[65] Kaimal, J. C., Wyngaard, J. C., Haugen, D. A., 1968: Deriving power spectra from a three-component sonic anemometer. *Journal of Applied Meteorology*, **7**: 827-837.

[66] Kaimal, J. C., Wyngaard, J. C. Izumi, Y., Cote, O. R., 1972: Spectral characteristics of surface-layer turbulence. *Quart. J. Roy. Met. Soc.*, **98**: 563-589.

[67] Keeling, C. D., Bacastow, R. B., Carter, A. F., Piper, S. C., Whorf, T. P., Heimann, M., Mook, W. G., Roelffzon, H., 1989: A three-dimensional model of atmospheric CO_2 transport based on observed winds; 1, Analysis of observational data. In: Aspects of climate variability in the Pacific and Western Americas (edited by Peterson, D. H.). *Geophys. Monogr.*, **55**: 165-236.

[68] Keeling, R. F., Piper, S. C., Heimann, M., 1996: Global and hemispheric CO_2 sinks deduced from changes in atmospheric O_2 concentration. *Nature*, **381**: 218-221.

[69] Kitzis, D., Zhao, C., 1999: CMDL/Carbon Cycle Gases Group standards preparation and stability. *NOAA Technical Memorandum* ERL CMDL-14.

[70] Lee, H. N., 1997: Improvement of surface flux calculations in the atmospheric surface layer. *Journal of Applied Meteorology*, **36**: 1416-1423.

[71] Lee, X., 1998: On micrometeorological observations of surface-air exchange over tall vegetation. *Agricultural and Forest Meteorology*, **91**: 39-49.

[72] Lenschow, D. H., Raupach, M. R., 1991: The attenuation of fluctuations in scalar concentrations through sampling tubes. *Journal of Geophysical Research*, **96D**: 15259-15268.

[73] Leuning, R., Moncrieff, J., 1990: Eddy-covariance CO_2 flux measurements using open- and closed-path CO_2 analysers: corrections for analyser water vapour sensitivity and damping of fluctuations in air sampling tubes. *Boundary-Layer Meteorology*, **53**: 63-76.

[74] Leuning, R., King, K. M., 1992: Comparison of eddy-covariance measurements of CO_2 fluxes by open- and closed-path CO_2 analysers. *Boundary-Layer Meteorology*, **59**: 297-311.

[75] LI-COR, 1996: LI-6262 CO_2/H_2O analyzer operating and service manual. Publication number 9003-59, Lincoln, NE, USA.

[76] Lindroth, A., Grelle, A., Morén, A-S., 1998: Long-term measurements of boreal forest carbon balance reveal large temperature sensitivity. *Global Change Biology*, **4**: 443-450.

[77] Malhi, Y., Baldocchi, D. D., Jarvis, P. G., 1999: The carbon balance of tropical, temperate and boreal forests. *Plant, Cell and Environment*, **22**: 715-740.

[78] Markkanen, T., Rannik, Ü., Keronen, P., Suni, T., Vesala, T., 2001: Eddy covariance fluxes over a boreal Scots pine forest. *Boreal Environment Research*, **6**: 65-78.

[79] Massman, W. J. website. `http://lamar.colostate.edu/~rwu4451/massman/coef_diff.html`

[80] Massman, W. J., 1991: The attenuation of concentration fluctuations in turbulent flow through a tube. *Journal of Geophysical Research*, **96D**: 15269-15273.

[81] Matyasovszky, I., 1990: Methods of spectral analysis of climatological time series I. *Időjárás*, **94**: 361-368.

[82] Matyasovszky, I., Weidinger, T., Bartholy, J., Barcza, Z., 1999: Current regional climate change studies in Hungary: a review. *Geographica Helvetica*, Swiss Journal of Geography, **54**: 138-146.

[83] McDermitt, D. K., Welles, J. M., Eckles, R. D., 1993: *Effects of temperature, pressure and water vapor on gas phase infrared absorption by* CO_2. LI-COR.

[84] McMillen, R., 1988: An eddy correlation technique with extended applicability to non-simple terrain. *Boundary-Layer Meteorology*, **43**: 231-245.

[85] Moncrieff, J. B., Malhi, Y., Leuning, R., 1996: The propagation of errors in long-term measurements of land-atmosphere fluxes of carbon and water. *Global Change Biology*, **2**: 231-240.

[86] Moncrieff, J. B., Massheder, J. M., de Bruin, H., Elberts, J., Friborg, T., Heusinkveld, B., Kabat, P., Scott, P., Soegaard, H., Verhoef, A., 1997: A system to measure surface fluxes of momentum, sensible heat, water vapour and carbon dioxide. *Journal of Hydrology*, **188-189**: 589-611.

[87] Moore, C. J., 1986: Frequency response corrections for eddy correlation systems. *Boundary-Layer Meteorology*, **37**: 17-35.

[88] Musselman, R. C., Fox, D. G., 1991: A review of the role of temperate forests in the global CO_2 balance. *J. Air & Waste Manage. Assoc.,* **41**: 798-807.

[89] Nagy, K., 1989: *Theoretical physics.* (in Hungarian) Tankönyvkiadó, Budapest, pp. 290-291.

[90] NOAA CMDL ftp site, 2001. `ftp://ftp.cmdl.noaa.gov/ccg/co2/flask/complete/hun.co2` for the complete dataset, `ftp://ftp.cmdl.noaa.gov/ccg/co2/flask/month/hunmm.co2` for the monthly data. GLOBALVIEW data: `ftp://ftp.cmdl.noaa.gov/ccg/co2/GLOBALVIEW/gv/hun*`

[91] NOAA CMDL website, 2000. `http://www.CMDL.NOAA.gov`

[92] Ohtaki, E., 1985: On the similarity in atmospheric fluctuations of carbon dioxide, water vapor and temperature over vegetated fields. *Boundary-Layer Meteorology*, **32**: 25-37.

[93] Paw U., K. T., Baldocchi, D. D., Meyers, T. P., Wilson, K. B., 2000: Correction of eddy-covariance measurements incorporating both advective effects and density fluxes. *Boundary-Layer Meteorology*, **97**: 487-511.

[94] Philip, J. R., 1963: The damping of a fluctuating concentration by continuous sampling through a tube. *Aust. J. Phys.*, **16**: 454-463.

[95] Quay, P. D., Tilbrook, B., Wong, C. S., 1992: Oceanic uptake of fossil fuel CO_2: Carbon-13 evidence. *Science*, **256**: 74-79.

[96] Running, S. W., Baldocchi, D. D., Turner, D. P., Gower, S. T., Bakwin, P. S., Hibbard, K. A., 1999: A global terrestrial monitoring network integrating tower fluxes, flask sampling, ecosystem modeling and EOS satellite data. *Remote Sens. Environ.*, **70**: 108-127.

[97] Saigusa, N., Oikawa, T., Liu, S., 1998. Seasonal variations og the exchange of CO_2 and H_2O between a grassland and the atmosphere: an experimental study. *Agricultural and Forest Meteorology*, **89**: 131-139.

[98] Sarmiento, J. L., Sundquist, E. T., 1992: Revised budget for the oceanic uptake of anthropogenic carbon dioxide. *Nature*, **356**: 589-593.

[99] Siegenthaler, U., Sarmiento, J. L., 1993: Atmospheric carbon dioxide and the ocean. *Nature*, **365**: 119-125.

[100] Schimel, D., Alves, D., Enting, I., Heimann, M., Joos, F., Raynaud, D., Wigley, T., Prather, M., Derwent, R., Ehhalt, D., Fraser, P., Sanhueza, E., Zhou, X., Jonas, P., Charlson, R., Rodhe, H., Sadasivan, S., Shine, K. P., Fouquart, Y., Ramaswamy, V., Solomon, S., Srinivasan, J., Albritton, D., Isaksen, I., Lal, M., Wuebbles, D., 1996: Radiative forcing of climate change. In: Climate change 1995: *The science of climate change* (edited by Houghton, J. T., Meira Filho, L. G., Callander, B. A., Harris, A., Kattenberg, A. and Maskell, K.). University Press, Cambridge. 65-132.

[101] Schimel, D. S., 1995: Terrestrial ecosystems and the carbon cycle. *Global Change Biology*, **1**: 77-91.

[102] Schmid, H. P., 1994: Source areas for scalars and scalar fluxes. *Boundary-Layer Meteorology*, **67**: 293-318.

[103] Schmid, H. P., 1997: Experimental design for flux measurements: matching scales of observations and fluxes. *Agricultural and Forest Meteorology*, **87**: 179-200.

[104] Stefanovits, P., 1971: *Brown Forest Soils of Hungary.* (in Hungarian) Akadémiai Kiadó, Budapest.

[105] Stull, R. B., 1988: *An introduction to boundary layer meteorology.* Kluwer Acad., Norwell, Mass. pp 666.

[106] Sundquist, E. T., 1993: The global carbon dioxide budget. *Science*, **259**: 934-941.

[107] Suyker, A. E., Verma, S. B., 1993: Eddy correlation measurement of CO_2 flux using a closed-path sensor: theory and field tests against an open-path sensor. *Boundary-Layer Meteorology*, **64**: 391-407.

[108] Taguchi, S., 1996: A three-dimensional model of atmospheric CO_2 transport based on analyzed winds: Model description and simulation results for TRANSCOM. *Journal of Geophysical Research*, **101D**: 15099-15109.

[109] Tans, P. P., Conway, T. J., Nakazawa, T., 1989: Latitudinal distribution of the sources and sinks of atmoapheric carbon dioxide derived from surface observations and an atmospheric transport model. *Journal of Geophysical Research*, **94D**: 5151-5172.

[110] Tans, P. P., Fung, I. Y., Takahashi, T., 1990: Observational constrains on the global atmospheric CO_2 budget. *Science*, **247**: 1431-1438.

[111] Tans, P. P., 1991: *An observational strategy for assessing the role of terrestrial ecosystems in the global carbon cycle: Scaling down to regional levels. Scaling Processes Between Leaf and Landscape Levels.* (edited by J. Ehleringer and C. Field). Academic Press. 71-105.

[112] Tans, P., Bakwin, P., Guenther, W., 1996: A feasible Global Carbon Cycle Observing System: a plan to decipher today's carbon cycle based on observations. *Global Change Biology*, **2**: 209-318.

[113] Trolier, M., White, J. W. C., Tans, P. P., Masarie, K. A., Gemery, P. A.,1996: Monitoring the isotopic composition of atmospheric CO_2: Measurements from the NOAA global air sampling network. *Journal of Geophysical Research*, **101**: 25897-25916.

[114] Valentini, R., Matteucci, G., Dolman, A. J., Schulze, E.-D., Rebmann, C., Moors, E. J., Granier, A., Gross, P., Jensen, N. O., Pilegaard, K., Lindroth, A., Grelle, A., Bernhofer, C., Grünwald, T., Aubinet, M., Ceulemans, R., Kowalski, A. S., Vesala, T., Rannik, Ü., Berbigier, P., Loustau, D., Gudmundsson, J., Thorgeirsson, H., Ibrom, A., Morgenstern, K., Clement, R., Moncrieff, J., Montagnani, L., Minerbi, S., Jarvis, P. G., 2000: Respiration as the main determinant of carbon balance in European forests. *Nature*, **404**: 861-865.

[115] Valentini, R., Gamon, J. A., Field, C. B., 1995: Ecosystem gas exchange in a California grassland: Seasonal patterns and implications for scaling. *Ecology*, **76**: 1940-1952.

[116] Valentini, R., De Angelis, P., Mattuecci, G., Monaco, R., Dore, S., Scarascia Mugnozza, G. E., 1996: Seasonal net carbon dioxide exchange of a beech forest with the atmosphere. *Global Change Biology*, **2**: 199-207.

[117] Webb, E. K., Pearman, G. I., Leuning, R., 1980: Correction of flux measurements for density effects due to heat and water vapour transfer. *Quart. J. Roy. Met. Soc.*, **106**: 85-100.

[118] Webb, E. K., 1970: Profile relationships: the log-linear range, and extension to strong stability. *Quart. J. Roy. Met. Soc.*, **96**: 67-90.

[119] Weidinger, T., Pinto, J., Horváth, L., 2000: Effects of uncertainties in universal functions, roughness length, and displacement height on the calculation of surface layer fluxes. *Meteorologische Zeitschrift*, Vol. **9**, No. 3: 139-154.

[120] Weidinger, T., Ács, F., Mészáros, R., Barcza, Z., 1999: Energy budget components in a forest clearcut: analysis of measurement results. *Időjárás*, **103**: 145-160.

[121] Vermetten, A. W. M., Ganzeveld, L., Jeuken, A., Hofschreuder, P., Mohren, G. M. J., 1994: CO_2 uptake by a stand of Douglas fir: flux measurements compared with model calculations. *Agricultural and Forest Meteorology*, **72**: 57-80.

[122] Wofsy, S. C., Goulden, M. L., Munger, J. W., Fan, S.-M., Bakwin, P. S., Daube, B. C., Bassow, S. L., Bazzaz, F. A., 1993: Net exchange of CO_2 in a mid-latitude forest. *Science*, **260**: 1314-1317.

[123] World Data Center for Greenhouse Gases website. World Meteorological Organization, 2001. `http://jcdc.kishou.go.jp/wdcgg.html`

[124] Yagüe, C., Cano, J. L., 1994: Eddy transfer processes in the atmospheric boundary layer. *Atmospheric Environment*, **28**: 1275-1289.

[125] Yamamoto, S., Murayama, S., Saigusa, N., Kondo, H., 1999: Seasonal and inter-annual variation of CO_2 flux between a temperate forest and the atmosphere in Japan. *Tellus*, **51B**: 402-413.

[126] Yi, C., Davis, K. J., Bakwin, P. S., Berger, B. W., Marr, L. C., 2000: Influence of advection on measurements of the net ecosystem-atmosphere exchange of CO_2 from a very tall tower. *Journal of Geophysical Research*, **105D**: 9991-9999.

[127] Zhao, C. L., Bakwin, P. S., Tans, P. P., 1997a: A design for unattended monitoring of carbon dioxide on a very tall tower. *J. of Atmospheric and Oceanic Technology*, **14**: 1139-1145.

[128] Zhao, C. L., Tans, P. P., Thoning, K. W., 1997b: A high precision manometric system for absolute calibration of CO_2 in dry air. *Journal of Geophysical Research*, 1**02D**: 5885-5894.